Contract No. Nonr 839 (38)
ARPA Order No. 529

Contract No. DAHC04-69-C-0073
ARPA Order No. 1442, Amendment 2
Program Code 9F30

FLOW FIELD DIAGNOSTICS IN RAREFIED SLIGHTLY IONIZED HYPERSONIC FLOW

by

Joel M. Avidor and Samuel Lederman

POLYTECHNIC INSTITUTE OF BROOKLYN

DEPARTMENT
of
AEROSPACE ENGINEERING
and
APPLIED MECHANICS

JUNE 1971

Distribution of this document is unlimited.

PIBAL REPORT NO. 71-18

125

Unclassified
Security Classification

DOCUMENT CONTROL DATA - R & D

(Security classification of title, body of abstract and indexing annotation must be entered when the overall report is classified)

1 ORIGINATING ACTIVITY (Corporate author)
Polytechnic Institute of Brooklyn
Dept. of Aerospace Eng. and Applied Mechanics
Route 110, Farmingdale, New York 11735

2a. REPORT SECURITY CLASSIFICATION
Unclassified

2b. GROUP

3 REPORT TITLE
FLOW FIELD DIAGNOSTICS IN RAREFIED SLIGHTLY IONIZED HYPERSONIC FLOW

4 DESCRIPTIVE NOTES (Type of report and inclusive dates)
Research Report

5 AUTHOR(S) (First name, middle initial, last name)
Joel M. Avidor
Samuel Lederman

6 REPORT DATE	7a. TOTAL NO OF PAGES	7b. NO OF REFS
June 1971	110	35

8a. CONTRACT OR GRANT NO
Nonr 839(38) and
DAHC04-69-C-0077

8b. PROJECT NO
ARPA Order Nos. 529 and 1442

c

d.

9a. ORIGINATOR'S REPORT NUMBER(S)
PIBAL Report No. 71-18

9b. OTHER REPORT NO(S) (Any other numbers that may be assigned this report)

10 DISTRIBUTION STATEMENT
Distribution of this document is unlimited.

11 SUPPLEMENTARY NOTES

12 SPONSORING MILITARY ACTIVITY
Office of Naval Research
and
U.S. Army Research Office-Durham

13 ABSTRACT

An experimental investigation was carried out in the PIB hypersonic shock tunnel in which two diagnostic techniques, the cylindrical electrostatic probe and the electron beam density probe, were applied to flow field surveys in rarefied slightly ionized hypersonic flow. Their relative merits have been evaluated. It was found that both can be applied for flow field investigations and particularly, density tracing and mapping, provided that diffusion effects are nonexistent or negligible. The correspondence between the ion and neutral densities in this case on a one-to-one basis is nonexistent.

In the course of this work, ion and neutral density profiles normal to a sharp flat plate and in the near wake of a 10^{o} half angle cone were obtained. Also using flush electrostatic probes, the ambipolar diffusion flux of the ionized particles to the plate was measured. A comparison with theoretical results obtained using the Rudman-Rubin formulation for the hypersonic flow about a sharp flat plate modified for slightly ionized flow was carried out. These show very good agreement for the ion density distribution in the viscous layer. In the case of the neutral density profiles good agreement again exists in the viscous layer; however, large deviations were observed between the measured and calculated

DD FORM 1 NOV 65 1473

Unclassified
Security Classification

14 KEY WORDS	LINK A		LINK B		LINK C	
	ROLE	WT	ROLE	WT	ROLE	WT
Electrostatic probe						
Flush probe						
Cylindrical probe						
Electron beam probe						
Field tracing						
Hypersonic flow						
Near wake						
Flat plate						
Axial density						
Diffusion effects						
Electro-optical system						
Collisional excitation						
Inelastic collisions						
Luminescence						

13. ABSTRACT (Contd.)

maximum density (ρ_{max}/ρ_{∞}) for $V_{\infty} > 0.2$.

The axial density distribution in the wake of the cone shows large deviation between ion and neutral density up to x/D_B=2.0. Good agreement between the ion and neutral density was obtained for the radial distribution as well as for the axial distribution for x/D_B larger than 2.0, where diffusion effects become minimal.

FLOW FIELD DIAGNOSTICS IN RAREFIED SLIGHTLY IONIZED HYPERSONIC FLOW

by

Joel M. Avidor and Samuel Lederman

This research was conducted in part under Contract Nonr 839(38) for PROJECT STRATEGIC TECHNOLOGY, supported by the Advanced Research Projects Agency under Order No. 529 through the Office of Naval Research; and in part under Contract DAHC04-69-C-0077, monitored by the U.S. Army Research Office-Durham and supported under ARPA Order No. 1442.

POLYTECHNIC INSTITUTE OF BROOKLYN

Department

of

Aerospace Engineering and Applied Mechanics

June 1971

PIBAL Report No. 71-18

FLOW FIELD DIAGNOSTICS IN RAREFIED SLIGHTLY IONIZED HYPERSONIC FLOW[+]

by

Joel M. Avidor[*] and Samuel Lederman[**]

Polytechnic Institute of Brooklyn
Preston R. Bassett Research Laboratory
Farmingdale, New York

ABSTRACT

An experimental investigation was carried out in the PIB hypersonic shock tunnel in which two diagnostic techniques, the cylindrical electrostatic probe and the electron beam density probe, were applied to flow field surveys in rarefied slightly ionized hypersonic flow. Their relative merits have been evaluated. It was found that both can be applied for flow field investigations and particularly, density tracing and mapping, provided that diffusion effects are nonexistent or negligible. The correspondence between the ion and neutral densities in this case on

---

[+] This research was conducted in part under Contract Nonr 839(38) for PROJECT STRATEGIC TECHNOLOGY, supported by the Advanced Research Projects Agency under Order No. 529 through the Office of Naval Research; and in part under Contract DAHC04-69-C-0077, monitored by the U.S. Army Research Office-Durham and supported under ARPA Order No. 1442.

[*] Research Associate.

[**] Associate Professor of Aerospace Engineering.

a one-to-one basis is nonexistent.

In the course of this work, ion and neutral density profiles normal to a sharp flat plate and in the near wake of a 10^{o} half angle cone were obtained. Also using flush electrostatic probes, the ambipolar diffusion flux of the ionized particles to the plate was measured. A comparison with theoretical results obtained using the Rudman-Rubin formulation for the hypersonic flow about a sharp flat plate modified for slightly ionized flow was carried out. These show very good agreement for the ion density distribution in the viscous layer. In the case of the neutral density profiles good agreement again exists in the viscous layer; however, large deviations were observed between the measured and calculated maximum density (ρ_{max}/ρ_{∞}) for $V_{\infty}>0.2$.

The axial density distribution in the wake of the cone shows large deviation between ion and neutral density up to $x/D_B=2.0$. Good agreement between the ion and neutral density was obtained for the radial distribution as well as for the axial distribution for x/D_B larger than 2.0, where diffusion effects become minimal.

TABLE OF CONTENTS

LIST OF ILLUSTRATIONS

LIST OF SYMBOLS

A_{jk}	spontaneous emission coefficient for the transition from state j to state k
C^*	$\frac{\mu T_\infty}{\mu_\infty T}$ = Chapman-Rubesin constant
C	$\frac{N_i M_i}{\rho}$ = charged species concentration
C_n	quenching coefficient for nitrogen
$\overline{C}$	$\sqrt{\frac{2kT}{\pi M}}$ = thermal velocity
D_B	cone base diameter
D_i	ion diffusion coefficient
d_s	sheath thickness
E	energy of incident beam electrons
E_j, E_k	molecular energy states
e	magnitude of electric charge
J	current density
k	Boltzmann's constant
ℓ	cylindrical probe length
L	$\frac{\gamma M_\infty^3}{Re_\infty}$ = reference length
M	mass
M_∞	Mach number
N	number density
N_j	density of molecules in state j
P	pressure
Re_∞	$\frac{\rho_\infty u_\infty}{\mu_\infty}$ = free stream unit Reynolds number
R_p	probe radius
T	temperature

x	coordinate in the streamwise direction
x_p	$\frac{e(V_p-V_\infty)}{kT_e}$ = normalized potential
y	coordinate normal to x axis
u	velocity in x direction
$\bar{V}_{\infty_x}$	$\frac{M_\infty\sqrt{C^*}}{\sqrt{Re_{\infty_x}}}$ - rarefaction parameter
V_∞	plasma potential
V_p	probe bias voltage
V	velocity in the y direction
S_{c_i}	$\frac{\mu}{\rho D_i}$ = ion Schmidt number
α	$\frac{T_i}{T_e}$ = ion to electron temperature ratio
α_p	dimensionless current
γ	ratio of specific heats
δ	$\frac{1}{\gamma^{\frac{1}{2}}M_\infty}$ = reference number
ϵ_o	dielectric constant
λ_{n-n}	neutral mean free path
λ_D	$\left[\frac{\epsilon_o kT_e}{N_e e^2}\right]^{\frac{1}{2}}$ = Debye shielding distance
μ	coefficient of viscosity
ν_{jk}	photon frequency corresponding to radiative transfer from molecular state E_j to E_k
ρ	density
σ	Prandtl number
$\sigma_j(E)$	cross section for excitation of the $B^2\Sigma$ state of N_2^+

Subscripts

ref	reference
o	stagnation conditions

∞	free stream conditions
w	conditions at the surface
e	electron
i	ion
p	probe

I. INTRODUCTION

The aerospace developments of the last decade stimulated a search for means and methods of determining relevant flow field parameters. These were important for the understanding of the phenomena encountered in space travel and reentry as pertaining not only to the fluid dynamic phase of the problem, but also to problems of communication and discrimination. Among the important parameters to be determined relevant to the problem at hand are the flow field configuration, neutral and ion densities, temperature, etc. To gain an understanding of phenomena observed, it was necessary, simultaneously with theoretical modeling, to obtain experimental data, not only from on-board measurements, but also from ground simulation facilities. To obtain these data, new diagnostic instrumentation and techniques had to be developed. In the development of these instruments one was aiming at developing an instrument which should combine simplicity, economy and ease of operation. Since in most cases under consideration the flow was slightly ionized, a natural choice for a diagnostic instrument was the electrostatic probe.

As is well-known, the electrostatic probe has been treated in innumerable publications over the last half a century (Refs. 1,2,3). Although in principle the electrostatic probe is the most simple instrument available, the interpretation of the measured collected currents is very complex. Depending on the regime of operation of the probe and its geometry, different theoretical as well as empirical

techniques for the interpretation of the collected currents in terms of the corresponding ionized particle densities emerged (Refs. 4,5,6). These techniques were applied in conjunction with other techniques and found to be very satisfactory when applied properly.

The application of the electrostatic probe as a field tracing diagnostic tool has been proposed. This diagnostic technique appeared to have the necessary merits for this purpose and particularly in highly rarefied flow regimes where other techniques and particularly optical techniques became inapplicable. In utilizing this field tracing technique in ground based simulation facilities (shock tunnels, ballistic ranges), two conditions have to be satisfied; namely, one must know the flow regime (λ_{n-n}) beforehand and the flow must have a certain degree of ionization. As indicated in some of the references (Ref. 7 and 8), flow field configurations were obtained using the electrostatic probe as the diagnostic tool. The technique, however, as pointed out in Ref. 7 can only be applied in nondiffusive regions if the ionized particle densities are to be interpreted in terms of the neutral density of the flow field. Since the flow fields in the above references consisted of diffusive and nondiffusive regions, and in view of the restriction placed on this technique, it became clear that these field configurations could be interpreted on a qualitative basis only. In order to obtain a better understanding of the phenomena occurring in these flow fields, it became necessary to determine flow field

configurations utilizing a different diagnostic technique. One of the most attractive tools for this purpose appeared to be the electron beam density probe. As discussed in the literature, this technique has been utilized extensively for this purpose (Refs. 9-11). It was, therefore, felt that this diagnostic tool in conjunction with the electrostatic probe tracing technique could be utilized in a complimentary fashion. It should be pointed out that the electron beam density probe in conjunction with the proper calibration technique is capable of providing absolute density measurements. It would, therefore, be possible, utilizing the electron beam, to define the region of applicability of the electrostatic probe tracing technique. In view of the above, an experimental program was initiated. It should be mentioned here that consistent with range of applicability of these techniques the experimental program was designed for the slightly ionized rarefied hypersonic flow of the PIB hypersonic shock tunnel. This program consisted of obtaining flow field configurations of models where diffusive as well as nondiffusive regions existed. In addition, flow fields of a highly complex nature were traced. The investigated flow fields consisted of the near wake of a pointed 10^{o} half angle cone at zero angle of attack, and the disturbed region about a sharp leading edge flat plate. Both ion and neutral density profiles were obtained. Comparison between the flow fields as obtained utilizing these two diagnostic techniques were made for both models. In addition, the obtained measurements

over the plate were compared with calculated values using the Rudman-Rubin solution for the hypersonic flow about a sharp leading edge flat plate. This solution was modified to include ionized particle behavior in the flow.

The authors would like to express their thanks to Dr. M.H. Bloom, Dean of Engineering and Director of Gas Dynamics Research, for his encouragement, stimulating discussions and support in the course of this work.

II. THEORY OF SLIGHTLY IONIZED HYPERSONIC FLOW ABOUT A SHARP LEADING EDGE FLAT PLATE

The slightly ionized hypersonic flow about a sharp leading edge flat plate is discussed here. Because the degree of ionization of the flow is very small and frozen, the equations governing the flow properties are unaffected by the presence of the ionized particles and the problem can be divided into two parts, the hypersonic flow about the sharp leading edge plate and the behavior of the ionized particles in this flow.

A. Hypersonic Flow About a Sharp Leading Edge Flat Plate

As discussed often in the literature (for example, Ref. 12), the flow field over a sharp leading edge body traveling at hypersonic speeds may be separated into four distinct regions (Fig. 1). The first region, the kinetic flow regime, is located in the immediate vicinity of the sharp leading edge. In this region, where property transfer is conducted at a molecular level, one must use the Boltzmann equation to adequately describe the flow field. This region gives way to a small transition region in which the flow field is becoming increasingly denser and hence more describable on a continuum basis. Continuing downstream, one enters the merged layer. The merged layer is characterized as a fully viscous region in which no discernible distinction can be made between the boundary layer and the shock layer. Also characteristic of this region are the velocity and temperature slips that occur

at a wall and a small region of rarefied flow in the upper portions of the viscous layer.

Progressing further downstream, the flow asymptotes into the interaction regime. The initial portion of this region is referred to as a strong interaction region in which a small inviscid layer is being formed. However, there exists a strong coupling between this inviscid layer and the adjacent viscous layer such that one cannot treat each layer independently. It is only until one proceeds further downstream into the weak interaction regime that the usual boundary layer techniques, as first described by Prandtl, are applicable.

It becomes desirable, therefore, for one to develop a set of continuum governing equations which are uniformly valid from the wall to the freestream and adequately describes the flow field from the merged layer downstream into the weak interaction region. Such an analysis was first carried out by Rudman and Rubin, (Ref. 13) in which they postulated one set of equations which were valid throughout the disturbance region.

Rudman and Rubin started with the governing Navier-Stokes equations non-dimensionalized with respect to local reference values. They postulated that if the shock layer on a slender body is considered small, such that the normal gradients are much larger than either of the two lateral planar gradients (this ratio being denoted as δ^{-1}) one may write a first order approximation to the full Navier-Stokes equations. An

exception occurred in the energy equations where δ^2 terms were retained in order to obtain a non-trivial solution (Ref. 13). Simultaneously, a second parameter $\Delta^2 = \frac{T_{ref}}{\gamma M_\infty^2}$ appeared in the expanded equations. Since T_{ref} represents the order of magnitude of the local temperature, one can easily show that $0.5 \geq \Delta^2 \geq .12$ depending upon the wall temperature (that is, cold or adiabatic wall) and, therefore, may also be considered small. Consequently, Δ^2 terms were also neglected which lead to the elimination of the streamwise pressure gradient. The consequences of this are discussed in Ref. 13. Within this approximation one can treat the x-momentum equation as a parabolic partial differential equation in which the inertia-viscous terms balance. This immediately makes possible the use of a finite difference, initial value technique to obtain the flow field description.

One may write this set of parabolic equations for a two-dimensional flow as follows:

Continuity: $(\rho u)_x + (\rho v)_y = 0$ (1)

x-momentum: $\rho u u_x + \rho v u_y = (\mu u_y)_y$ (2)

y-momentum: $\rho u v_x + \rho v v_y = -P_y + \frac{4}{3}(\mu v_y) + (\mu u_y)_x - \frac{2}{3}(\mu u_x)_y$ (3)

Energy: $\rho u T_x + \rho v T_y = -(\gamma-1) P (u_x + v_y) + \frac{\gamma}{\sigma}(\mu T_y) + \gamma(\gamma-1) M_\infty^2 \mu u_y^2 + \frac{4}{3}\mu(\gamma-1) v_y^2$ (4)

state: $P = \rho T$ (5)

where p, ρ, T, and u are non-dimensionalized with respect to their respective freestream values; μ with $\mu_\infty M_\infty$; v with $u_\infty \delta$; x with L and y with δ. Note that $\delta = \frac{\delta}{L} = \frac{1}{\gamma^{1/2} M_\infty}$ and $L = \frac{\gamma M_\infty^3 \mu_\infty}{\rho_\infty u_\infty}$.

For a detailed derivation and an in-depth discussion of these equations, one should refer to Ref. 13 .

The following initial and boundary conditions were used in the numerical solution for the problem in question. The initial profiles used were the uniform freestream conditions. It was shown by Rudman and Rubin that their solution of the flow is not sensitive to the initial condition for $\bar{V}_\infty \leq 0.4$. For larger values of $\bar{V}_\infty$ the solution of the flow depends on the initial conditions applied at the leading edge.

Slip boundary conditions are enforced on the surface of the plate; namely,

$\underline{Y = 0 \quad X \geq 0}$

$$U = \lambda U_y , \quad V = 0 , \quad T = T_w + \frac{2\gamma}{\gamma+1} \frac{\lambda}{\sigma} T_y \tag{6}$$

$\underline{Y \to \infty \quad X \geq 0}$

$$\left.\begin{matrix} T \\ u \\ \rho \end{matrix}\right\} \to 1 \tag{7}$$

$$V \to 0$$

A numerical solution of these equations was carried out for the flow conditions in question on a CDC 6600. The conditions are as follows: $M_\infty = 18.0$, $T_o = 7560^\circ R$, $T_w/T_o = 0.075$, $\sigma = 0.737$, $\gamma = 1.4$, $c^{*1/2} = 0.85$.

B. Charged Particle Density Profiles

In general, the ionized flow about a body can be divided into an inviscid and viscous region; the viscous layer is then divided into two, the sheath and ambipolar region (Ref. 14-16). In the latter, convection and diffusion operate simultaneously, and charge neutrality is maintained. The thickness of this diffusion layer is of the same order of magnitude as the viscous momentum layer, i.e., of order $\frac{1}{\sqrt{Re}}$. In the sheath, charge separation takes place; convection is unimportant. The main transport mechanisms in the sheath are diffusion and mobility of ions and electrons. The thickness of this region is about 10 times the Debye shielding distance, evaluated from plasma properties at the sheath edge.

Under the flow and plasma conditions about the plate in this work, the sheath is much thinner than the disturbed region, which includes the viscous and outer compression regions; thus charged particle diffusion across the layer was assumed to be essentially ambipolar in nature.

Following the formulation by Chung (Ref. 16) the charge specie conservation equation in the quasi-neutral region of the disturbed layer about the plate can be written as

$$\rho u C_x + \rho v C_y = \left\{ \frac{\rho D_i}{1+(M_e/M_i)^{\frac{1}{2}}} \left[C + C \frac{T_e}{T_i} \right]_y \right\}_y \qquad (8)$$

In deriving this equation, charge neutrality $N_i = N_e$ has been invoked and diffusion in the x-direction neglected. Nondimensionalizing this equation in the same manner as the governing equation for the hypersonic flow about the plate

where ρ, T_i, T_e, u and C are non-dimensionalized with respect to their respective freestream value; μ with $\mu_\infty M_\infty$; v with $u_\infty \delta$; x with L and y with f, and $d = \frac{\rho D_i}{\rho_\infty D_{i_\infty} M_\infty}$, we obtain

$$\rho u C_x + \rho v C_y = \frac{1}{S_{ci}} \left\{ d \left[C \left(1 + \frac{T_e}{T_i} \right) \right]_y \right\}_y \qquad (9)$$

Here, $S_{c_i} = \frac{\mu}{\rho D_i}$ is the ion Schmidt number. The assumed boundary conditions in this case were

$y = 0 \quad x \geq 0$	$y \to \infty \quad x \geq 0$
$C = C_w + \lambda C_y$	$C \to 1$

(10)

The equation governing the charge particle distribution was solved simultaneously with the hypersonic flow about the plate. In the calculation the electron temperature T_e was assumed to be frozen and T_i the ion temperature was assumed equal to the static temperature of the gas at any point in the flow field.

The choice of C_w had some effect on the charge particle density profile, as shown in Fig. 2. C_w=0 was used to agree with the cylindrical probe measurements of the ion density near the plate surface. The effect of the ion Schmidt number (Sc_i) on the ion density distribution in the disturbed region about the plate under our experimental conditions is exhibited in Fig. 3. The ion density profile appeared to be insensitive to the value of Sc_i.

III. LANGMUIR PROBES IN FLOWING PLASMAS

The cylindrical electrostatic probe has been found to be an attractive diagnostic tool for low density plasma flows due to its excellent spatial resolution and relative simplicity of construction. Recent reviews by de Leeuw (Ref. 17) and Chen (Ref. 18) gave detailed accounts of Langmuir probe theory and its application.

One of the most realistic collisionless probe theories published to date is that of Laframboise (Ref. 4) who has used the mathematical framework of Bernstein and Rabinowitz (Ref. 3) to calculate entire probe characteristics for both cylindrical and spherical probes at rest in a two-temperature plasma. Laframboise assumes that the plasma consists of two species of charged particles, one positive and one negative, each having a Maxwellian velocity distribution with its own characteristic temperature and that whenever a particle of either species strikes the probe surface, it is annihilated and removed from the problem. Laframboise calculations are based on the Vlasov equations for two species, coupled by Poisson's equation for the electric field, and the results are, therefore, not expected to be valid unless binary collisions can be ignored and the electric field consistent with Poisson's equation is the dominant influence on the motion of the charged particles.

For a plasma where the positive particles are singly charged ions and the negative ones are electrons, Laframboise's results may be summarized as follows:

For $x_p < 0$

$$J_i = eN\sqrt{\frac{KT_e}{2\pi M_i}}\,\alpha_{p_i}\left(x_p,\ R_p/\lambda_D,\ \frac{T_i}{T_e}\right) \tag{11}$$

$$J_e = eN\sqrt{\frac{KT_e}{2\pi M_e}}\,e^{x_p} \tag{12}$$

For $x_p > 0$

$$J_i = eN\sqrt{\frac{KT_i}{2\pi M_e}}\,e^{-T_e/T_i\,x_p} \tag{13}$$

$$J_e = eN\sqrt{\frac{KT_i}{2\pi M_e}}\,\alpha_{p_e}\left(x_p,\ R_p/\lambda_D,\ \frac{T_i}{T_e}\right) \tag{14}$$

When the probe is at plasma potential, $x_p=0$, either species arrives at the probe surface at a rate given by its random kinetic flux, $\frac{N\bar{c}}{4}$, and when a species is repelled, its flux to the surface is reduced from this value by the Boltzmann factor. When it is attracted, on the other hand, the situation becomes more complex. When the electrons are attracted, their flux increases over the random kinetic value by the factor α_{p_e}, calculated by Laframboise. When the probe is made negative so as to attract ions, the ion flux soon reaches a magnitude of the order $eN\sqrt{\frac{kT_e}{2\pi M_i}}$, which is $\sqrt{\frac{T_e}{T_i}}$ times the random ion flux and may be much larger than the latter if $T_e \gg T_i$. Again, α_{p_i} represents a dimensionless correction factor which emerges from theory.

Both α_{p_i} and α_{p_e} depend not only on the dimensionless potential difference between the probe and the plasma, x_p, but also on the properties of the plasma through R_p/λ_D and T_i/T_e, as well as on probe geometry. Both are generally of order unity at moderate probe potentials and R_p/λ_D values. The magnitude of α_{p_i} and α_{p_e} for cylindrical and spherical

probes are given in Ref. 4 for

$$|X_p| < 25$$
$$0 < T_i/T_e < 1 \qquad (15)$$
$$0 < R_p/\lambda_D < 10^2$$

Figure 4, which is reproduced here from Laframboise work, shows the dependence of σ_{p_i} on R_p/λ_D for $T_i/T_e=0$. Included in Fig. 4 is the orbital motion limited current boundary. Current collection is said to be orbital motion limited at the energy E, when no absorption radius exists for the energy E and the current is limited by the large angular momentum of the particles. The orbital motion limited current represents the maximum current of particles of a given energy that can be collected in the collisionless case by a given potential. From this figure, it is seen that as R_p/λ_D decreases, the current σ_{p_i} reaches the orbital motion limit and levels off to a constant value.

Since the publication of Laframboise results, many experimental investigations were carried out to verify the applicability of the static probe theory to probes in collisionless flowing plasmas (Ref.19). In his work, Sonin examined the behavior of free molecule cylindrical Langmuir probes in supersonic flows. Those experiments indicated that under flow conditions, the theory of Laframboise represents the ion current characteristics adequately at large R_p/λ_D. Departure from theoretical ion-currents were observed in the small probe limit, when the ratio of cylindrical probe radius R_p to plasma Debye length λ_D was less than about 3. Similar

departure was observed by Lederman et al.in their experiments with cylindrical probes in rarefied ionized hypersonic flow (Ref. 20). The leveling off of the α_{p_i} curves for small values R_p/λ_D in Laframboise results (see Fig. 4) was not compatible with those experimental results, α_{p_i}, exceeded markedly the theoretical collisionless values at low R_p/λ_D.

In many experiments by Lederman et al. conducted in the hypersonic shock tunnel, the parameter R_p/λ_D was much smaller than unity. This resulted from the combined effect of the plasma conditions (N_{i_∞}, T_e) and small probe radii used to minimize gasdynamical effects on collisions. Also in the course of this work, length limitations required for the achievement of spatial resolution in ion density distribution measurements resulted in length-to-diameter ratio $\ell/2R_p < 100$. It appeared that experimental information on the effect on ion current collection of the parameter $\ell/2R_p<100$ and $R_p/\lambda_D< 3$ in rarefied hypervelocity ionized flow is needed.

This lead to an experimental investigation by Lederman et al. (Ref. 5) which determined the behavior of biased electrostatic probes in the regime of high rarefaction, and low degree of ionization hypervelocity flow. Using the slightly ionized flow in a hypersonic shock tunnel, data for various diameter and length-to-diameter ratio ($\ell/2R_p$) probes was obtained under known plasma conditions ($N_{i_\infty} \sim 3 \times 10^8 el/cm^3$, $T_{e_\infty} \approx 3000^\circ K$, $T_i/T_e \to 0$). The free stream ion number density was measured with microwave resonant cavities and the electron temperature was obtained using cylindrical probes operating in the electron

retarding field region. These experimental results showed that the current collection ability of a probe operating in the above-mentioned regime and the resulting current density is greatly enhanced with the decrease of the diameter of the cylindrical collecting probe and the subsequent decrease of the R_p/λ_D ratio. This effect thus presents a significant departure from Laframboise theory at the point where, according to that theory, the current should reach its orbital motion limited value and should no longer increase. The experimental values of the normalized nondimensional current α_{p_i} for R_p/λ_D as obtained by Lederman et al. are presented in Fig. 5 . The observed experimental increase in the ion current at small value of R_p/λ_D can be attributed to collisions of the orbiting ions as pointed out by Shih and Levi (Ref. 21). Since the Coulomb cross section for ion-ion collisions increases rapidly as the ion temperature decreases, in the limit of small ion temperature, which was the case in Lederman's work, there always exists ion-ion collisions in sufficient numbers to destroy orbital motion. Shih showed in this work that there is an increase in current collection by the probes due to small collisional effects in the region where orbit motion limit should have been reached in a collisionless plasma as predicted by Laframboise.

Lederman et al also formed a relation between current density and the length-to-diameter ratio as shown in Fig. 6 , thus permitting the use of very small probes to achieve better spatial resolution. The increase in current density collected

by probes with $\ell/2R_p<100$ can be attributed to end effects when the Debye length is large compared with the probe radius and the flow speed is high. Under those conditions, the ion current collected by the probe consists of ions entering the side sheath and of ions entering through the front of the sheath. For short enough probes, the latter dominates, thus causing the large increase in observed current collected by short probes.

IV. ELECTRON BEAM DENSITY PROBE

The optical electron beam density probe was suggested and developed by Schumacher and Gadamer (Ref.22) and was first applied to an actual flow investigation by Gadamer (Ref. 23), who showed that it can be used to accurately determine the local densities in a rarefied gas flow. The technique employs a narrow, well-collimated, high energy, electron beam which is projected at right angles to the flow through the region of interest. Because of the relatively small collision cross-section of the gas atoms for 20 keV electrons, the interaction of the gas with the beam is weak and results mainly in the scattering at small angles of some of the primary electrons. At the electron energy used, many of the electron-atom interactions are of the elastic type. There occur, however, sufficient inelastic collisions, resulting in electronic excitation and subsequently de-excitation, to give rise to luminescence, which is largely confined to the beam region itself. By focusing the luminescence onto an optical slit, which is at right angles to the beam, the light issuing from a small elemental gas volume is selected and can subsequently be measured through the utilization of a photomultiplier. Under certain conditions, the photo-current measured is a direct indication of the molecular number density in the elemental volume under consideration.

It should be pointed out that, at gas densities corresponding to a gas pressure of 200μHg at room temperature, the average

time between atomic collisions of order 10^{-11} sec. for most gases becomes comparable to the lifetimes of excited states of the atoms of order 10^{-7} sec. for allowed transitions. Under these conditions, a measurable fraction of the electron beam excited atoms collide with other atoms before they can emit the excitation energy in the form of radiation. This makes the observed intensity of the electron beam luminescence less than one would otherwise predict. The effect is generally referred to as collisional quenching. Since the collision frequency and, therefore, the collisional quenching effects are temperature dependent as well as density dependent, it is almost imperative to work with gas densities, at which collisional quenching can be neglected. For the visible spectrum of nitrogen, Gadamer (Ref.23) found no quenching effects up to 100 μHg.

In addition, there exists the possibility of the luminescence being carried downstream in a high velocity gas flow. As pointed out before, for the nitrogen first negative system the lifetime is approximately 10^{-7} sec. Since the velocity in the HST is approximately 3×10^{6} cm/sec., the drift in this case is about 0.03 cm, and it is, therefore, possible to obtain good spatial resolution by observing the center portion of the beam having a 2-mm diameter.

A. Origin of Luminescence in Nitrogen

The electron beam technique involves the ionization and excitation of nitrogen molecules with a beam of highly energetic electrons (10-30 keV). The resulting spontaneous

emission in the spectral region 3500-5000 Å is predominantly that of the first negative system of nitrogen N_2^+ (1-). Analysis by Muntz (Ref. 24) and Petrie (Ref. 25) proposed the excitation process to be directly from the neutral ground state molecules ($N_2 X^1\Sigma$) to the excited states of the molecular ion ($N_2^+ B^2\Sigma$) by inelastic collisions with high energy electrons (See Fig. 7). This analysis discounted other paths of excitation to $N_2^+ B^2\Sigma$ such as cascade population, double excitation, and secondary excitation of ground state ions. The observed emission corresponds to the electronic transition $N_2^+ B^2\Sigma \rightarrow N_2^+ X^2\Sigma$ (the ground state of the molecular ion) with the average lifetime of the excited ions on the order of 10^{-7} seconds. Muntz (Ref. 24) also showed that for low density gas flows at room temperature the excited gas particles should experience little interference due to gas kinetic collisions during the process of excitation and emission.

The luminescence caused by the de-excitation of the N_2^+ molecules can be examined in the following manner. The rate of emission of photons of frequency $\nu_{j,k}$ corresponding to radiative transition from molecular state E_j to E_k per cm^3 of the luminescing gas is

$$\phi(\nu_{jk}) = A_{jk} N_j \qquad (16)$$

where N_j is the density of molecules per cm^3 in the parent state E_j and A_{jk} is the spontaneous-emission coefficient for the transition. Under the weak excitation condition employed here, N_j is produced by binary encounters between beam

electrons and neutral ground state N_2 molecules; the rate of production of N_j is then

$$\left(\frac{\partial N_j}{\partial t}\right)_{EXC} = K_j(E)\, P i(\vec{r}) \qquad (17)$$

where E is the energy of the incident electrons, P the pressure of N_2, $i(\vec{r})$ the spatially dependent flux of beam electrons, and $k_j(E)$ is related to the cross-section for excitation of the $B^2\Sigma$ state of N_2^+ by

$$K_j(E) = 2.22 \times 10^{29} \left(\frac{273}{T°K}\right) \sigma_j(E) \qquad (18)$$

The $B^2\Sigma$ state is de-excited in two ways. First, the molecule can radiate to all lower states yielding a spectrum which includes the 3914 Å line (the most intense radiation) and the rate of radiation is given by

$$\left(\frac{\partial N_j}{\partial t}\right)_{RAD} = -\sum_{K=0}^{j-1} A_{jK} N_j = -A_j N_j \qquad (19)$$

where A_j is the reciprocal of the radiation lifetime of state N_j and the radiation lifetime of state N_j is the average time spent by the molecules in state N_j.

The excited molecule can also lose its energy in collisions with other molecules; this process, known as quenching, is described by

$$\left(\frac{\partial N_j}{\partial t}\right)_{QUEN.} = C_n P N_j \qquad (20)$$

Here C_n is the quenching coefficient for nitrogen. In the steady state, the production of N_j is equal to its total removal rate

$$N_j A_j + C_n P N_j = K_j(E) P i(\vec{r}) \qquad (21)$$

hence,

$$\phi(\vec{r}) = A_{jK} N_j = \frac{A_{jK} K_j(E) P i(\vec{r})}{A_j + C_n P} \qquad (22)$$

Since for a constant temperature, P is proportional to the number of N_2 particles present, Eq. (22) shows that there exists a linear relation between the radiant intensity and the density of nitrogen as long as quenching effects are small ($C_n << A_j$). This linear relationship is the basic principle of the electron beam density probe.

V. EXPERIMENTAL APPARATUS

A. Experimental Facility

The experiments reported throughout this work were performed in the hypersonic shock tunnel of the Polytechnic Institute of Brooklyn, located at the Graduate Center in Farmingdale. The schematic layout of the H.S.T., together with its principal components, is shown in Fig. 8 . The HST employs a variable-area shock tube where the driver is 6 inches I.D. and 24 feet long, and the driven is 3 inches I.D. and 28 feet long. The driver gas was helium at room temperature and the driven gas, air or nitrogen. The shock processed gas at the end of the shock tube is expanded through a conical nozzle into the test section. A uniquely designed valve located at the end wall of the shock tube prevents the driver gas from flowing into the test section, thus avoiding damage and contamination of the instrumentation. A detailed description of the facility and its performance capability is given in Ref. 26 .

B. Flow Conditions

The operating initial conditions of the shock tunnel were fixed throughout this investigation. With an initial driven pressure of 38 mmHg air or nitrogren and driver pressure of 1800 psia helium, a shock Mach number of about 7 was obtained. This resulted in a pressure of about 350 psia and temperature of 4000^{o}K behind the reflected shock. The shock processed gas was then expanded through a 10^{o} half-angle and 52-inch

exit diameter conical nozzle into the test section. The flow conditions in the test section were obtained in the following way. The stagnation conditions behind the reflected shock were obtained from shock tube tables for equilibrium air or nitrogen for the measured shock velocity, and the flow properties in the nozzle and the test section were calculated using the CAL program for nonequilibrium nozzle flows (Ref. 27). Calculation of the flow properties using this program showed that the flow becomes frozen at about 25 in.downstream from the throat for stagnation conditions $T_o \approx 4000^oK$ and $P_o \approx 350$ psi. Table I lists the flow conditions at positions along the nozzle and Table II lists those in the test section. At the various stations along the nozzle a rake of cylindrical electrostatic probes aligned parallel to the flow direction was used to determine the uniformity of the flow. Stagnation heat transfer and ion density surveys made under test conditions in the test section showed the flow is uniform through a core 26 inches in diameter. This region is only a portion of the nozzle exit diameter because of boundary layer growth in the nozzle due to the low Reynolds number flow. The relatively large uniform region allows one to introduce fairly large models for surface measurements and flow field investigation.

C. Electron Beam Density Probe

The electron beam density probe technique is based on the stimulation of emission from a gas by collisional excitation using a beam of energetic electrons (larger than 10 keV). Inelastic collisions between the gas molecules and

the beam electrons result in electronic excitation and subsequently de-excitation giving rise to luminescence which is mostly confined to the beam region. The local emitted intensity is directly proportional to the local gas number density of molecules. With the luminescent light yield detected at different points along the beam with a photomultiplier, spatial density measurements can be carried out. An electron density probe basically consists of two systems; one, the electron gun which is used to generate a narrow collimated, high energy electron beam, and the other is the electro-optical system for point-wise luminescence detection. The electron density probe used in this investigation is described in the following section.

D. Electron Gun and Electro-Optical Systems

The electron gun assembly, complete with diffusion pump and gauges, is mounted on the hypersonic shock tunnel as shown in Fig. 9 . An external view of the gun, battery, power supplies, and instrumentation is shown in Figs. 10 and 11.

The electron beam is produced by a specially designed electron gun , which consists of a tungsten filament and one accelerating grid (the filament is a plug-in type allowing easy replacement). The advantage of a tungsten filament electron gun over a commercial electron gun with a Barium Cathode is twofold. First, the filament can be exposed to atmospheric pressure without losing its emission capability, and second, no differential pumping is needed to maintain high vacuum in the gun chamber since it can operate at higher

pressure, about 10^{-4} Torr, compared to at least 10^{-} required for a commercial gun. The gun is housed in a chamber constantly evacuated by a 230 liter/sec. oil vapor diffusion pump (Kinney KDB-200) and maintained at approximately 10^{-5} Torr pressure. The pressure in the gun chamber is monitored by an ionization gauge (Veeco RG-31A). In order to reduce oil deposits in the gun chamber caused by backstreaming, the diffusion pump was equipped with a nitrogen cold trap (Kinney KDB-200). A special diffusion pump oil with low backstreaming properties was used (Convalex-10 manufactured by Bendix).

From the gun chamber, the electron beam passes into a 1-inch diameter and an 18-inch long drift tube, and from there into the test section through an aperture of low gas conductance. This restricts the inflow of gas from the test section and confines the electron beam geometrically. The aperture consists of a cylindrical hold 2 mm in diameter and 1 inch long drilled into a brass insert, which can easily be replaced.

Careful alignment and focusing of the beam is necessary to allow it to pass through the aperture into the test section. This is achieved by an electromagnetic focusing and deflection system, Fig. 12. This system, which consists of two deflection coils and one focusing coil (Celco AF 304-200) is mounted on the drift tube. Regulated power supplies (KEPCO) were used to supply the control current to the coils. After passing through the test section the electron beam impinges on a brass block which serves as the beam collector. The beam

collector is electrically isolated from ground by a teflon insulator, so that the collected beam current can be measured. The current to the filament is supplied by a 6 volt heavy duty battery and can be adjusted by a rheostat to control the emission. The battery which is at beam potential is placed in a big plexiglass box because of the high voltage with respect to ground.

The cathode potential is supplied by a Universal Voltronic high voltage, unregulated, D.C. power supply which can be varied between zero and 32 KV. The anode is kept at ground potential or a few volts positive bias with respect to ground. The grid voltage is obtained from a voltage divider circuit, which allows ample adjustment of the beam current (see Fig. 12).

The function of the electro-optical system is to measure the intensity of the radiation issuing from a small gas volume in the electron beam. In accordance with this requirement, the instrument must have a high sensitivity to detect a very weak light source, and it must spectrally discriminate between the light emitted by the nitrogen due to excitation by the beam electrons and other sources of luminescence present during a test in the hypersonic shock tunnel. Furthermore, only light which originates in a well-defined region of the electron beam should be allowed to be picked up by the photomultiplier.

Good sensitivity is obtained by using an optical system of low f-number in conjunction with a high gain photomultiplier.

Two achromatic lenses, f 3.7 and f 5.8, are used to form a real image of the electron beam. In the image plane an iris is used to spatially define the section at the electron beam, from which light is received. A narrow band-pass filter is used to select the most intense nitrogen line (3914Å) and the intensity of the transmitted light is then measured with an uncooled photomultiplier EMI 9502S having an S-11 spectral response (a peak at 4000Å). The spectral response curve of the photomultiplier and the transmission curve of the narrow band-pass filter are given in Fig. 13.

It should be noted that the lens-to-beam and lens-to-iris distances are approximately 192 and 275 mm, respectively, giving magnification close to 1.5. Thus the 3 mm diameter iris opening, when imaged on the 2 mm wide electron beam, is only 2 mm in diameter. This defines the elemental volume in the beam luminescence where the measurements were made.

The photomultiplier tube and the optics are housed in a container made of aluminum tubing (Fig. 14). This combined electro-optical system is mounted on a frame inside the test section (see Fig. 9), which by itself is mounted rigidly to the electron gun housing. This arrangement has the advantage that optics remain aligned with the electron beam. The photomultiplier tube and the optics are moved from point-to-point along the beam by a remotely controlled driving system and the position of the system is monitored by a potentiometer-ammeter readout. One of the problems encountered by the fact that the photomultiplier is inside the test section where high

vacuum is maintained, was electrical breakdown between the high voltage connections leading to the photomultiplier at about 50 μHg. Suitable precautions have been taken to prevent this from happening.

The cathode voltage to the EMI 9502S photomultiplier was supplied by a highly regulated D.C. power supply (N.J.E. S-326). See Fig. 14 for the tube circuitry. The anode current was displayed on a Tektronix 565 oscilloscope and recorded by a Polaroid camera. This kind of recording system is used because of the very short test duration.

In order to obtain simultaneously density measurements at two points during one test, a second electro-optical system almost identical to the first one, was constructed. Both systems were arranged in such a way that their focal points intersect with the beam and the distance between the focal points was kept at 1" during all tests of the near wake density survey, and 0.2" for all the tests in the flow field about the plate. Both systems were connected rigidly to a plate which could be moved along the beam with the driving system designed for this purpose.

E. Langmuir Probes and Associated Circuitry

Cylindrical Langmuir probes were made by allowing a length of tungsten wire to protrude from a piece of Teflon tubing used as insulation, having an inside diameter of approximately the diameter of the wire. Tungsten wires 0.001-0.080 inches in diameter were used for all probes. With the

desired length of wire protruding from the tube, the interface between the Teflon tube and the tungsten wire was filled with an epoxy, thus making a firm bond. This process eliminated any possibility of faulty current leakage through the Teflon-wire interface. A stainless steel tube was used as a protective outer shield for the probe. To facilitate Langmuir probe boundary layer surveys over the entire flat plate surface, a group of 25 identical probes 0.020 inches in diameter and 0.5 inches long was arranged in a rake for simultaneous acquisition of data. The probes were of the "plug-in" type allowing easy replacement or interchanging.

A second rake of probes was constructed for the investigation of the effect of density increase on ion current collected by cylindrical electrostatic probes. The rake consisted of four rows of eight probes each. One row contained eight probes of the same diameter and length to check the uniformity of the flow and the next two rows contained two sets of probes of the same $\ell/2R_p$ ratio but of variable diameter ranging from 0.001 inch to 0.080 inch. The last row consisted of probes with same diameter but different length to investigate fineness ratio effects.

Langmuir probes were cleaned ultrasonically in acetone solution before being installed in the rake. Probe current collection appeared to be very reproducible in different tests for the same test conditions, thus discounting any possibility of contamination after installation and between tests.

Figure 15 shows the construction and circuit for the Langmuir probe. Probe voltage was supplied by a regulated D.C. power supply. During all the tests reported here, probes were biased at -9 volts for ion collection. The probe current during a test is displayed on a 565 Tektronic oscilloscope and recorded with a Polaroid camera.

F. Flat Plates and Imbedded Flush Electrostatic Probes

Two completely different plates were used in this work. The first was made of aluminum and a stainless steel sharp leading edge (0.005") as shown in Fig. 16. This plate was used for the investigation of the slightly ionized flow in the disturbed region over the plate. Holes were bored into the surface to accommodate the flush probes. Four rows of those probes were imbedded flush with the surface. The probes were circular in shape, all made out of brass, insulated from the plate with plexiglass sleeves, and varied in size from 1/16" to 3/4" diameter. After installing the probes in the plate, the combination plate probes were then ground for a smooth-surface finish. Again, the flush probes were cleaned before installing the plate in the test section, and reproduction between tests was very good. The plate was mounted on a movable string to allow one to position the plate at different axial locations with respect to the stationary cylindrical probe rake.

The second plate was used for flow field investigation with the electron beam density probe, Figs. 17 and 18. Actually, two plates were used for this purpose; the first, made of 1/16 inch

aluminum sheet with a 15° bevel on the undersides, was 12 inches by 18 inches. This plate was used to obtain density profiles at the same axial positions where ion density profiles were already measured with the electrostatic probe. The second plate was made of 0.015 inch thick spring steel sheet 6 inches by 6 inches. This plate was used for density measurements in the vicinity of the leading edge (x=2.0 inches). This plate was introduced for measurements near the leading edge in order to avoid reported observed influence of a finite thickness plate on the flow field development near the leading edge of the plate (Ref. 28). These plates were connected to the drift tube of the electron gun system, and a 2 mm diameter orifice machined into the plate allowed the beam to emerge through the plate and impinge on the beam collector. Since the electron beam density probe was fixed in position in the tunnel, measurements were made starting with the rear stations and moving forward. As each station was completed, a new orifice was machined at the next location forward. This procedure prevented any disturbance to the measuring region from orifices ahead of the testing location.

G. The Cone

As mentioned previously, density distribution in the near wake of a 10° half angle 4" base diameter cone was also investigated. The cone was made of aluminum with a stainless steel tip and suspended from a frame with 0.020" diameter piano wires, as shown in Figs. 19,20. It was found in previous work of Lederman (Ref. 29) that this size wire does not introduce any

disturbance in the wake region. The frame on which the cone was suspended was mounted on a movable string to allow one to position the cone at different axial positions with respect to the electron beam density probe.

VI. EXPERIMENTAL RESULTS

A. Test Duration

One of the problems generally encountered working in hypersonic shock tunnels is the test duration and where is the test in the time history of the recorded data. In previous work by Lederman et al. (Ref. 20) and in the present work, the test duration of the ionized flow in the hypersonic shock tunnel of PIB was established using cylindrical electrostatic probes and microwave cavities.

Using these methods, the ionized flow under the present test conditions was found to be about 0.4 msec. In the course of the present investigation using the electron beam density probe and stagnation pressure measurements, a uniform flow region of a longer duration which starts after the ionized flow in the time history of the recorded data was utilized. Those two flow regimes are apparent from the following figures (Fig. 21 through Fig. 23).

In Fig.21a, two traces of ion current collected by cylindrical electrostatic probes are shown. It is evident from these traces that after the initial flow containing ionized particles a region of non-ionized or at most very slightly ionized flow exists.

In Fig. 21b, the corresponding background radiation of the freestream flow without beam excitation is shown. It is interesting to note that radiation occurs at the exact time of the ionized flow and vanishes simultaneously with the vanishing of the ionization of the flow.

In the next figure, Fig. 22, two traces are indicated. As seen, the traces of both oscillographic recordings correspond to the photoluminescence in the freestream. (a) corresponds to the freestream "off beam" luminescence whereas (b) corresponds to the freestream "on beam" luminescence. It is seen that the initial luminous flux corresponding to the ionized portion of the flow is followed in (a) by a non-radiating flow region as in Fig. 21a obtained under "off beam" conditions and in Fig. 21b by a photoluminescence current due to beam excitation of the non-radiating flow. This behavior can be correlated with the stagnation pressure measurements in the freestream as shown in Fig. 23, where the upper trace presents the "on beam" photocurrent (density) measurement and the lower traces correspond to stagnation pressure.

Because of the timewise difference in the location of the test as obtained with the cylindrical electrostatic probes and the electron beam density probe, and the fact that no ionized particles are present in the flow where density measurements were made, it was suggested that the density measurements were actually made in the region where the driver gas, Helium in this case, arrives at the test section. In order to verify that the density measurements were made in the region where the flow in the test section consists of the driven gas, air or nitrogen in our case, and not Helium, the following measurements were made.

The electron beam density probe was operated during

tests conducted in the hypersonic shock tunnel and the photoluminescence current recorded during each test. In these tests two different narrow band-pass filters were used in the electro-optical system in order to observe the 0-0 and 0-1 vibrational bands of the first negative N_2^+ system. The one for the 0-0 band was 3914 Å with 100 Å half-band width and the other filter for the 0-1 band was 4227 Å with 39 Å half-band width. Since beam excited Helium radiates at 3965 Å, a wave length which is transmitted by the 3914/100 Å filter, hence just using this filter in these tests could not determine the arrival of the Helium at the test section. In order to overcome this problem, the second interference filter 4227/39 Å was introduced into the electro-optical system. Since in this range of wave length no beam excited radiation of the Helium exists, hence the photoluminescence current is only due to radiation of the beam excited nitrogen.

By comparing the photocurrent obtained during a freestream run with the 3914/100 Å interference filter to the photocurrent obtained with the 4227/39 Å interference filter, and taking into account the relative emission of the 0-0 and 0-1 vibrational bands, and the transmission of each filter, it was established that the flow consists of nitrogen.

B. Langmuir Probe Response in Transition Regime

An experimental investigation on the effect of neutral density increase (mainly decrease in mean free path λ_{n-n}) on the current collection of cylindrical probes in slightly ionized hypersonic flow was carried out during the course of

this work. This information was needed in order to reduce the data obtained by cylindrical electrostatic probes in the flow field about the plate. Since there exists a compression zone at the outer edge of the disturbed region about the sharp leading edge flat plate in question where the local neutral density ρ might be a few times higher than the free stream density ρ_∞, it was felt that the probes used R_p=0.010" will operate in a transition regime in this region and not as free molecular cylindrical probes. In order to investigate the effect of density increase, it was decided to utilize the flow in the nozzle of the HST as the test medium. Here the density could be continuously varied maintaining the velocity almost constant. The slight changes in ion temperature T_i as one moves from the test section into the nozzle up to about 40 inches from the throat (length of nozzle 175 inches) can be neglected particularly since $\frac{T_i}{T_e} \approx 0$ at any point along the nozzle and the random ion velocity as defined varies only as the square root of the electron temperature T_e. Following the same procedure as in Lederman's work (Ref. 5), cylindrical electrostatic probes of the same $\ell/2R_p$ ratio but of variable diameter ranging from 0.001 inches to 0.080 inches were arranged in a rake mounted on a moveable sting.

The different diameters of the probes provided a variation of R_p/λ_d in each position where measurements were performed. All probes were biased at -9 volts ($X_p \approx -35$) for ion collection. To correlate the collected ion current

density to the corresponding ion number density two microwave resonant cavities were used; they were mounted on the rake and gave an independent measurement of the ion density in each test at the different positions along the nozzle.

The sting with the probes and cavities was moved stepwise from the test section into the nozzle. In this configuration the probes were always aligned with the flow direction. A number of tests were run under the same initial test conditions, at different stations in the nozzle. The ion densities as obtained by the cavities and the ion current of each probe were recorded.

The charged particle number density obtained by the microwave resonant cavity measurements were compared to the nonequilibrium calculations of the nozzle flow. Figure 24 shows the experimental as well as the theoretical results. The scatter of the experimental points is within the accuracy one can expect from the resonant cavity measurements. The electron number densities obtained by the microwave cavity technique at each axial station in the nozzle was used to compute the R_p/λ_D parameter for each probe and the corresponding α_p. The results of these tests are shown in Fig. 25 where the parameter α_p as a function of R_p/λ_D is plotted for two different positions in the nozzle. The lower correspond to a higher density as well as a higher charge particle density at a station further upstream in the nozzle (see Table I).

One can see from this figure that within the scatter

of the data there seems to be a decrease in α_p for the same R_p/λ_D when the density increases. This result agrees in principle with the theoretical prediction of Talbot and Chou (Ref. 30). They have shown that for cylindrical Langmuir probes in the transition regime the effect of collisions on the probes is to reduce the ion current to the probe and thus reduce the inferred number density.

C. Ion Density Distribution About the Plate

Cylindrical electrostatic probes arranged in a rake were used in the course of this work to obtain ion density profiles in the field of a sharp leading edge flat plate in slightly ionized rarefied hypersonic flow. Tests were performed on the plate at Mach 18 and zero angle of attack; all tests reported in this section were conducted in air (commercial dry bottled air), and the flow conditions in the test section are listed in Table II. The arrangement of the probe rake with respect to the plate is shown in Fig. 16. As can be seen from this figure, the rake was perpendicular to the plate surface and fixed in position with respect to the tunnel. Since the rake was stationary, the plate was moved in order to obtain ion density profiles at various axial positions along the centerline of the plate. The probes on the rake were aligned parallel to the freestream flow direction and biased at -9 volts with respect to ground($x_p \approx -35$) for ion collection.

Figure 26 represents a sample of the oscilloscope traces as obtained in these tests. As can be seen, these traces

show, after an initial peak, a region of relatively uniform amplitude which could be considered as the response in the established uniform flow. This region will be referred to as the flat portion. In reducing the data, only the flat portion of the probe response was used, the reason being that recently it was shown by Bornstein (Ref. 31) that the peak portion of the probe response depends on the load resistor of the probe (R_L) and the plasma properties in question.

Using the procedure devised by Lederman et al. (Ref. 5) and discussed previously, ion number density was determined from the ion current collected by the probes. Since the ion number density N_i depends on the nondimensional current density α_{p_i} which is a function of N_i itself, an iteration scheme had to be used to reduce the data, and a computer program has been devised which carried out the data reduction.

Figure 27 through Fig. 30 show the ion density profiles obtained at x=3.0, 6.0, 9.0, 12.0, 15.0 inches along the plate. The data presented is in a normalized form, where the ion density at each point in a given profile was calculated using the flat portion of the probe response, and then normalized with the freestream value obtained in each test by the probes located outside the disturbed region about the plate. In each of these figures is included the calculated ion density profile as obtained from the numerical solution of the slightly ionized hypersonic flow about the plate. In this calculation, the following conditions and properties were used. The free

stream electron to ion temperature ratio was $(\frac{T_e}{T_i})_\infty = 42.0$. The ion diffusion coefficient D_i was evaluated as outlined in Appendix A. The value of the charged species concentration at the wall used as $C_w=0$, to agree with the ion density obtained near the wall using the cylindrical electrostatic probes. As was pointed out before, the value of the Schmidt number has a very small effect on the ion density profiles and for the problem in question, $S_{c_i}=1.0$ was used in all the calculations carried out. The calculated ion density shows very good agreement with the measured values up to the point where the outer compression region starts. At this point, one observes that the calculated ion density starts to increase and reaches values of one and a half to over three times its free stream value, something the measured ion density profiles do not exhibit.

This may be attributed to the fact that the theory does not apply at this region.

D. Density Profiles on the Plate

Density profiles in the disturbed region about a sharp leading edge flat plate in a rarefied hypersonic flow were obtained in the course of this work using an electron beam density probe. Experiments were conducted in the hypersonic shock tunnel on a plate at zero angle of attack, Mach number 18, temperature ratio $T_w/T_o=0.075$, and Reynolds number of 1500/inch.

The following arrangement of the plate and the optics was used in the density survey. The plate was mounted on the

drift tube of the electron gun; the beam was allowed to emerge through a small orifice in the plate surface and impinge on the beam collector mounted 12 inches away from the plate. The radiation emitted due to the beam emerging from the model surface and traversing the test section was monitored during each test with the electro-optical system which could be positioned at any point along the beam. The surface position of the optics was determined visually by positioning the electro-optical system such that the center of the beam lens coincides with the plate surface.

Prior to each test the electro-optical system was positioned at a desired distance away from the plate surface and the photomultiplier voltage was turned on. The electron beam was in continuous operation before each test; nominal operation conditions were 20 KeV accelerating potential and 300 μA beam current. Once the test was initiated the data was displayed on Tektronix 565 oscilloscope and recorded by a Polaroid camera. In each test the data recorded included the photomultiplier output and the beam current signal. Since ambient pre-test pressure in the test section was always less than 10^{-4} mmHg, and at this pressure the photomultiplier had zero output (except for noise), hence the recorded portion of the data before the arrival of the test gas gave the zero signal level for the recorded data. Figure 31 presents typical data traces recorded during a test. The upper trace corresponds to the photomultiplier output. As can be seen, after some initial disturbance there is a gradual increase in the

photoluminescence current which,after a certain period of time, levels off to a constant value. The lower trace corresponds to the beam current signal, which remains relatively constant throughout the test.

A series of density profiles normal to the plate surface were obtained, ranging from 2 to 9 inches from the leading edge. Because of the extremely short test duration pointwise measurements had to be performed in order to obtain a density profile. Figure 32 through Fig. 35 present the normalized density profiles in the disturbed region about the plate. The density at each point of the profile was normalized with respect to the freestream density after corrections were made for changes in beam current between tests and taking into account variation in the photomultiplier output depending on its position with respect to the plate. It should be noted here that the accuracy of positioning the electro-optical system at any given point normal to the plate was ±0.025 inches. This fact had an effect on the accuracy of the density measurements in the shock layer where rapid density changes occur in a relatively narrow region.

E. Flush Probe Measurements and Size Study

Flush probe ion saturation current collection gives information concerning the ambipolar diffusion flux to the plate surface and the charge number density at the sheath edge of the plate. Via boundary layer theory, charged particle density at the boundary layer edge can also be determined. In this experimental investigation, flush

probes were used only to determine the ambipolar diffusion flux to the plate surface.

Measurements were also made of the current voltage characteristics of the flush probes. This was achieved by changing the bias of the different diameter probes at each test and recording the collected ion current. This pointwise measurement of the current voltage characteristic was due to the fact of extremely short test duration whereby no sweeping of the probe bias was possible during a test. Figure 39 shows a typical current voltage characteristic of a circular flush probe biased as a single probe. For all probes large and small, except the 3/4" diameter, no ion saturation current could be observed. Even for the largest probe, 3/4", the ion saturation was ambiguous. The ion current was found to be a very strong function of the bias potential and probe size. Therefore, a series of size studies was undertaken to investigate these effects.

Flush probe studies were made by using the ion current collected by the 3/4" diameter probe at a bias of -3 volts, as a reference. The reason for this choice was the fact that since no ion saturation current was reached even for this probe as shown in Fig. 40, the low value of V_p would partially satisfy the desire to minimize the sheath size which is proportional to $V_p^{3/4}$ and at the same time, provide a reasonable current signal. Thus, by taking the ion current collected by the 3/4" flush probe at a bias of -3 volts, it was felt that fringing effects were kept minimal and that this current is close to the ion saturation current. Ion

current density J_i, to a smaller sized flush probe at a particular x was then normalized by the current density of a 3/4" probe. This normalized current density was then plotted against the parameter d_s/R_p as shown in Fig. 41 to demonstrate the fringing field effects; here d_s is the sheath thickness at the biased flush probe and R_p the probe radius. For the determination of d_s use was made here of the simple free-fall sheath relationship given by the Child-Langmuir Law cited by Brown (Ref. 32),

$$d_s^2 = \frac{8}{9}\left(\frac{I}{\alpha}\right)^{1/2}\left(\frac{eV_p}{KT_e}\right)^{3/2}\lambda_D^2 \qquad (23)$$

where

$$\alpha = T_i/T_e$$

λ_D is the Debye shielding distance based on the plasma conditions at the sheath edge. λ_D was calculated from the ion density near the surface of the plate as measured by the cylindrical electrostatic probes, and the electron temperature T_e was assumed to be constant and equal to its freestream value since the flow is frozen.

The combined sheath area effect was first demonstrated by applying a constant bias potential to all probes of different sizes under the same flow conditions. To vary d_s/R_p even more, different bias potentials up to -200 volts were applied to these probes.

F. Ambipolar Diffusion Flux Along the Flat Plate

The ambipolar diffusion flux of the ionized particles to the plate surface at different axial locations along the plate was obtained during the course of this work using three

different approaches.

In the first approach, following the formation of Chung (Ref. 16) the current density at the plate surface is related to the ambipolar diffusion coefficient and the gradient of ion number density at the plate surface in the following manner:

$$J = eD_a \left(\frac{\partial N_i}{\partial y}\right)\Big|_w \qquad (24)$$

where

$$D_a = D_i \left(1 + \frac{T_e}{T_i}\right)$$

Since of interest was the ambipolar diffusion flux along the plate, hence, the ion current density distribution as a function of x was calculated using this relation (Eq. 24) together with the numerical calculation of the slightly ionized hypersonic flow about the plate in question. It was assumed here that the ion and neutral particle temperature are equal (T_i=T) and that the electron temperature is constant throughout the region since the flow is frozen (T_e=3000^{o}K). The ambipolar diffusion coefficient was determined at each point as outlined in Appendix A.

The second method consisted again of utilizing Eq. (24) together with the value of $\partial N_i/\partial y|w$ obtained from the experimental ion density profiles at the various axial station. The density and temperature distribution in the disturbed region about the plate was obtained here from the numerical calculation.

The third method used to establish the ambipolar diffusion flux to the plate was to measure the ion current collected by

the 3/4" diameter flush electrostatic probes imbedded at different axial positions along the plate and biased at -3 volts for ion collection.

Figure 42 presents the ambipolar diffusion flux along the surface of the plate as obtained using those three methods. Figure 43 shows the non-dimensional current density distribution along the plate where the current density collected by the flush probes was non-dimensionalized with the current collected by the probe located at the furthest downstream position (x=16½ inches) from the leading edge. Included in this figure is the non-dimensional ambipolar flux of the ionized particles as obtained from the numerical solution for the flow in question.

G. Cone Wake Density Measurements

As mentioned above in previous work by Lederman and Avidor (Ref. 7), it was suggested that ions in a preionized flow can be used for flow field tracing and that in chemically frozen flow fields, the ion density distribution measured can be interpreted in terms of neutral density distribution, provided diffusion is negligible. In this work and another investigation (Ref. 8), ion density distribution in the near wake of slender and blunted bodies was obtained in a slightly preionized hypersonic flow generated in a hypersonic shock tunnel. The present investigation of density measurements in the near wake of a cone was initiated because the wake provides the different flow fields in which diffusion is more or less significant, and thus provides the necessary flow field

to determine the correctness or incorrectness of the flow field diagnostics as suggested by Lederman et al.

Utilizing an electron beam density probe for this purpose, tests were conducted on a sharp 10^{o} half angle cone with a 4-inch base diameter at Mach number 18 and zero angle of attack. All tests on the cone wake reported here were conducted in pure nitrogen (commercial dry bottled nitrogen), and the flow conditions in the test section are listed in Table II.

For any wake measurements, the model suspension system is of critical importance. For the present tests, the model was suspended on 0.020 inch diameter wire. It was found in previous work by Lederman (Ref. 29) that this size wire did not introduce any observable disturbance in the wake region under the same flow conditions as those in question here.

A further experimental detail concerned the positioning of the model with respect to the electron beam. The model was suspended on wires from a frame mounted to a movable sting, which allowed one to position the cone at different axial stations (x/D_B) with respect to the beam's position which was fixed. The $x/D_B=0$ position was obtained before each test by projecting the beam through the test section and letting it impinge on the shoulder of the cone, and from this reference point, the cone was moved to a desired x/D_B position by moving the sting. Thus, after the cone was set in position at a given x/D_B, the electro-optical system was moved to a desired radial position by moving it along the beam. In each

test two data points were obtained in any radial profiles, each by one electro-optical system. Because of the short test duration, one cannot move the electro-optical systems to obtain a continuous density profile during the test run. Density measurements obtained in the near wake of the cone include axial density distribution from x/D_B=0.25 to x/D_B= 3.0 . At x/D_B=1.0 and x/D_B=3.0 a radial density profile was obtained which extended to the outer edges of the flow field. Before presenting the data, one aspect of the work should be emphasized. All of the density measurements are direct "point" measurements. The resolution of "point" size in this case is 2 mm. Figure 44 shows an oscilloscope trace of the electroluminescence intensity for a freestream run and one taken in the wake of the cone. The traces include a sharp change in photocurrent occurring when the flow arrives at the beam station and then the photocurrent increases for awhile and levels off to a constant value over a period of 0.5-1.0 msec. The traces also include the beam current as monitored during each test.

The fluctuations observed in the current trace are due to the fact that the beam collector which was biased at +9 volts with respect to ground was actually a biased electrostatic probe collecting electrons from the slightly ionized flow. This current, however, was found to be negligible in the region where the tests were conducted. It was found that no observable attenuation of the beam current did exist during the test duration. It is also worth mentioning here that during the course of this work, it was found that the

repeatability of tests was excellent.

Figure 45 presents the axial density distribution in the near wake of the cone as obtained in the present work. The density at each point on the axis of the wake was normalized with the freestream density. Included in this figure for the purpose of comparison is the ion density distribution in the near wake of the cone as obtained by Lederman et al.with cylindrical electrostatic probes (Ref. 29). The next two figures, Fig. 46 and 47, show two radial profiles measured at x/D_B=1.0 and x/D_B=3.0. Those were obtained by positioning the cone at the particular x/D_B and measuring the density by moving the electro-optical system in the radial direction, starting at the wake axis and moving out to the outer edges of the flow field. Again, the density is presented in a normalized form where at each point the density was normalized with the local freestream value. These figures also include the radial ion density profiles as obtained by Lederman et al.(Ref. 29).

VII. DISCUSSION OF RESULTS

As pointed out above and shown in Fig. 24 through Fig. 27, the normalized profiles of the ion density about the flat plate at the several stations investigated agree within the experimental error remarkably well with the theoretically calculated profiles up to the point where the outer compression region starts. At this point one can observe a departure between the measured and calculated profiles. Although there is no complete explanation of this behavior possible at this time, it should be noted that the absolute ion density values may have been underestimated through the use of the upper curve in Fig. 25. This curve was obtained at a density which was lower than the actual density in the compression region, as seen in the same figure, the lower curve- an increase in density would result in a decrease in α_p which would in turn result in a higher number density value at the given point. Furthermore, it should be indicated that the numerical solution in the compression region is of questionable validity.

In Figs. 32 through 35, the experimentally obtained neutral density profiles normal to the plate are shown. Superimposed on these are the theoretically obtained profiles. It is evident from these figures that good agreement between the theoretical and experimental density profiles exist. Slight deviations can be observed in the position of the maximum density. The absolute values of the theoretical and experimental maximum density (ρ_{max}/ρ_∞) deviate more

significantly. This deviation appears to decrease with the increase in x (decrease in $\bar{V}_{\infty_x}$)(see Fig. 36). This kind of behavior was observed by a number of other investigators (Refs. 28,33,34). The next two figures, Figs. 37 and 38, consist of a superposition of an experimentally obtained neutral and ion density profile. Because of the large difference in Reynolds number for the ionized flow and the nonionized flow (see Table II) the correlating parameter used in this superposition was $\bar{V}_{\infty_x}$.

As can be seen, there is no agreement between the two profiles. In the viscous region the ion density drops down to much lower values than the density. This could partly be explained by the large ambipolar diffusion of the ionized particles because of the relatively large electron to ion temperature ratio $(\frac{T_e}{T_i})$ under the test conditions in question. In the compression region the density shows a definite overshoot whereas the ion density does not.

In Fig. 42, the ambipolar diffusion flux of the ionized particles to the plate, as determined experimentally and theoretically, is shown. It is clearly evident from this figure that the theoretical and experimental values may deviate by a factor of two. This deviation could be ascribed partially to the experimental scatter of the data, the fringing effects on ion current collection by the flush electrostatic probes as indicated in Fig. 41, and the uncertainty in the calculated values because of initial condition effects on the numerical solution for $\bar{V}_{\infty} > 0.4$

($x < 4$). Figure 43 presents the nondimensionlized ambipolar flux to the plate. Again, significant deviation occurs for $x < 4$.

In the next few figures the comparison between ion and neutral density distributions in the near wake of the cone is shown. Figure 45 presents the axial distribution and as one can see, there is a significant deviation between the ion and neutral density up to about $x/D_B = 2.0$. Figure 46 shows the radial distribution and as is evident from this figure, the difference between the ion and neutral density is in particularly large in the core of the wake. It should be noted that the overshoot in the density and ion density indicating the location of the shock is at the same radial position and about the same strength ($\frac{\rho_{max}}{\rho_\infty}$, $\frac{N_{i_{max}}}{N_{i_\infty}}$). Figure 47 shows the radial distribution at $x/D_B = 3.0$; in this case very good agreement exists between the ion and neutral density profiles even in the center core region.

In view of the above, it is quite evident that the electrostatic probe technique can only be utilized for flow field determination in regions where diffusion of the ionized particles is negligible. In these regions a one-to-one correlation can be obtained for the ion and neutral densities.

Finally, it should be noted that two flow regimes were utilized in the course of this investigation. One, containing ionized particles of approximately 0.4 msec. duration; the other of a higher density following the ionized flow region and containing a negligible amount of ionized particles.

VIII. SUMMARY AND CONCLUSIONS

Two diagnostic techniques, the cylindrical electrostatic probe and the electron beam density probe, were applied to flow field surveys in the disturbed region about a flat plate and in the near wake of a 10^{o} half angle cone in a rarefied slightly ionized hypersonic flow. Their relative merits have been evaluated. It was found that both can be applied for flow field investigations and particularly density tracing and mapping, provided that diffusion effects are nonexistent or negligible. In cases where diffusion is significant, the electrostatic probe technique may provide highly misleading data. The correspondence between the ion and neutral densities in this case are, on a one-to-one basis, nonexistent. On the other hand, the electron beam density probe is applicable in diffusive and nondiffusive regions. Its limitations, however, are at extremely low densities where the signal-to-noise ratio becomes intolerable, or at the high density range where collisions cause quenching of the beam. From the above, it is evident that both of those techniques are supplementary; whereas the former has no limitation on the density regime, the latter is not limited by diffusion effects.

It can, therefore, be concluded that:

i) The electrostatic probe can be utilized as a field tracing tool in regions where diffusion is nonexistent or negligible irrespective of density.

ii) The electron beam density probe provides a unique

technique for tracing and determination of flow configurations irrespective of diffusion effects, provided it is operated in the proper density regime.

iii) Ion density profiles normal to the plate agree very well in the viscous layer with results obtained from the numerical solution using the Rudman-Rubin theory for the hypersonic flow about the plate modified by Chung's formulation for the ambipolar diffusion of the ionized particles in the disturbed region.

iv) Neutral density profiles obtained normal to the plate indicate a certain deviation from the theoretically predicted result. The experimentally obtained data agree with data obtained by other investigators under similar flow conditions.

IX. REFERENCES

1. Langmuir. I, and Mott-Smith, H.M.: Theory of Collectors in Gaseous Discharges . Phys. Rev., 28, p. 727, 1926.
2. Allen, J.E., Boyd, R.L.F., Reynolds, P.: The Collection of Positive Ions by Probes Immersed in a Plasma . Proc. Phys. Soc. B., 70, p. 297, 1957.
3. Bernstein, I.B., Rabinowitz, I.N.: Theory of Electrostatic Probes in a Low Density Plasma. Phys. of Fluids, 2, p. 112, 1959.
4. Laframboise, Y.G.: Theory of Spherical and Cylindrical Langmuir Probes in a Collisionless Maxwellian Plasma at Rest. University of Toronto, UTIAS Report No. 100, 1966.
5. Lederman, S., Bloom, M.H., and Widhopf, G.F.: Experiments on Cylindrical Electrostatic Probes in a Slightly Ionized Hypersonic Flow. AIAA J., 6, pp. 2133-2139, 1968.
6. Kiel, R.E.: Electrostatic Probe Theory for Free Molecular Cylinders. AIAA J., 6,p.708, 1968.
7. Lederman, S., Bloom, M.H. and Avidor, J.: The Electrostatic Probe: Some Applications to Hypersonic Flow Diagnostics. Israel Journal of Technology, 8, No. 1-2, pp. 73-85, 1970.
8. Lederman, S., Bloom, M.H., and Widhopf, G.F.: Field Tracing With Electrostatic Probes in Low Density, Slightly Ionized Flows. International Congress on Instrumentation in Aerospace Simulation Facilities, 1969 Record, pp. 43-50.
9. Harbour, P.J. and Lewis, J.H.: Preliminary Measurements of the Hypersonic Rarefied Flow Field on a Sharp Flat Plate Using an Electron Beam Probe., (C.L. Brundin, ed.),

"Rarefied Gas Dynamics, Supp. 4, 2, p. 1031, Academic Press, New York, 1967.

10. Lillicrap, D.C. and Berry, C.J.: Experimental Model for High-Speed Rarefied Flow Over a Sharp Flat Plate. Phys. of Fluids, 13, No. 5, May 1970.

11. Zempel, R., Mallin, J. and Muntz, E.: An Electron Beam Excitation Technique for the Measurements of Low Densities In Hypersonic Shock Tunnel Flows. General Electric Missile and Space Division Report No. R-63-SD-21, 1963.

12. Hays, W.D. and Probstein, R.F.: Hypersonic Flow Theory, Academic Press, Inc., New York, 1959.

13. Rudman, S. and Rubin, S.G.: Hypersonic Viscous Flow Over Slender Bodies Having Sharp Leading Edges. AIAA J., 6, 10, pp. 1883-1889, October 1968.

14. Su, C.H.: Compressible Plasma Flow Over Biased Body. AIAA J., 3, pp. 842-848, 1965.

15. Lam, S.H.: General Theory for the Weakly Ionized Gases. AIAA J., 2, pp. 256-262, 1964.

16. Chung, P.M. and Blankenship, V.D. Theory of Double Electrostatic Probes Comprised of Two Parallel Plates. AIAA J., 4, pp. 442, 1966.

17. de Leeuw, J.H.: Elelectrostatic Probes, Published in "Physio-Chemical Diagnostics of Plasmas", (T.P. Anertson, et al., eds.) Northwestern University Press, Evanston, Illinois, pp. 65, 1963.

18. Chen, F.F.: Electrostatic Probes, Published in "Plasma Diagnostic Techniques" (R.H. Huddlestone and S.L. Leonard, eds.), Academic Press, New York, pp. 113-119, 1965.

19. Sonin, A.A.: The Behavior of Free Molecule Cylindrical Langmuir Probes in Supersonic Flows and Their Application to the Study of the Blunt Body Stagnation Layer. University of Toronto, Institute of Aerospace Studies, UTIAS Report No. 109, 1965.

20. Bloom, M.H. and Lederman, S.: Measurements of the Ionized Flow in a Shock Tunnel by Means of Resonant Cavities and Electrostatic Probes. Polytechnic Institute of Brooklyn, PIBAL Report No. 1019, 1967.

21. Shih, C.H. and Levi, E.: The Effect of Collisions on Cold Ion Collection by Means of Langmuir Probes. Presented at the AIAA Third Fluid and Plasma Dynamics Conference, Los Angeles, California, June 28-July 1, 1970, AIAA Paper No. 70-757.

22. Schumacher, B.W., Gadamer, E.O.: Electron Beam Fluorescence Probe for Measuring the Local Gas Density in a Wide Field of Observation. Canadian Journal of Physics, 36, pp. 659-671, 1959.

23. Gadamer, E.O: Measurement of the Density Distribution in a Rarefied Gas Flow Using the Fluorescence Induced by a Thin Electron Beam. UTIAS Report No. 83, 1962.

24. Muntz, E.P.: Measurement of Rotational Temperature, Vibrational Temperature, and Molecule Concentration in Non-Radiating Flows of Low Density Nitrogen. UTIAS Report No. 71, 1961.

25. Petrie, S.J.: Analysis of the Thermo-Chemical State of an Expanded Air Plasma. AFFDL-TR-64-91, 1965.

26. Visich, M., Lederman, S. and Mak, W.H.: Combustion Driven Shock Tunnel of the Polytechnic Institute of Brooklyn. PIBAL Report No. 847, 1965.

27. Lordi, J.A., Mates, R.E. and Moselle, J.R.: Computer Program for the Numerical Solution of Nonequilibrium Expansions of Reacting Gas Mixtures. Cornell Aeronautical Laboratory, Rept. No. AD-1689-A-6, 1965.

28. Lillicrap, D.C. and Berry, C.J.: Experimental Model for High-Speed Rarefied Flow Over a Sharp Flat Plate. Phys. of Fluids, 13, No. 5, May 1970.

29. Lederman, S., Bloom, M.H. and Widhopf, G.F.: Laboratory Measurements of Electron-Density Distribution in the Near Wake. AIAA J., 7, pp. 1421-1429, 1969.

30. Talbot, L. and Chou, Y.S.: Langmuir Probe Response in the Transition Regime. In "Rarefied Gas Dynamics," (C.L. Brundin, ed.) Academic Press, New York, Vol. II, pp. 1723-1737, 1969.

31. Bornstein, J: Behavior of a Cylindrical Electrostatic Probes in a Transitional Regime. M.S. Thesis, Polytechnic Institute of Brooklyn, June 1971.

32. Brown, S.C.: Introduction to Electrical Discharges in Gases, J. Wiley and Sons, New York, 1965.

33. Cresci, R.J. and Schmidt, E.M.: Rarefied Flow Field Measurements Over Planar, Two- and Three-Dimensional Bodies. Presented at Seventh Rarefied Gas Dynamics Symposium, Pisa, Italy, 1970.

34. Rubin, S.G. and Lin, T.C.: Rotational Non-Equilibrium Near a Hypersonic Leading Edge. Presented at Seventh International Rarefied Gas Dynamics Symposium, Pisa, Italy, 1970.

35. Mason, E.A.: Estimated Ion Mobilities for Some Air Constituents. Planet.Space. Sci., 18, pp. 137-144, 1970.

APPENDIX A

DIFFUSION AND AMBIPOLAR DIFFUSION COEFFICIENT FOR No^+ IN AIR

Most data on the motion of ions in neutral gases is given in terms of mobility, μ_i, which is related to the diffusion coefficient, D_i, by Einstein's relation

$$D_i = \frac{KT_i}{e}\mu_i \qquad (A.1)$$

the mobility μ_i which is usually given in literature represents the value of μ_i at the standard gas number density of $N_o = 2.69 \times 10^{25}$ particles/m^3, which corresponds to standard conditions of 760 Torr and 273°k. The mobility at other densities is related to μ_{io} by the equation

$$\mu_i\,(N,T) = \frac{N_o}{N}\mu_{io}(T) \qquad (A.2)$$

but $N_o/N = \rho_o/\rho$, ρ_o is the gas density at standard conditions.

Mason (Ref. 35) gives values for $\mu_{io}(T)$ for N_o^+ in air which can be approximated by the following expression

$$\mu_{io}(T) = 2.75 + 1.466 \times 10^{-3}T \qquad \left[\frac{CM^2}{Volt\text{-}sec}\right] \qquad (A.3)$$

in the range $0°k \leq T \leq 1000°k$. The ambipolar diffusion coefficient is related to the diffusion coefficient of the ion in the following way:

$$D_a = D_i\left(1 + \frac{T_e}{T_i}\right) \qquad (A.4)$$

Substituting Eq. (A.1) into (A.4) and using the expression $\mu_i(N,T)$, we obtain

$$D_a = \frac{K}{e}\frac{\rho_o}{\rho}\left(T_i + T_e\right)\left[2.75 + 1.466 \times 10^{-3}T_i\right] \qquad (A.5)$$

Eq. (A.5) was used in all the calculations concerning ion mobility in the flow.

TABLE I

FLOW CONDITIONS ALONG THE NOZZLE

(IONIZED FLOW REGION)

x	40 in.	50 in.	67 in.	105 in.
$T(^{o}k)$	315	225	167	115
P(Atm)	3.96×10^{-4}	1.15×10^{-4}	4.15×10^{-5}	10^{-5}
ρ(Atm)	4.75×10^{-4}	1.92×10^{-4}	9.4×10^{-5}	3.3×10^{-5}
N_i (el/cm^3)	1.5×10^{10}	9×10^{9}	4×10^{8}	9×10^{8}
$T_e(^{o}k)$	3000	3000	3000	3000

TABLE II

FLOW CONDITIONS IN THE TEST SECTION

	Ionized Flow Region	Nonionized Flow Region
T_∞	~70°k	~70°k
P_∞	2.6×10^{-6} Atm	1.3×10^{-5} Atm
ρ_∞	1.1×10^{-5} Atm	5.5×10^{-5} Atm
M_∞	~18.0	~18.0
R_{e_∞}	~300/in.	~1500/in.
T_{i_∞}	~70°k	--------
T_{e_∞}	~3000°k	--------
N_{i_∞}	3×10^8 el/cm^3	--------
λ_{n-n}	~0.1 in.	~0.020 in.
λ_D	0.01 in.	--------

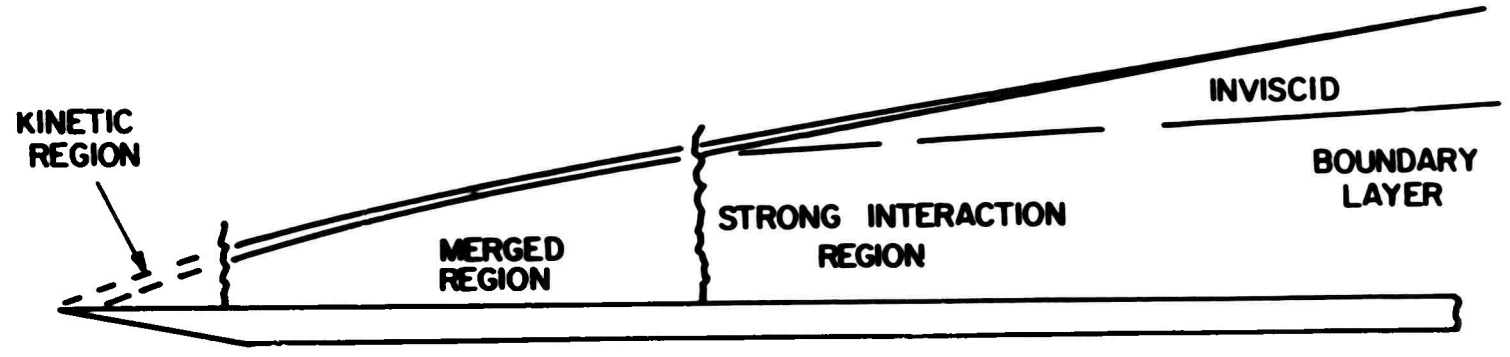

FIG. 1 FLOW PATTERN ABOUT SHARP LEADING EDGE FLAT PLATE IN HYPERSONIC FLOW

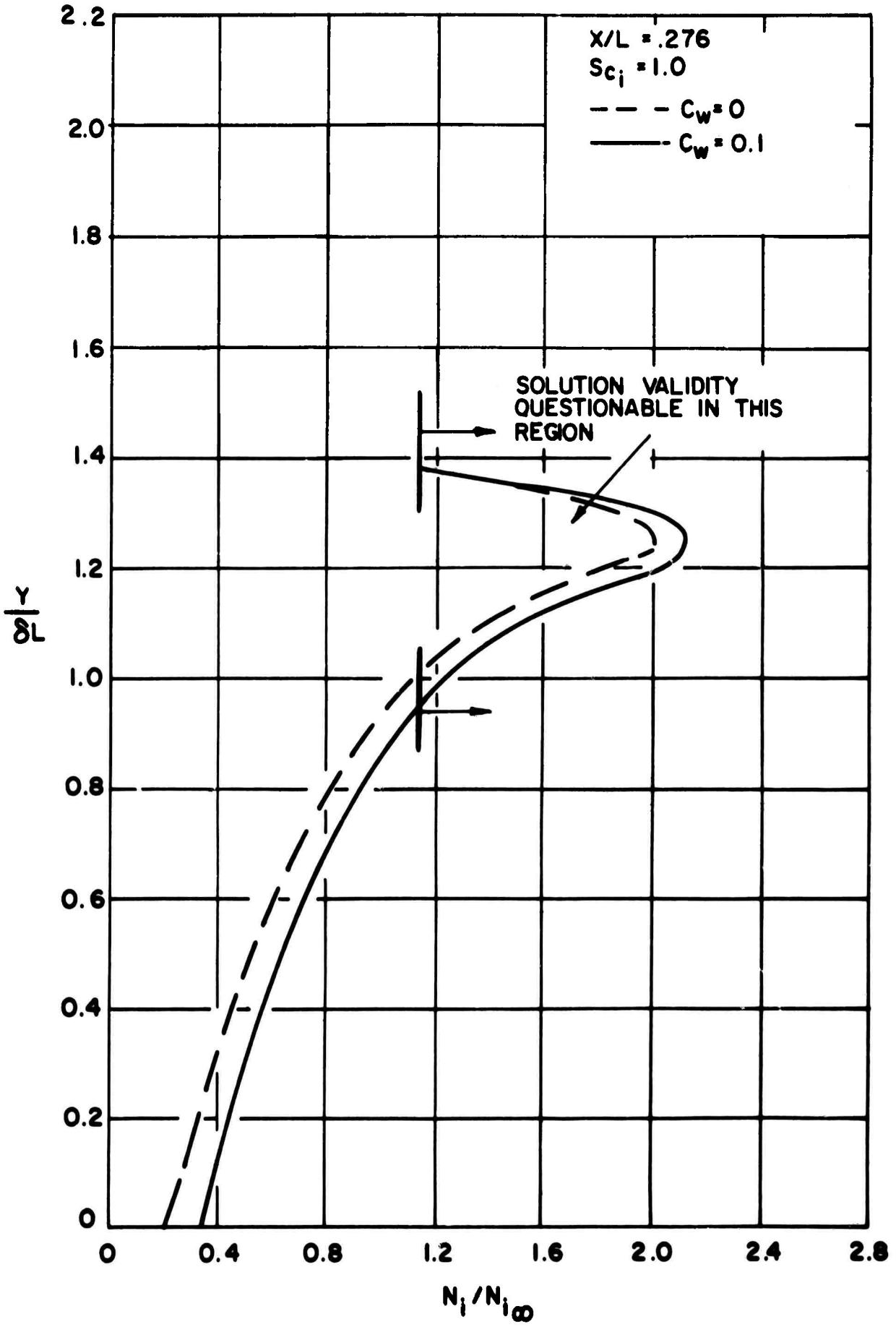

FIG. 2 EFFECT OF C_w ON CALCULATED ION DENSITY PROFILE

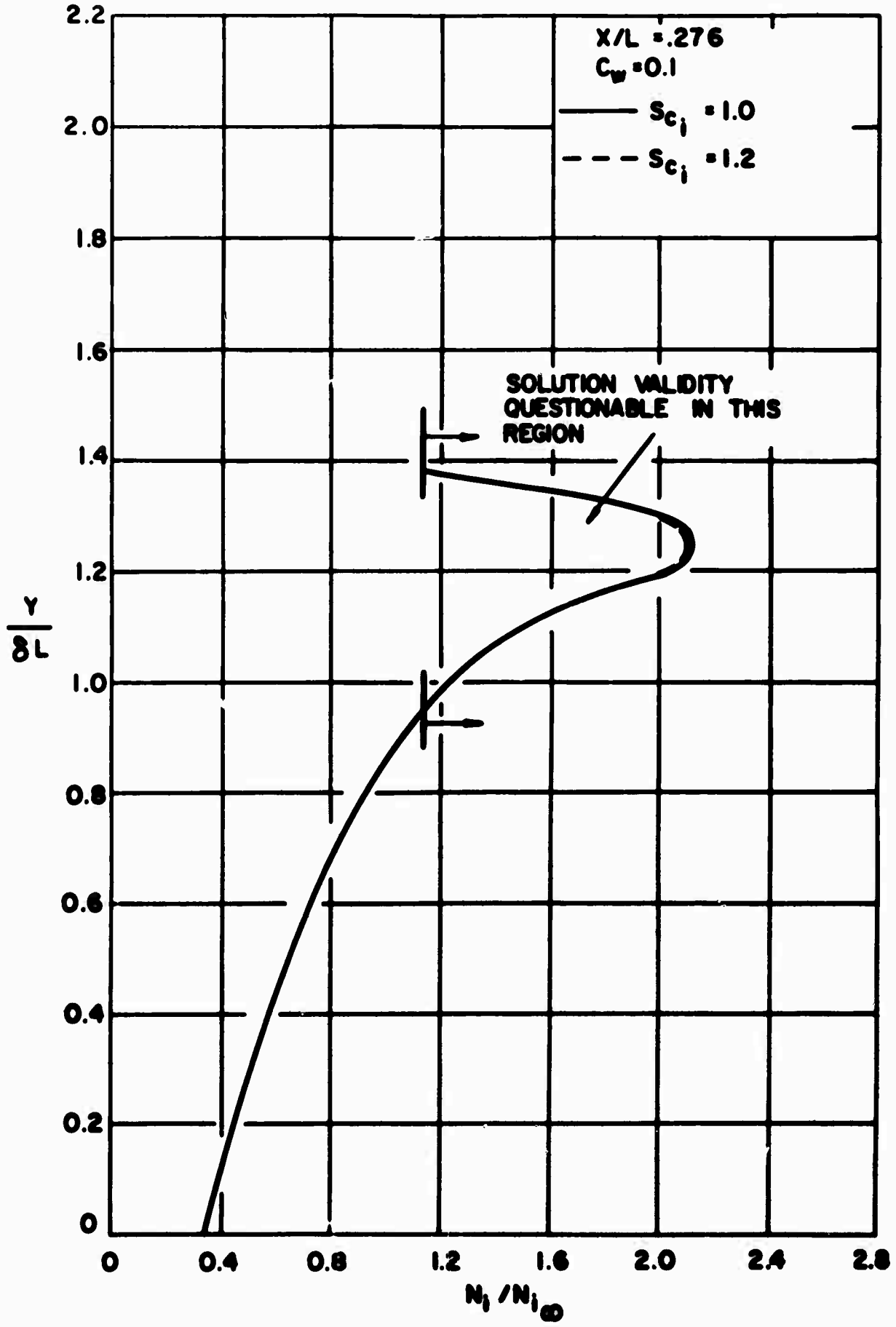

FIG. 3 EFFECT OF SCHMIDT NUMBER ON CALCULATED ION DENSITY PROFILE

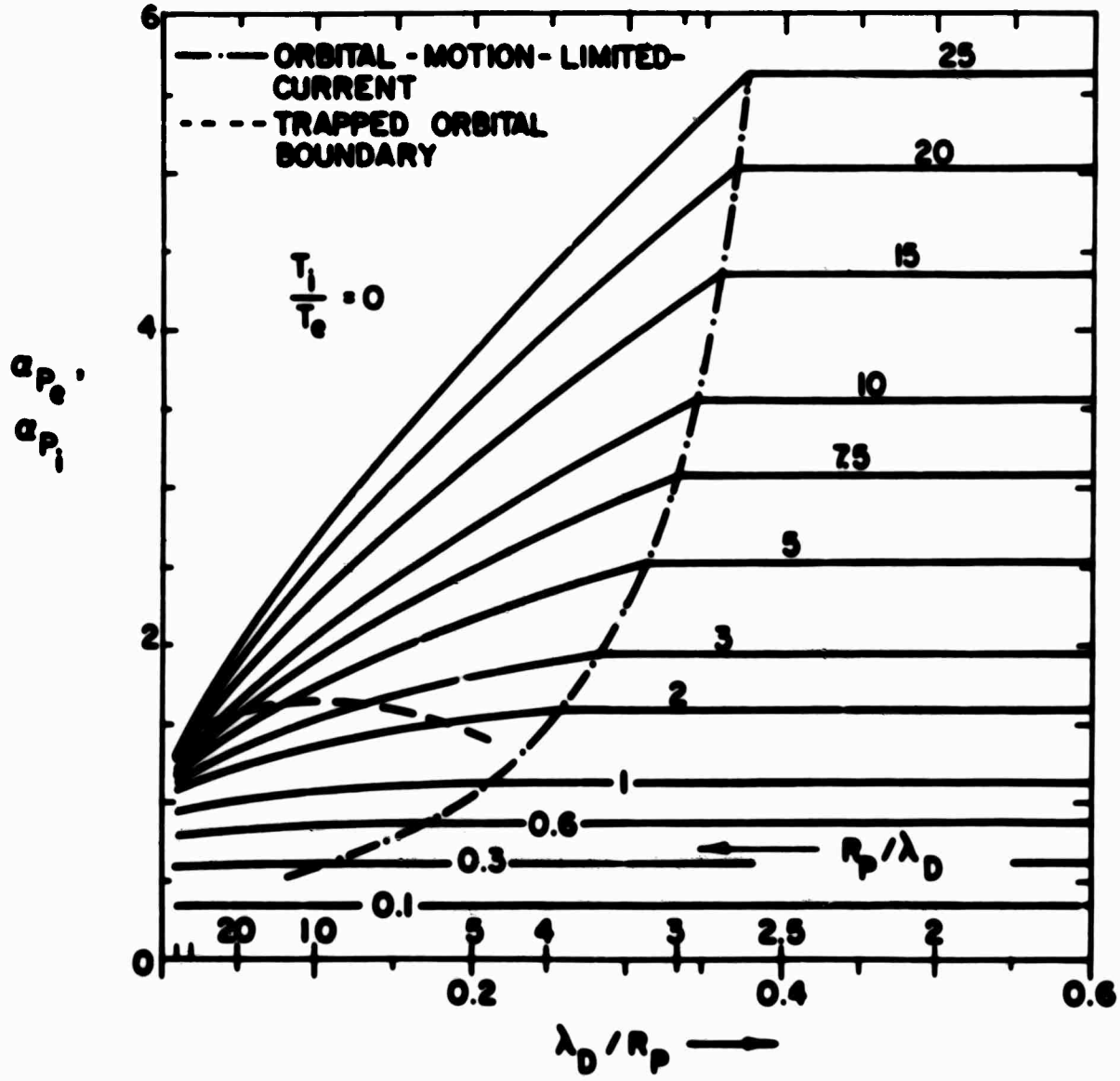

FIG. 4 ION CURRENT VS λ_D/R_p FOR VARIOUS VALUES OF $-eV_p/kT_e$; CYLINDRICAL PROBE; $T_i/T_e = 0$.

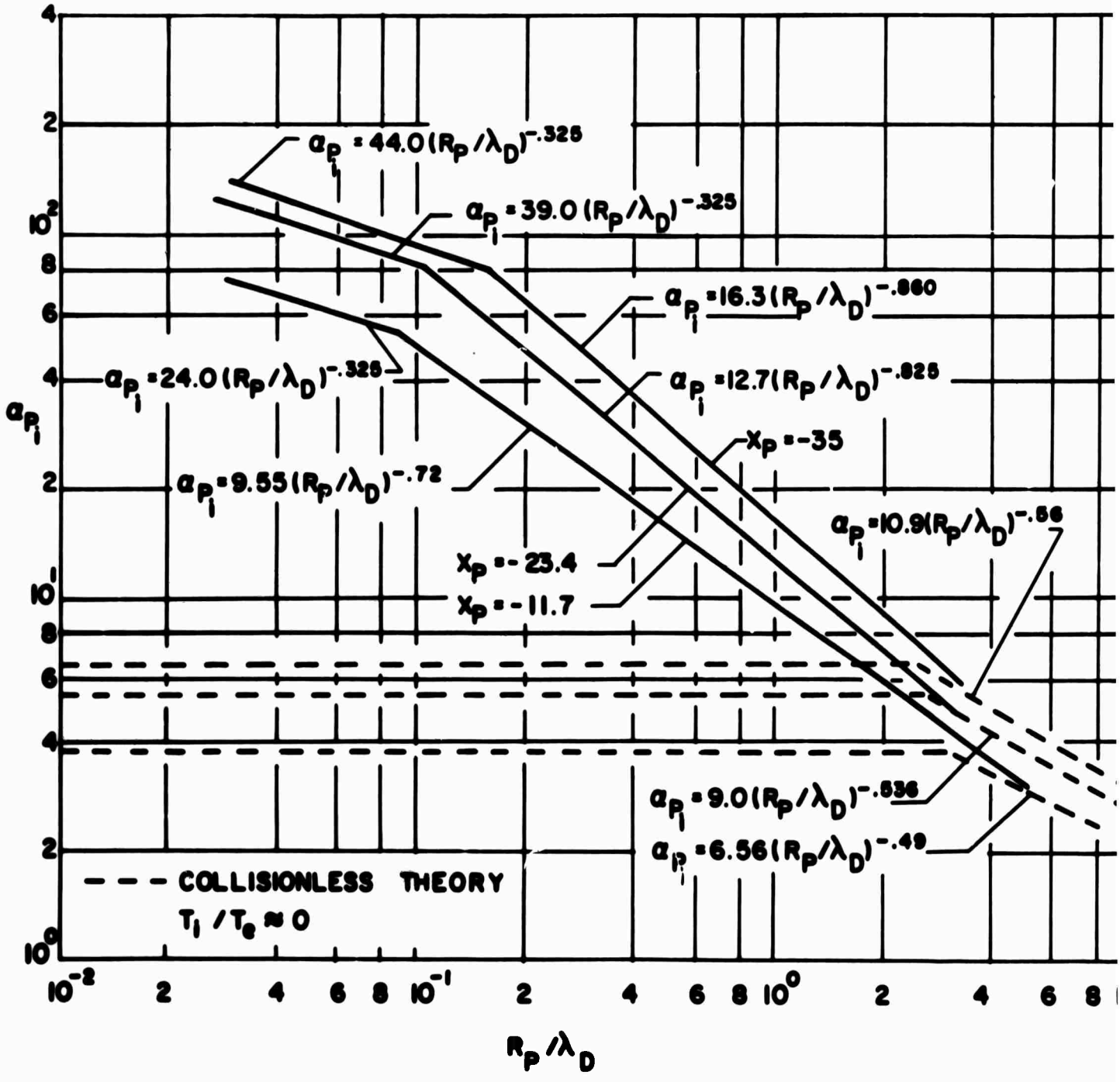

FIG. 5 DIMENSIONLESS ION CURRENT α_P AS A FUNCTION OF R_P/λ_D

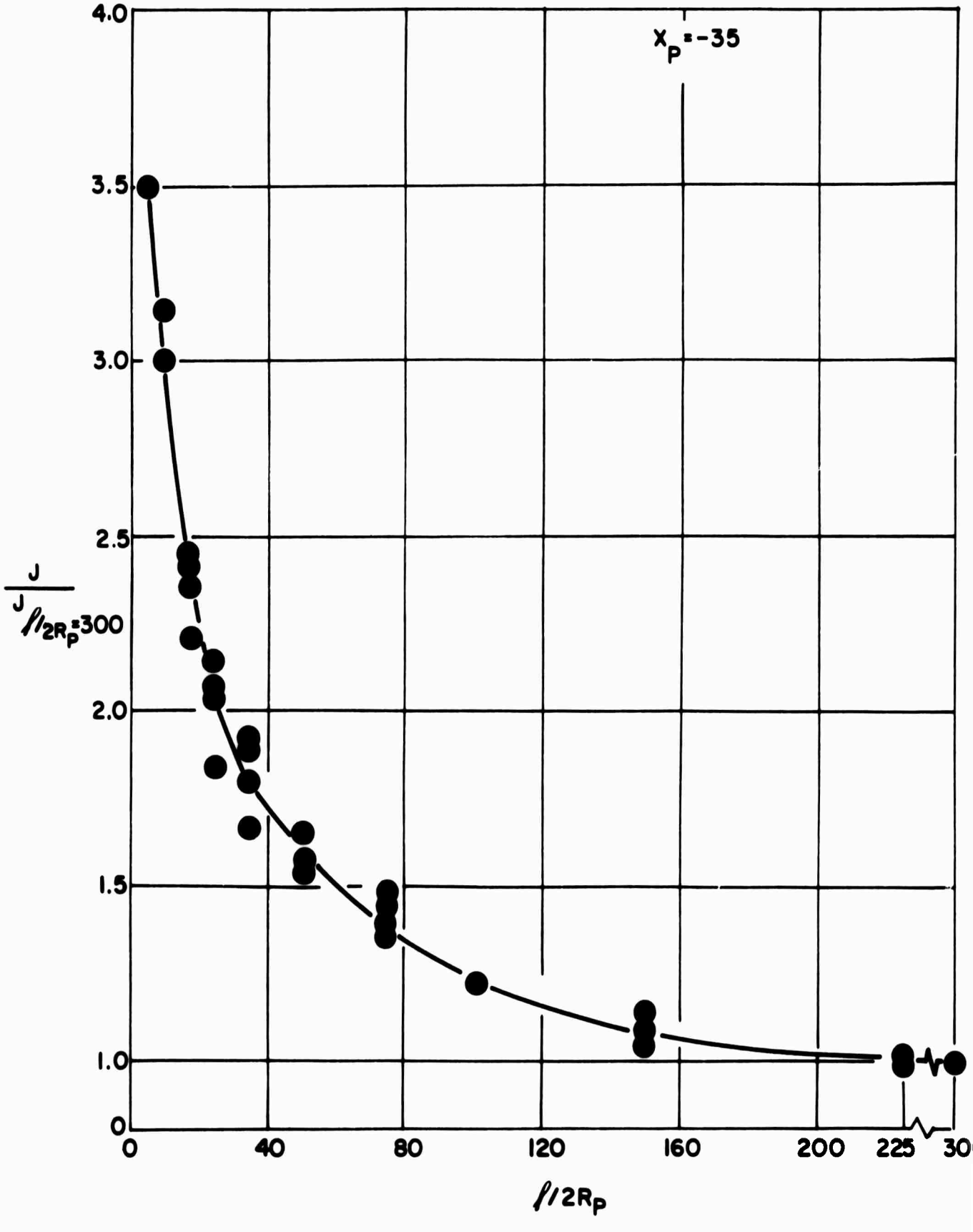

FIG. 6 NONDIMENSIONAL CURRENT DENSITY AS A FUNCTION OF THE PROBE LENGTH TO DIAMETER RATIO

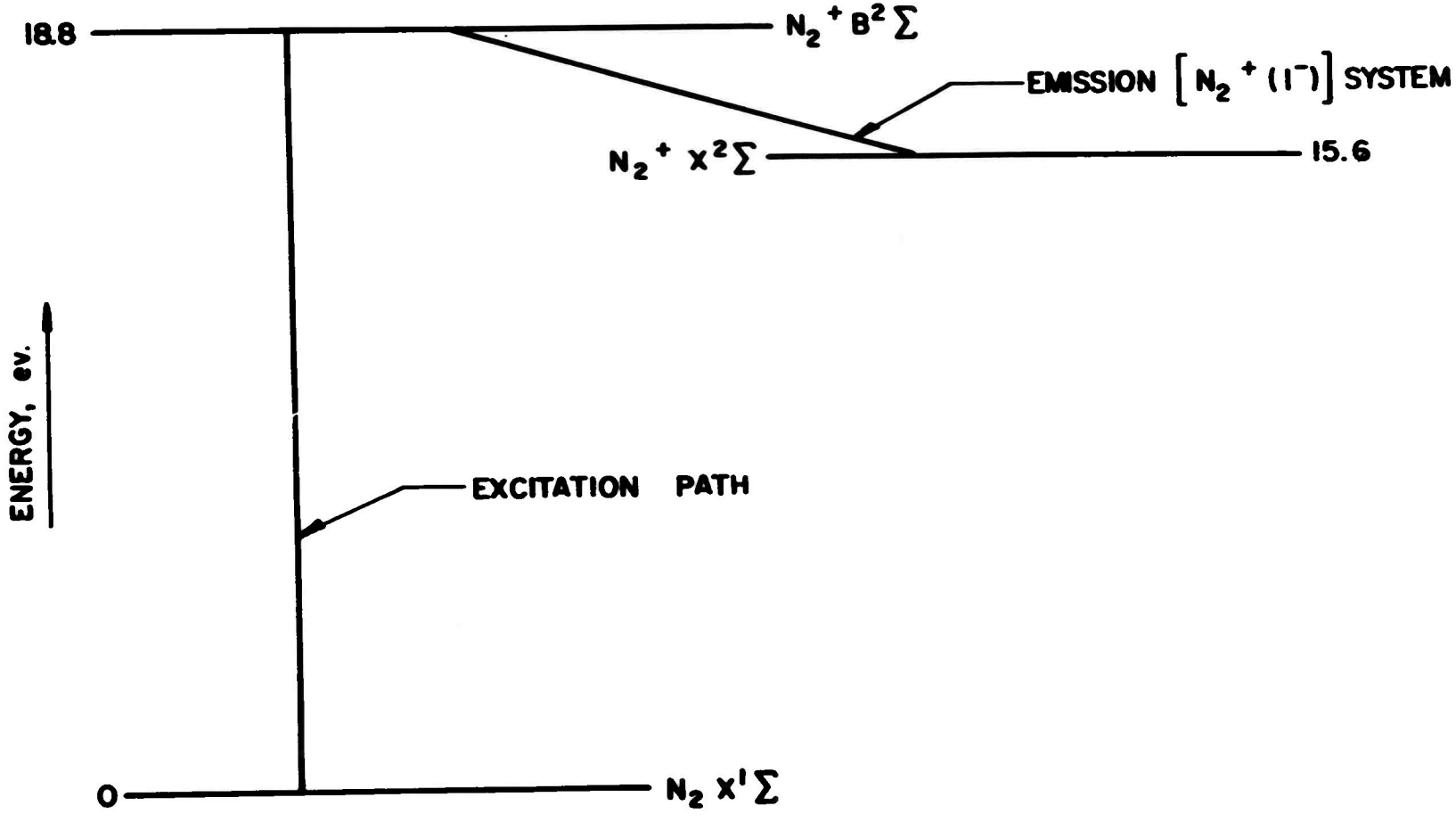

FIG. 7 SIMPLIFIED, GENERAL EXCITATION - EMISSION DIAGRAM

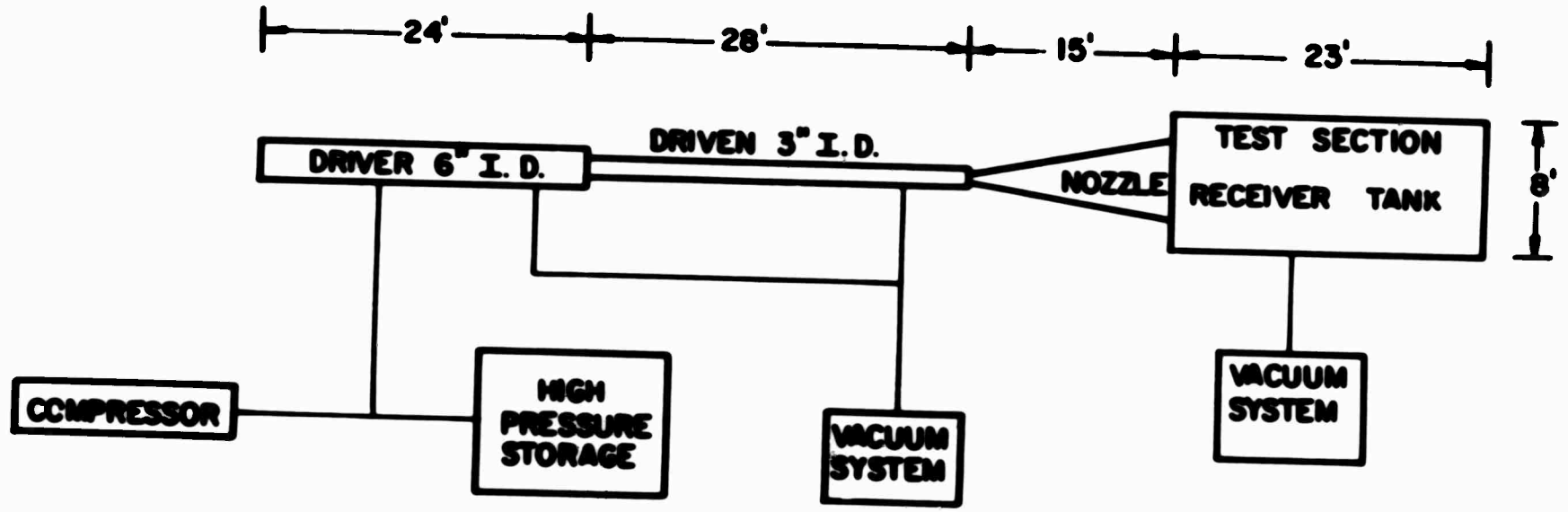

FIG. 8 BASIC COMPONENTS OF THE PIB HYPERSONIC SHOCK TUNNEL

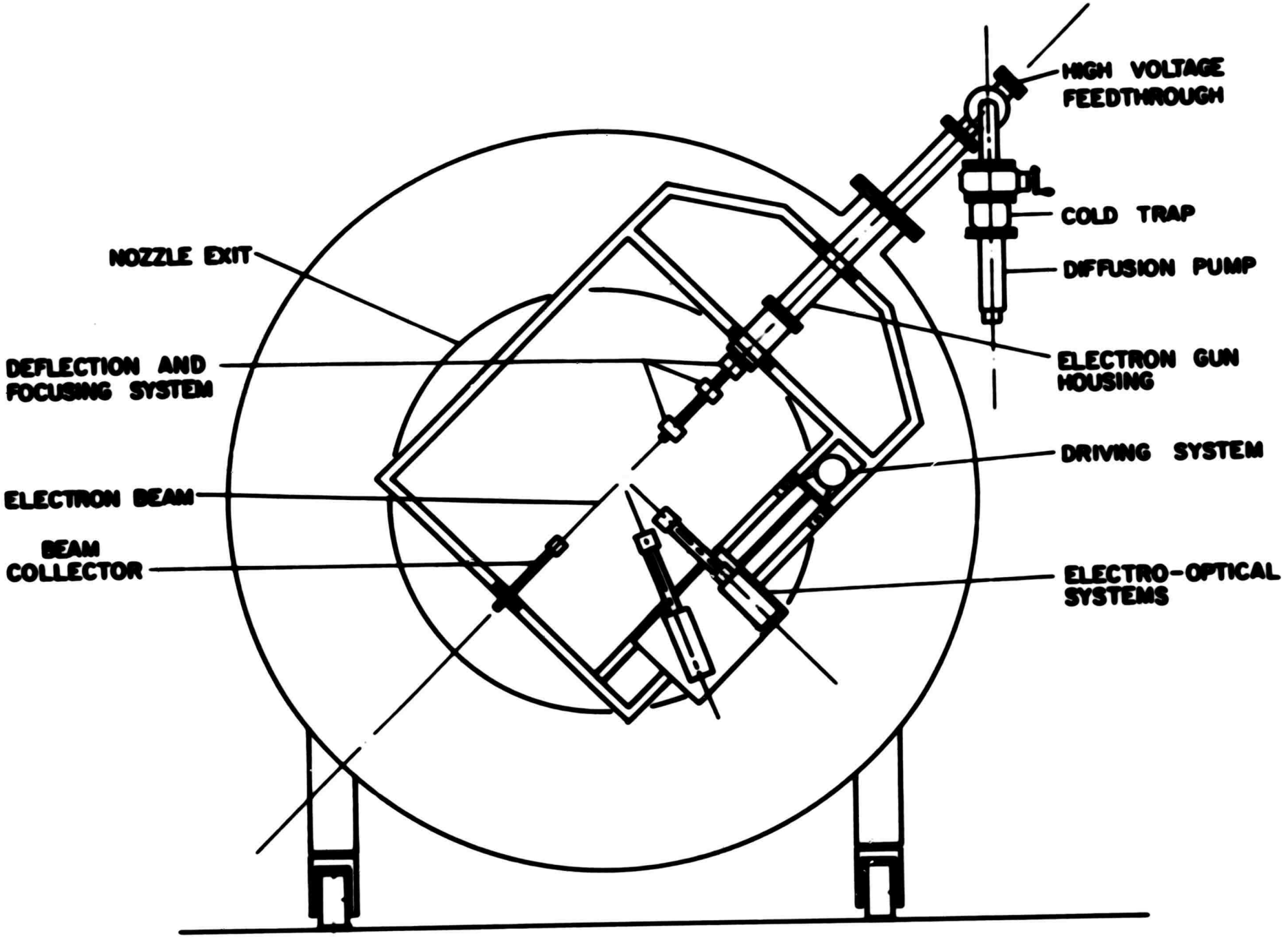

FIG 9 SCHEMATIC DIAGRAM OF ELECTRON BEAM APPARATUS

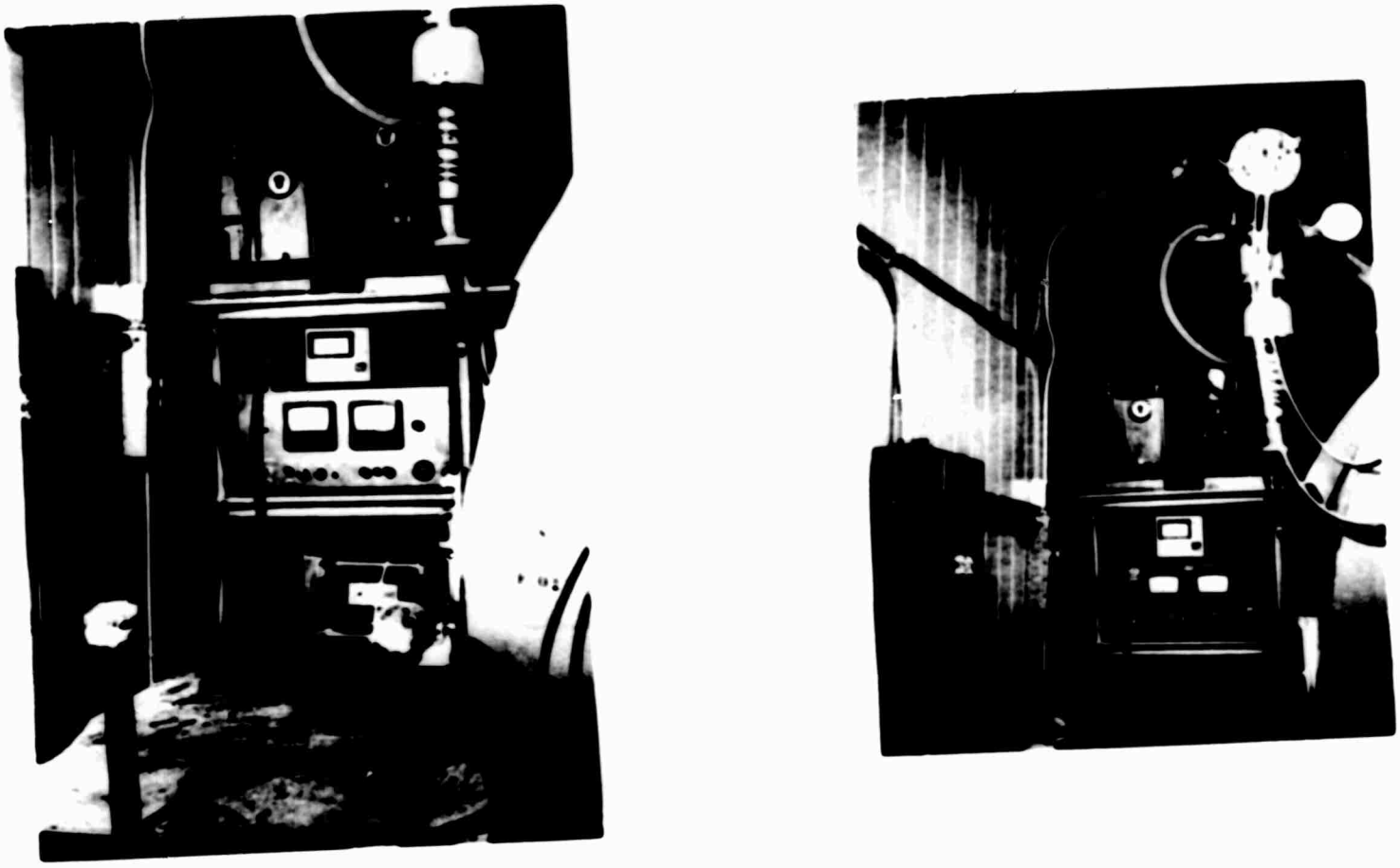

FIG. 10 EXTERNAL VIEW OF THE ELECTRON GUN SYSTEM PUMPS AND PRESSURE GAUGES

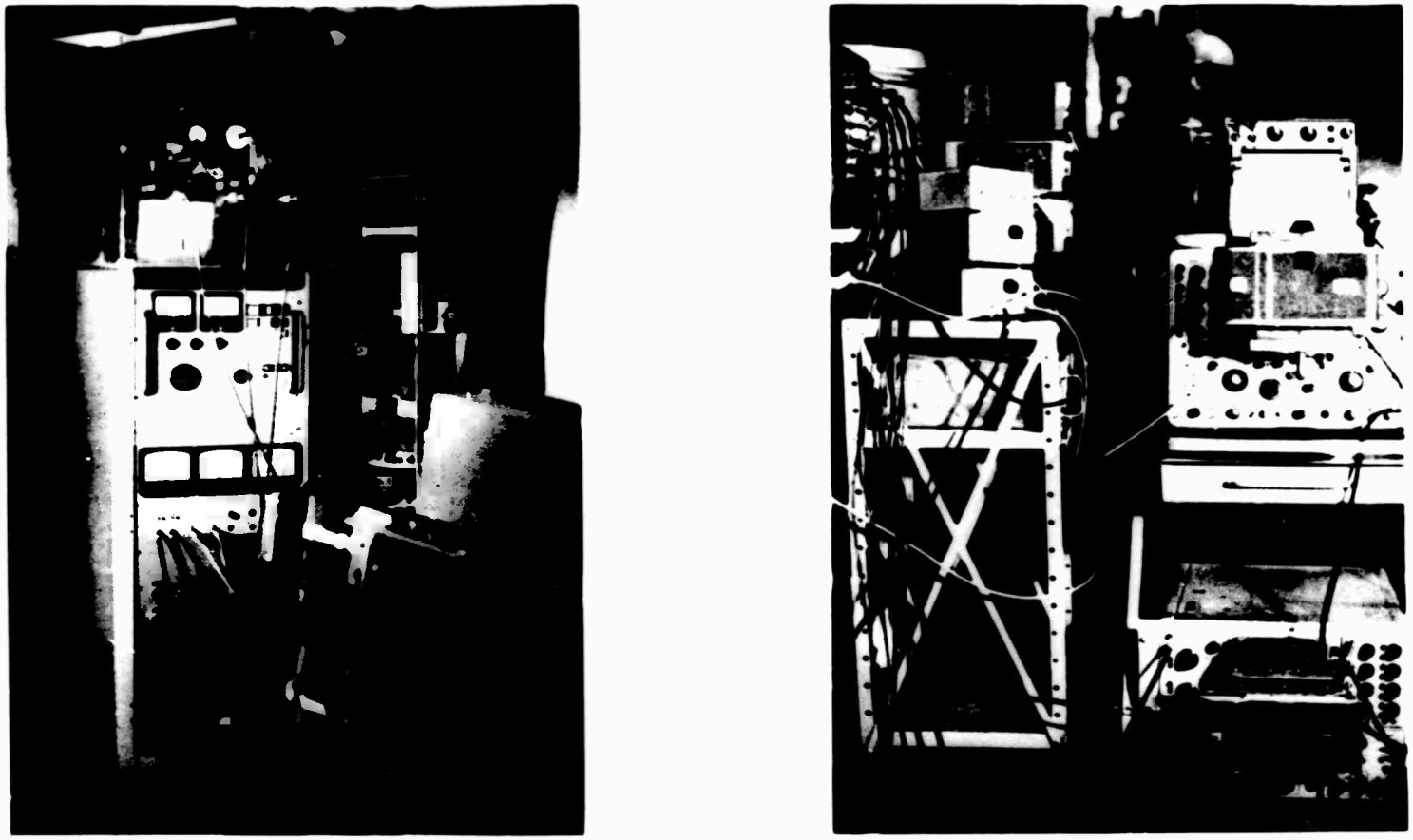

FIG. 11 PHOTOGRAPHIC VIEW OF HIGH VOLTAGE POWER SUPPLY, BATTERY, AND DATA RECORDING SYSTEM

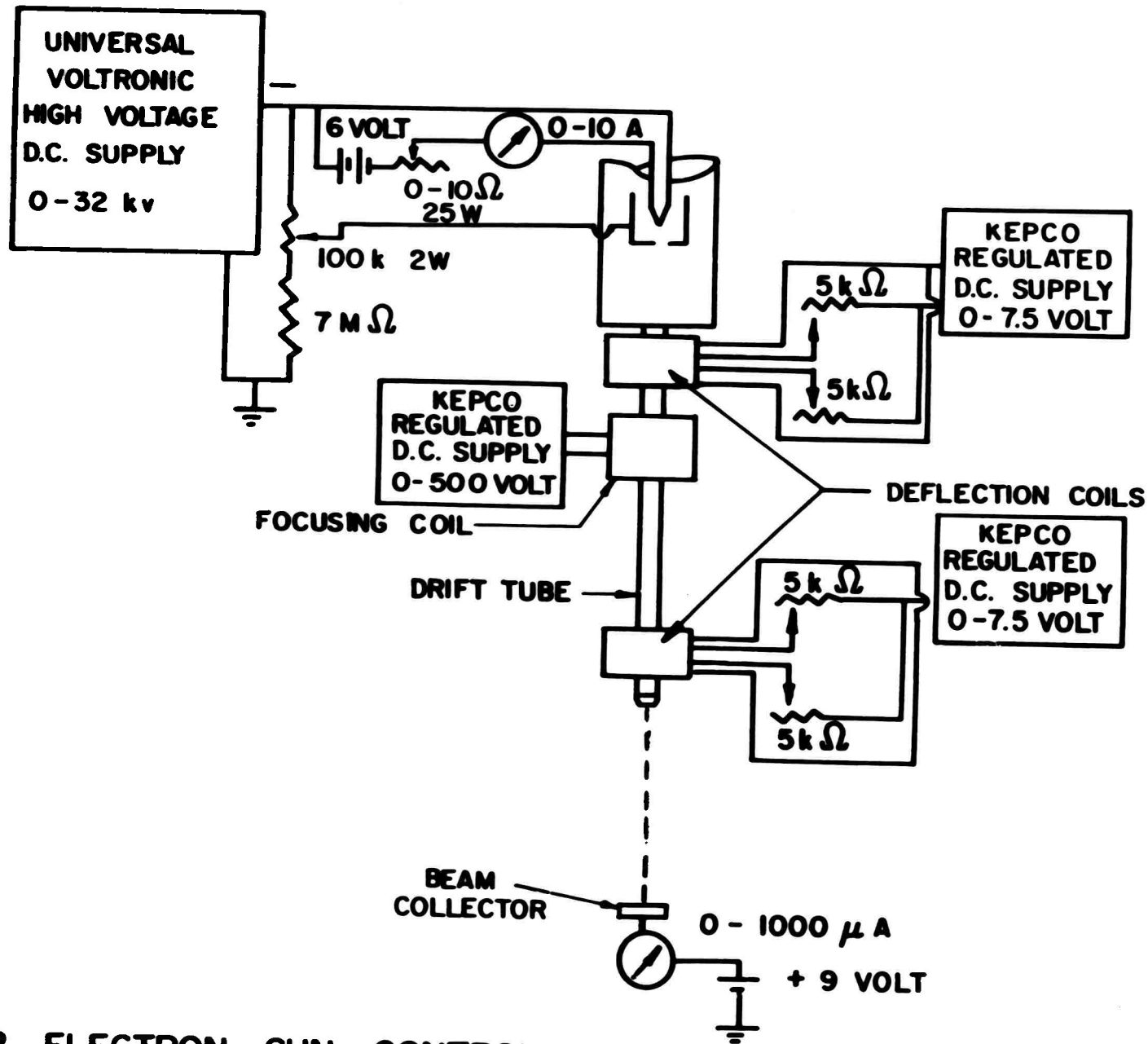

FIG. 12 ELECTRON GUN CONTROL SYSTEM

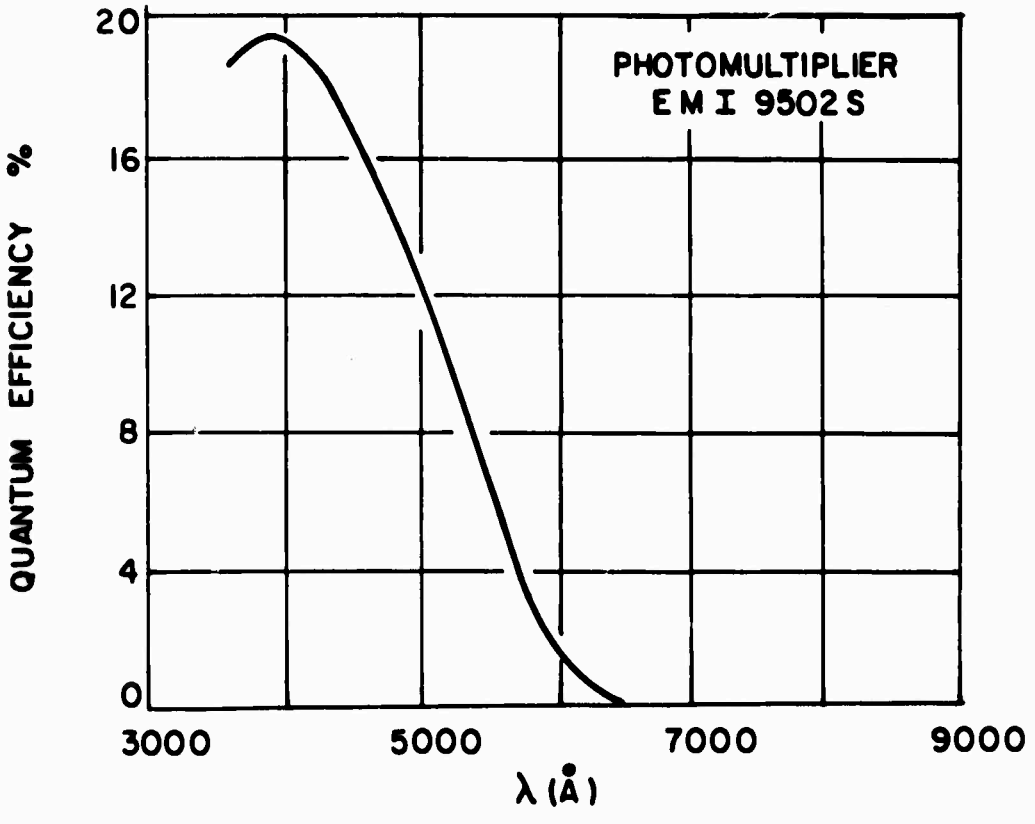

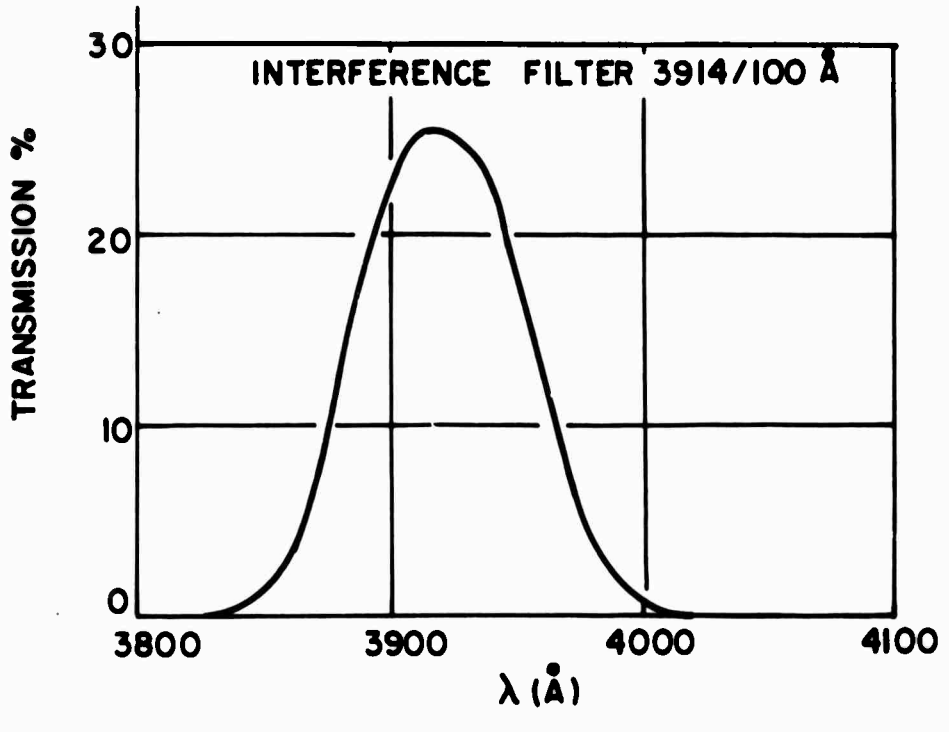

FIG.13 THE EMI PHOTOMULTIPLIER QUANTUM EFFICIENCY AND BELOW THE TRANSMISSION CURVE OF THE INTERFERENCE FILTER

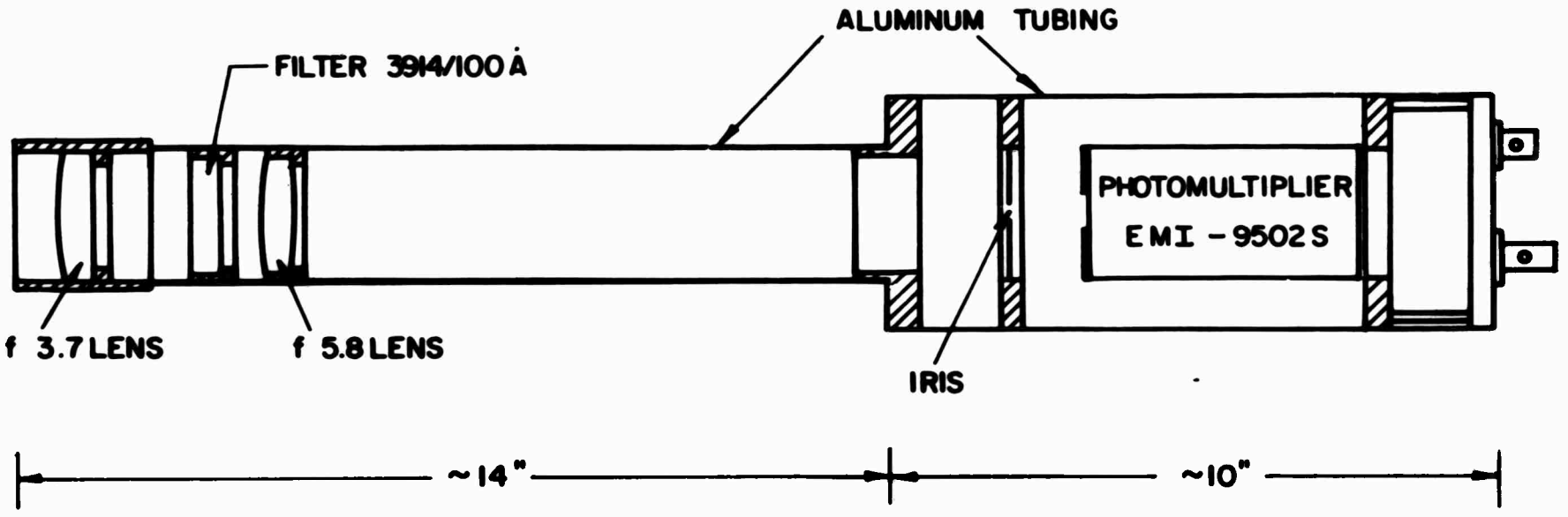

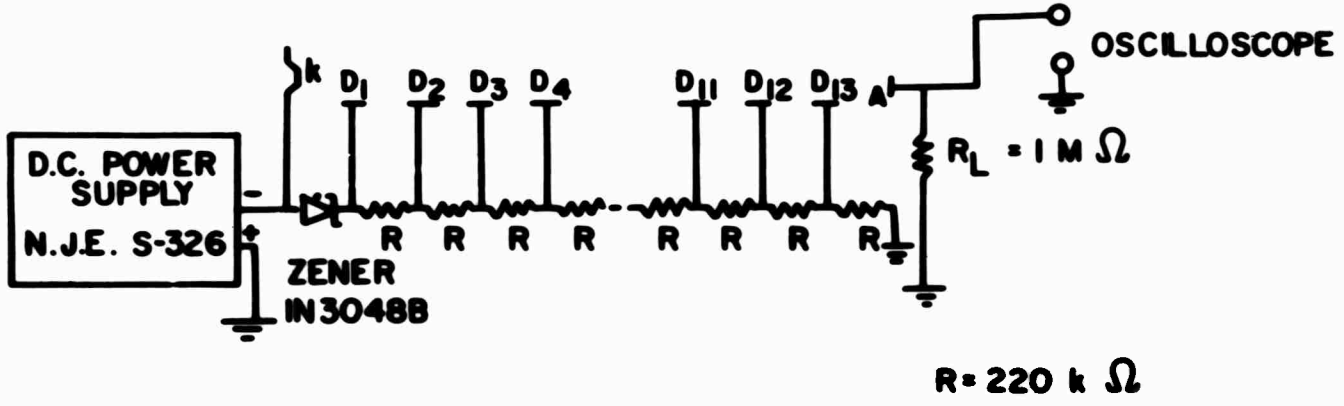

FIG. 14 THE ELECTRO-OPTICAL SYSTEM AND PHOTOMULTIPLIER CIRCUITRY

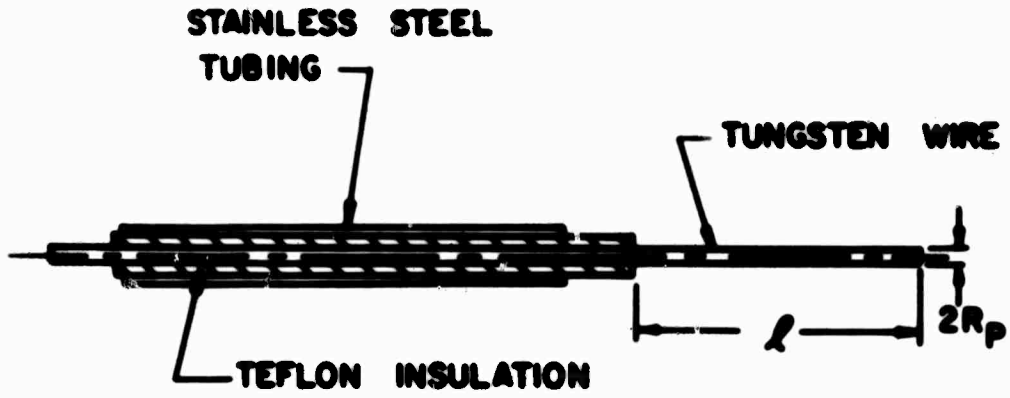

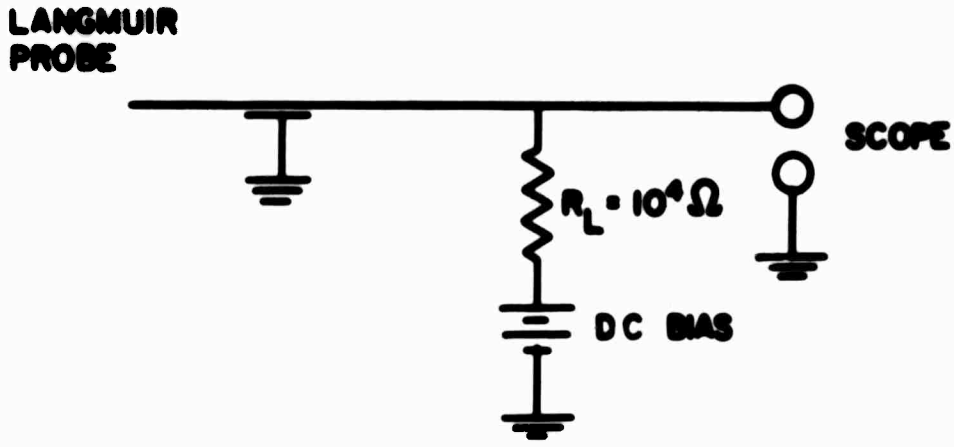

FIG. 15 LANGMUIR PROBE CONSTRUCTION AND CIRCUIT

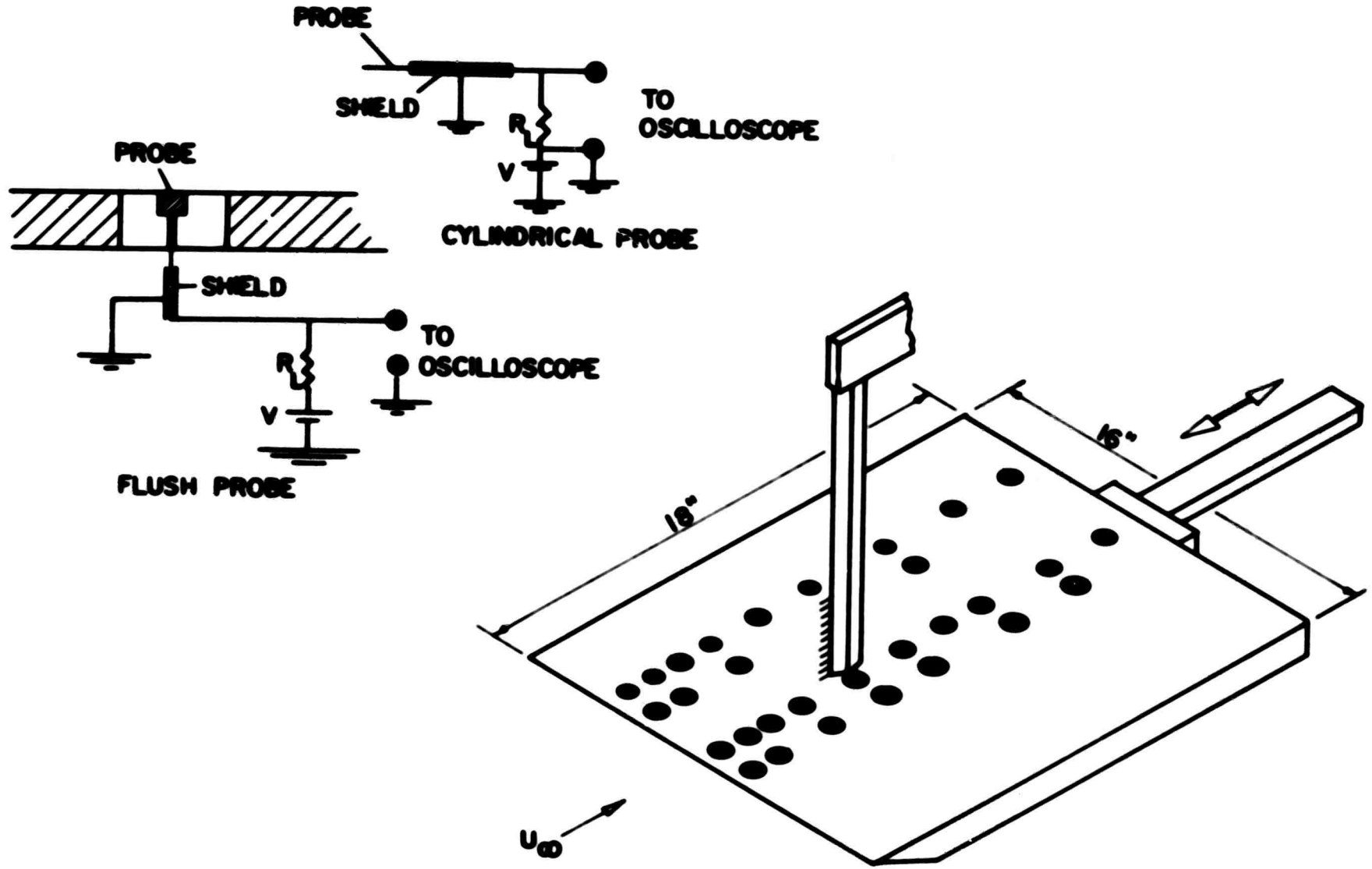

FIG. 16 PLATE WITH FLUSH PROBES, CYLINDRICAL PROBE RAKE AND ELECTROSTATIC PROBE CIRCUITRY

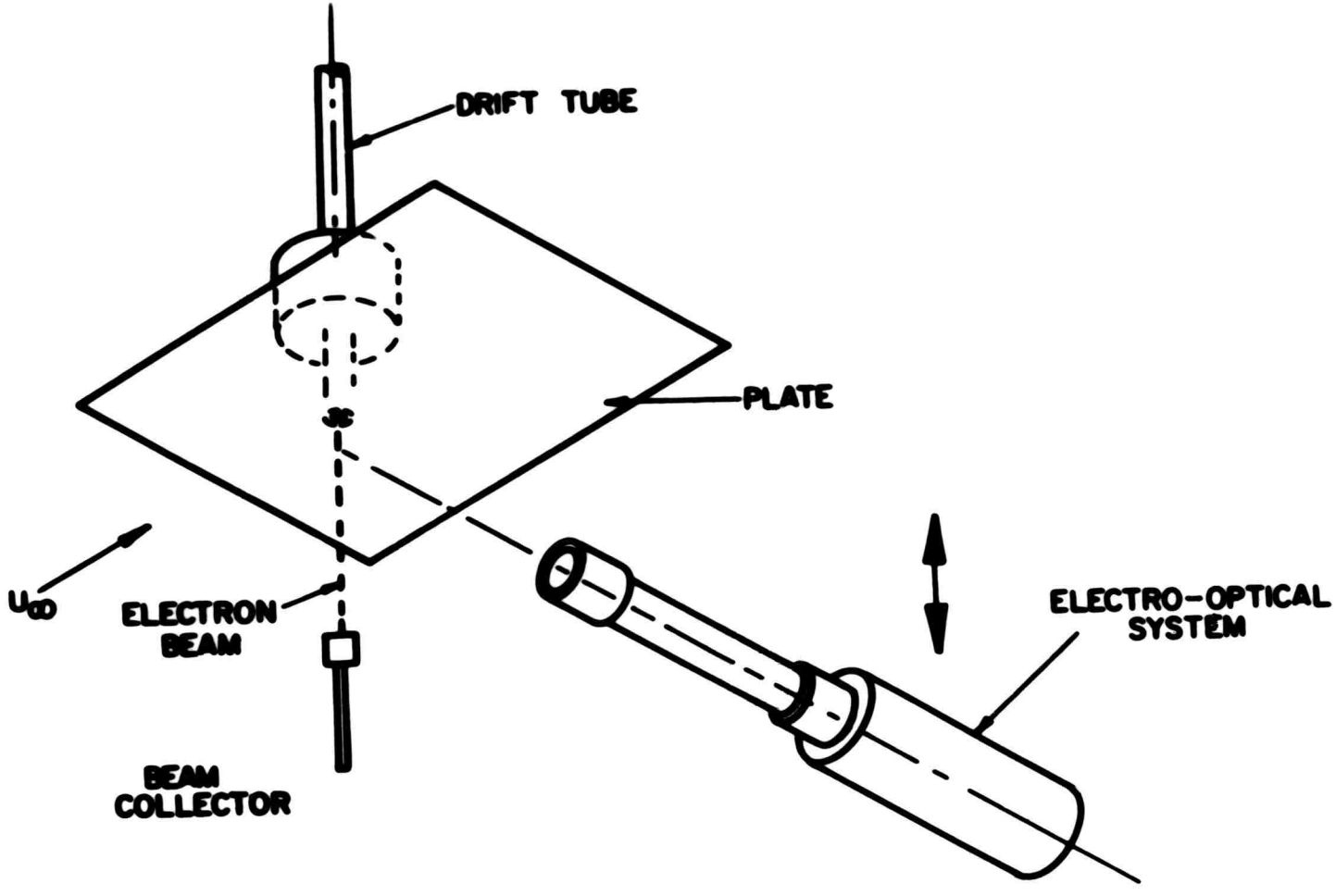

FIG. 17 SETUP FOR DENSITY MEASUREMENTS ABOUT THE PLATE

FIG. 18 PHOTOGRAPHIC VIEW OF THE PLATE, ELECTRON GUN AND ELECTRO-OPTICAL SYSTEMS

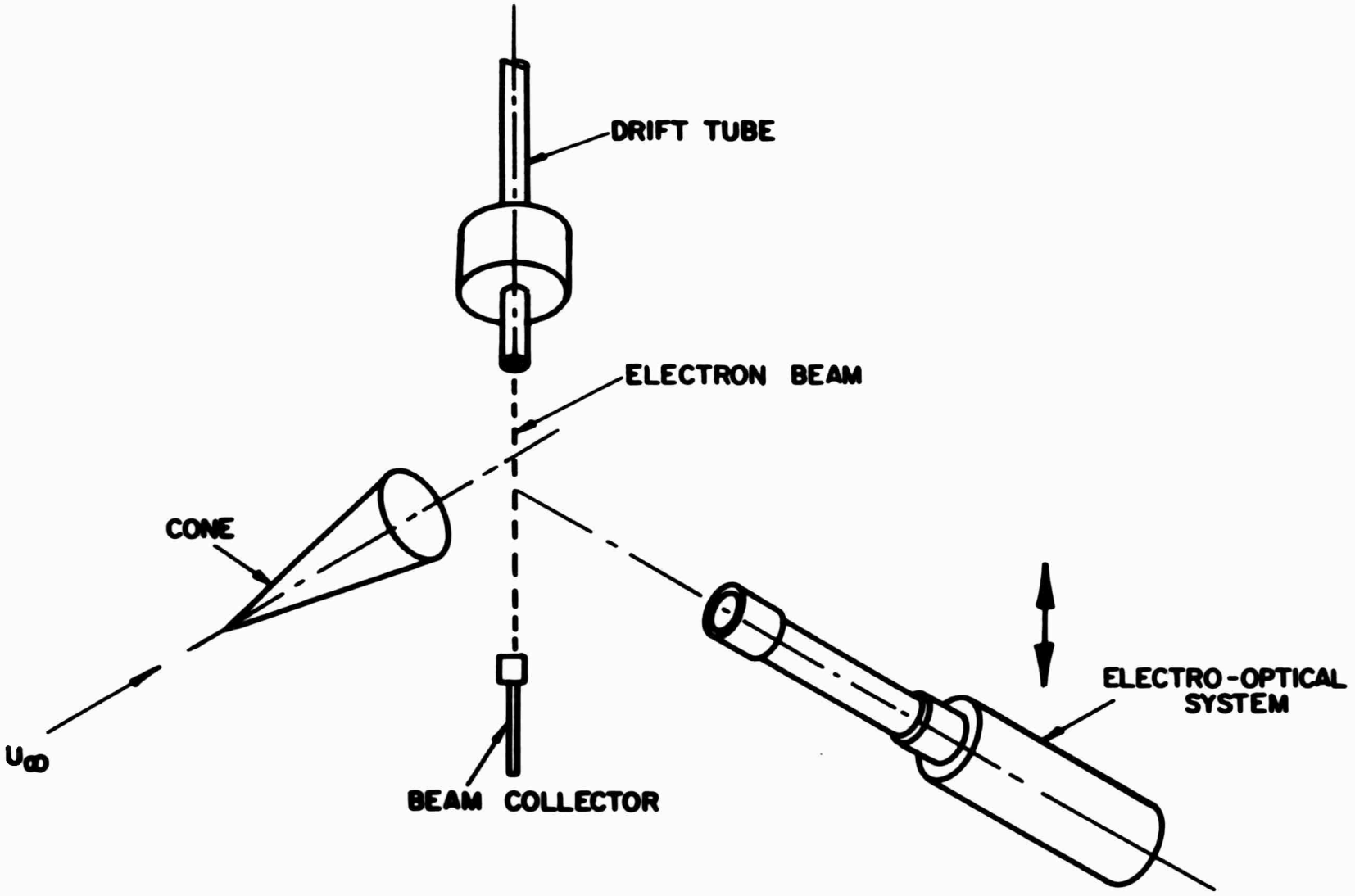

FIG. 19 EXPERIMENTAL SETUP FOR CONE WAKE DENSITY SURVEY

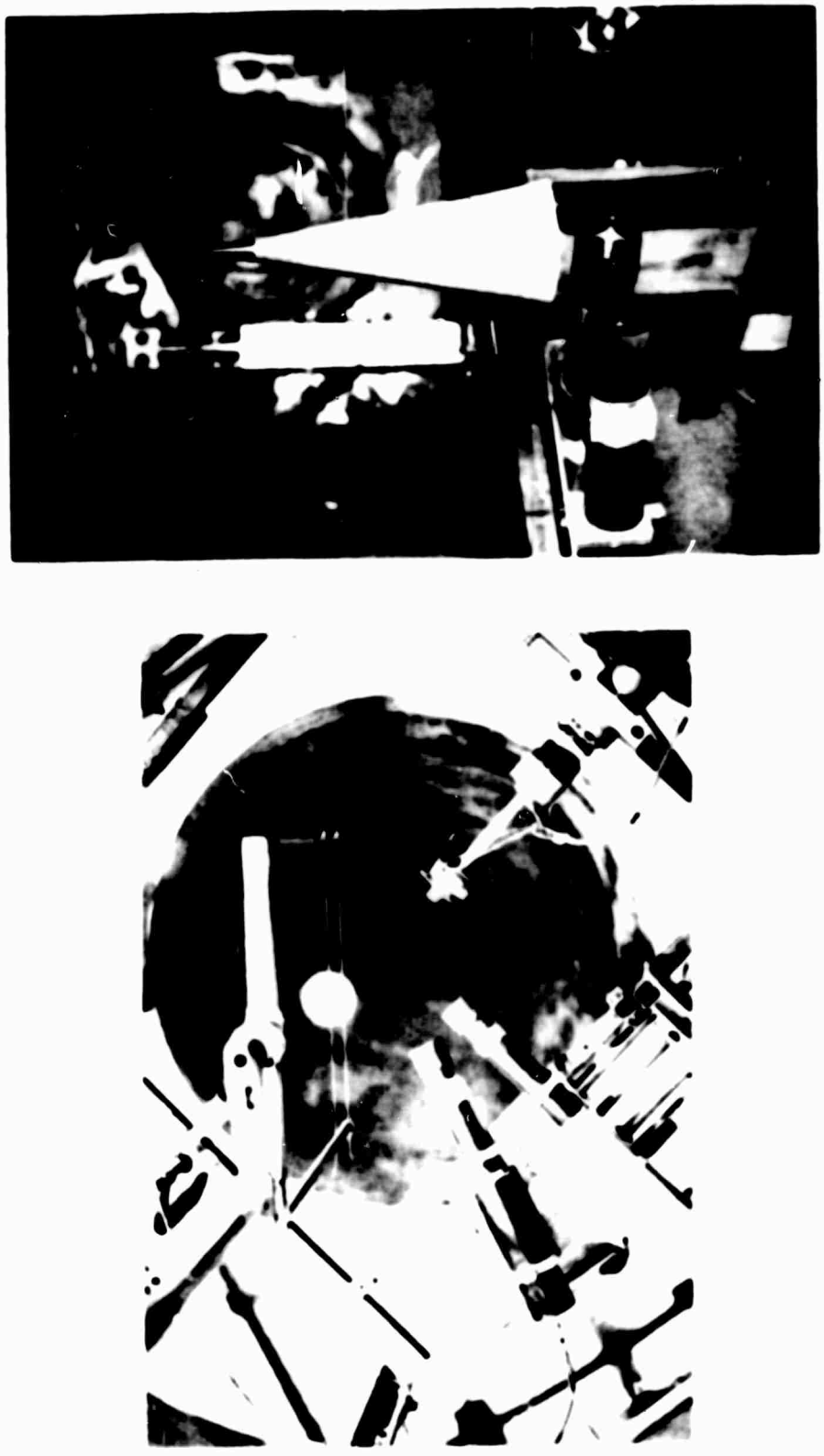

FIG. 20 PHOTOGRAPHIC VIEW OF THE CONE SUSPENDED IN THE TEST SECTION

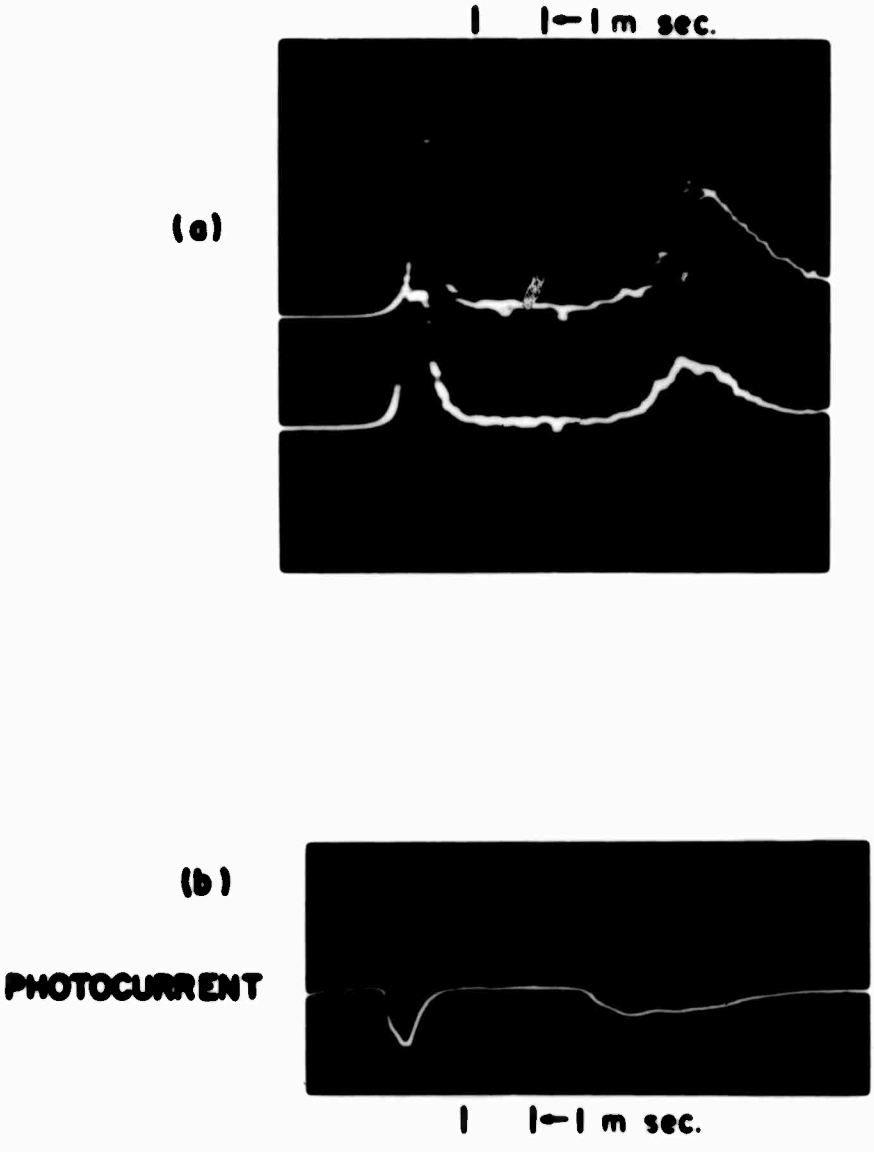

FIG. 21 (a) RESPONSE OF CYLINDRICAL ELECTROSTATIC PROBES
(b) FREE STREAM PHOTOCURRENT, NO ELECTRON BEAM

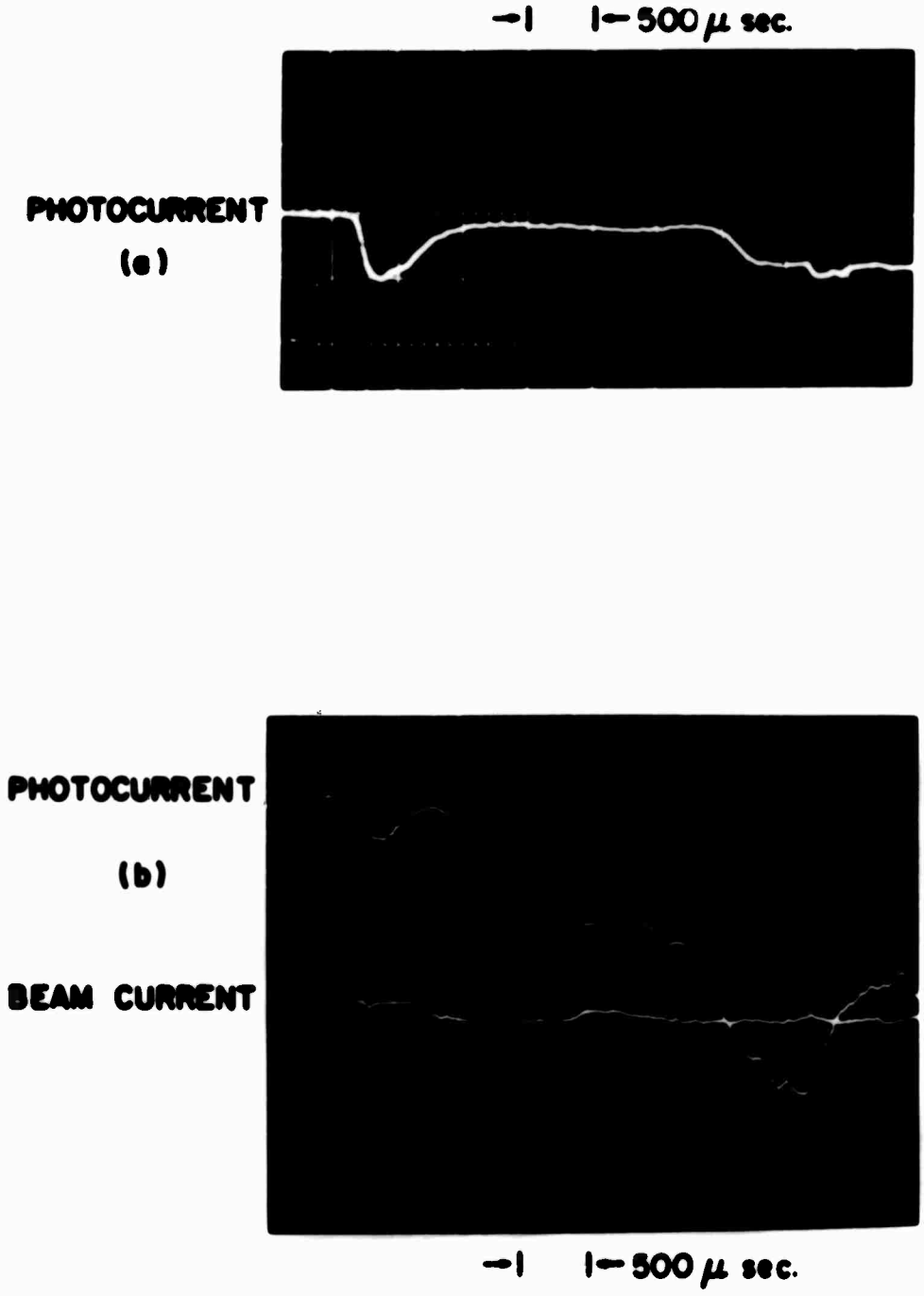

FIG. 22 (a) FREE STREAM PHOTOCURRENT, NO ELECTRON BEAM

(b) FREE STREAM PHOTOCURRENT, WITH ELECTRON BEAM

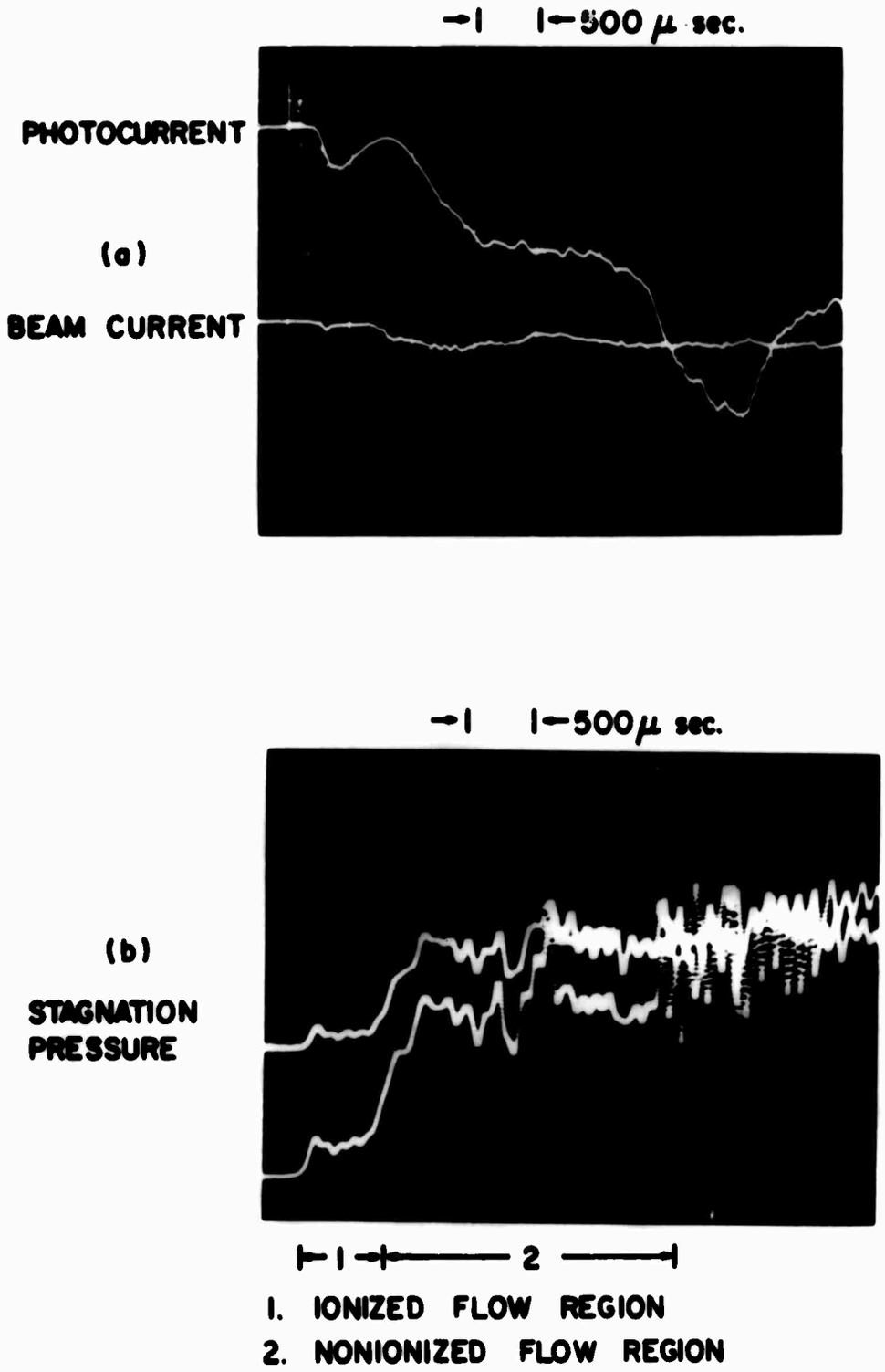

FIG. 23 (a) FREE STREAM PHOTOCURRENT, WITH BEAM
(b) FREE STREAM STAGNATION PRESSURE

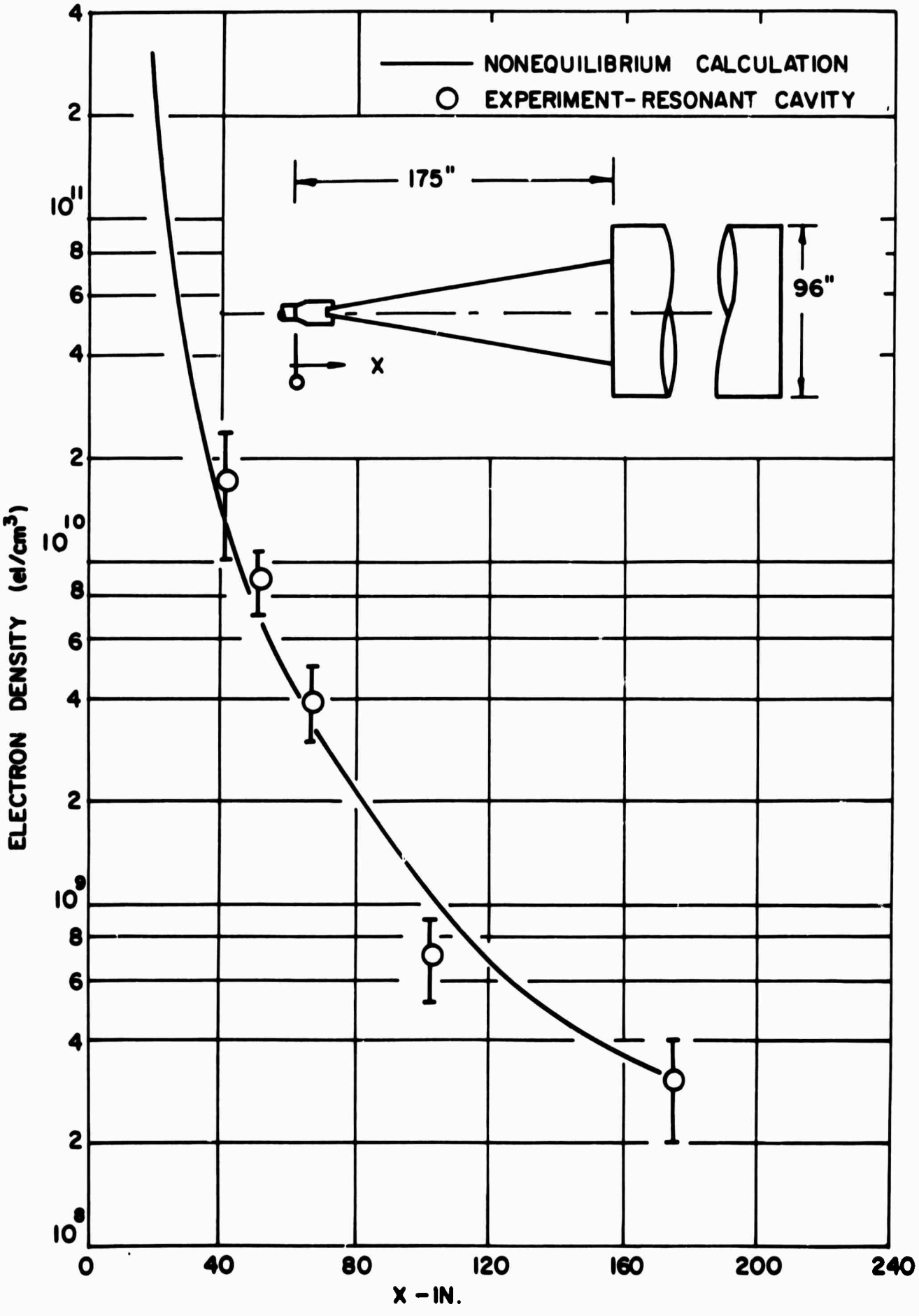

FIG.24 ELECTRON NUMBER DENSITY ALONG THE NOZZLE

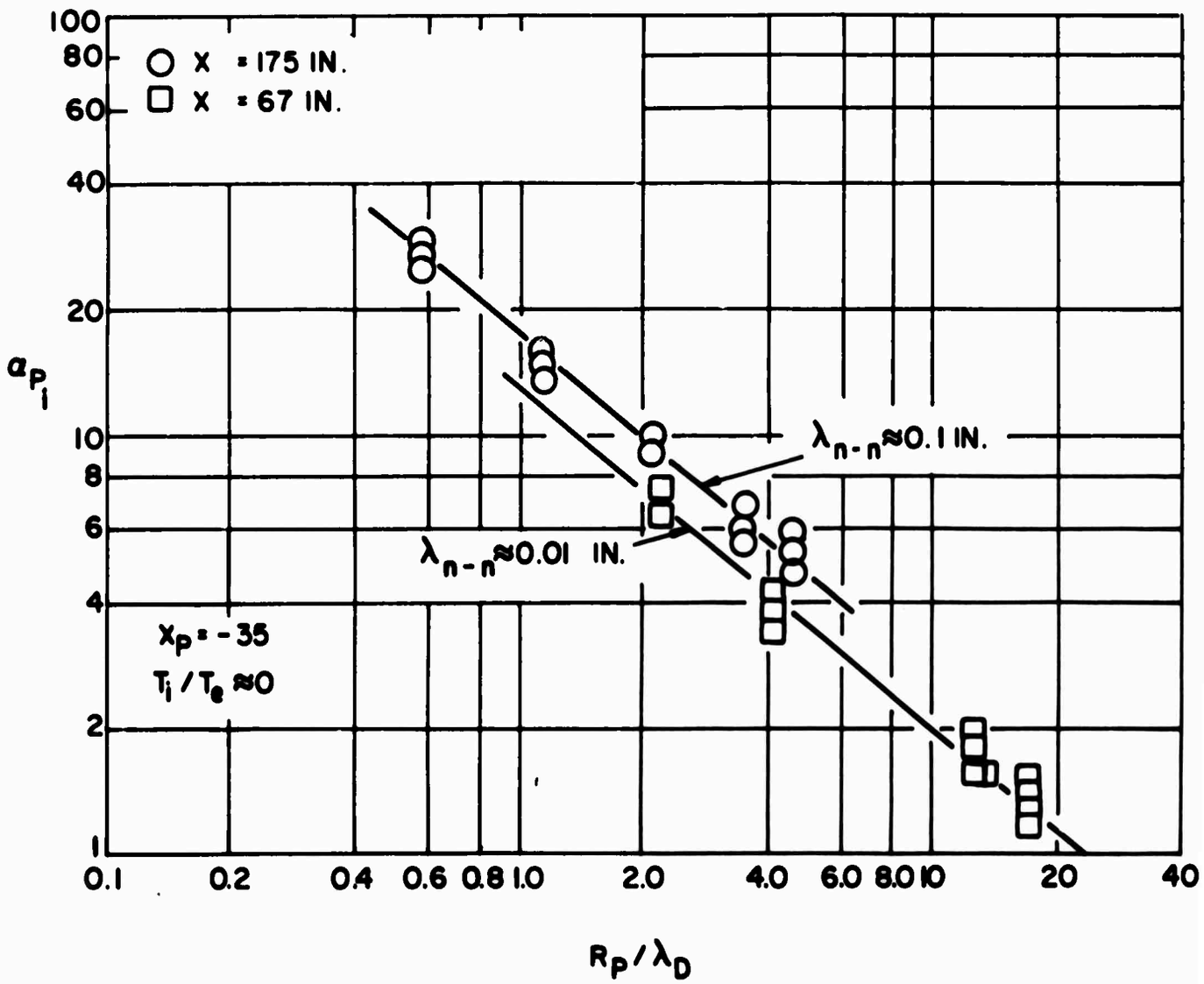

FIG. 25 DIMENSIONLESS ION CURRENT (α_{P_i}) DEPENDENC
ON NEUTRAL MEAN PATH λ_{n-n}

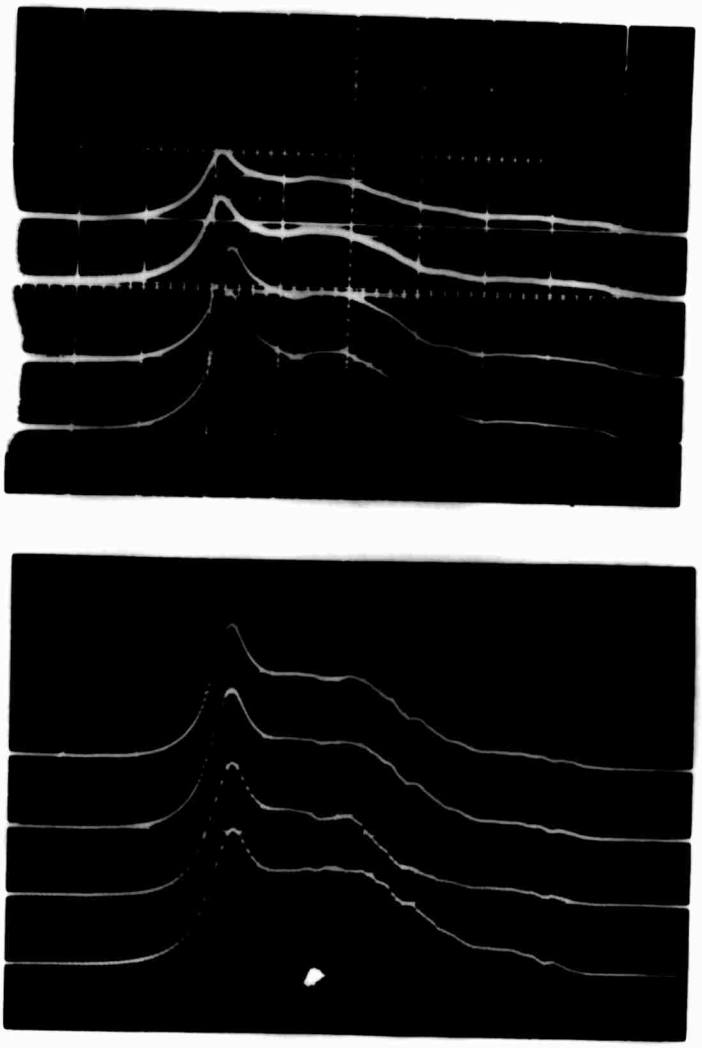

FIG. 26 RESPONSE OF ELECTROSTATIC PROBES IN THE FLOW ABOUT THE PLATE. TOP TO BOTTOM REPRESENT PLATE SURFACE TO FREE STREAM RESPONSE

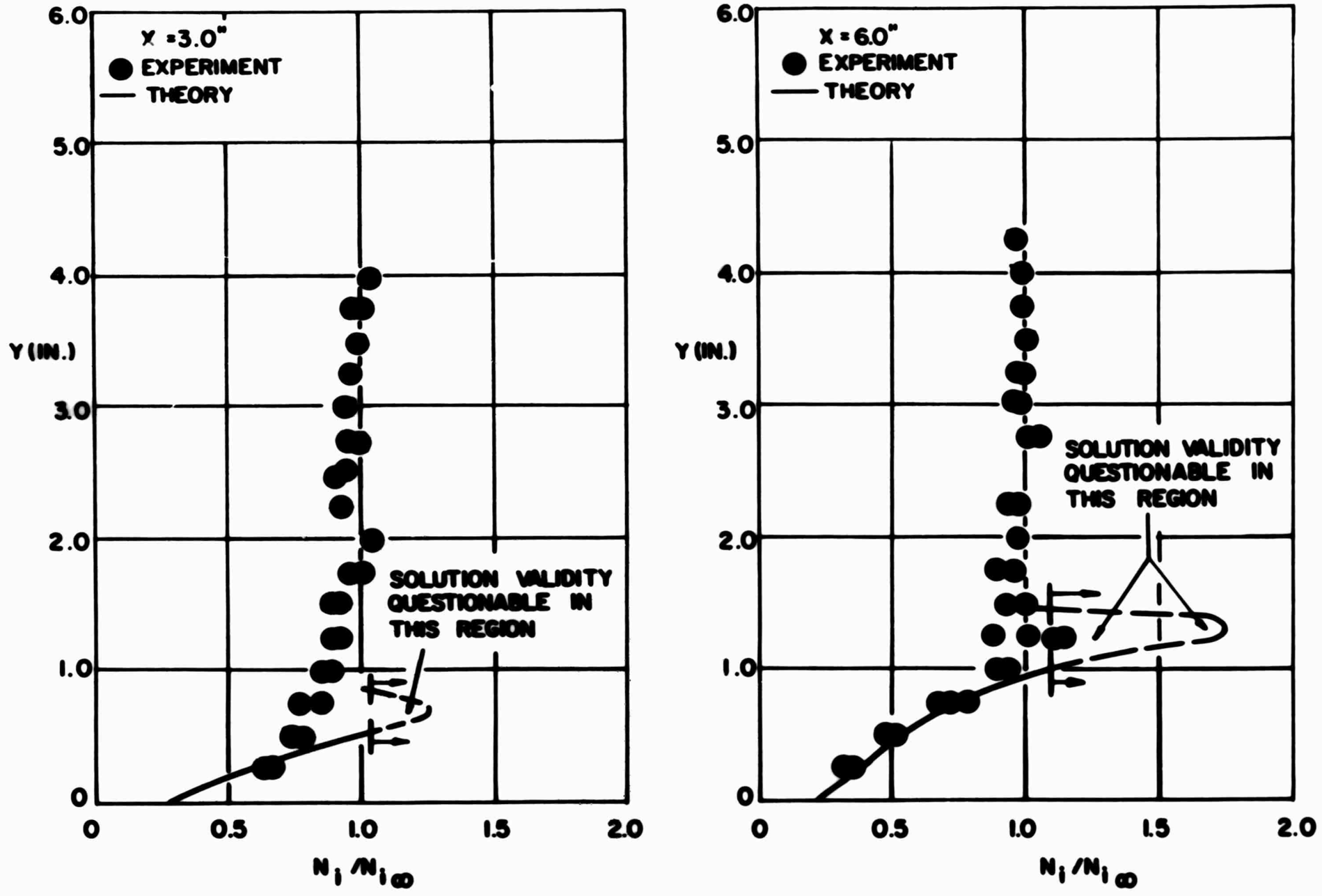

FIG. 27 NORMALIZED ION DENSITY PROFILE NORMAL TO THE PLATE

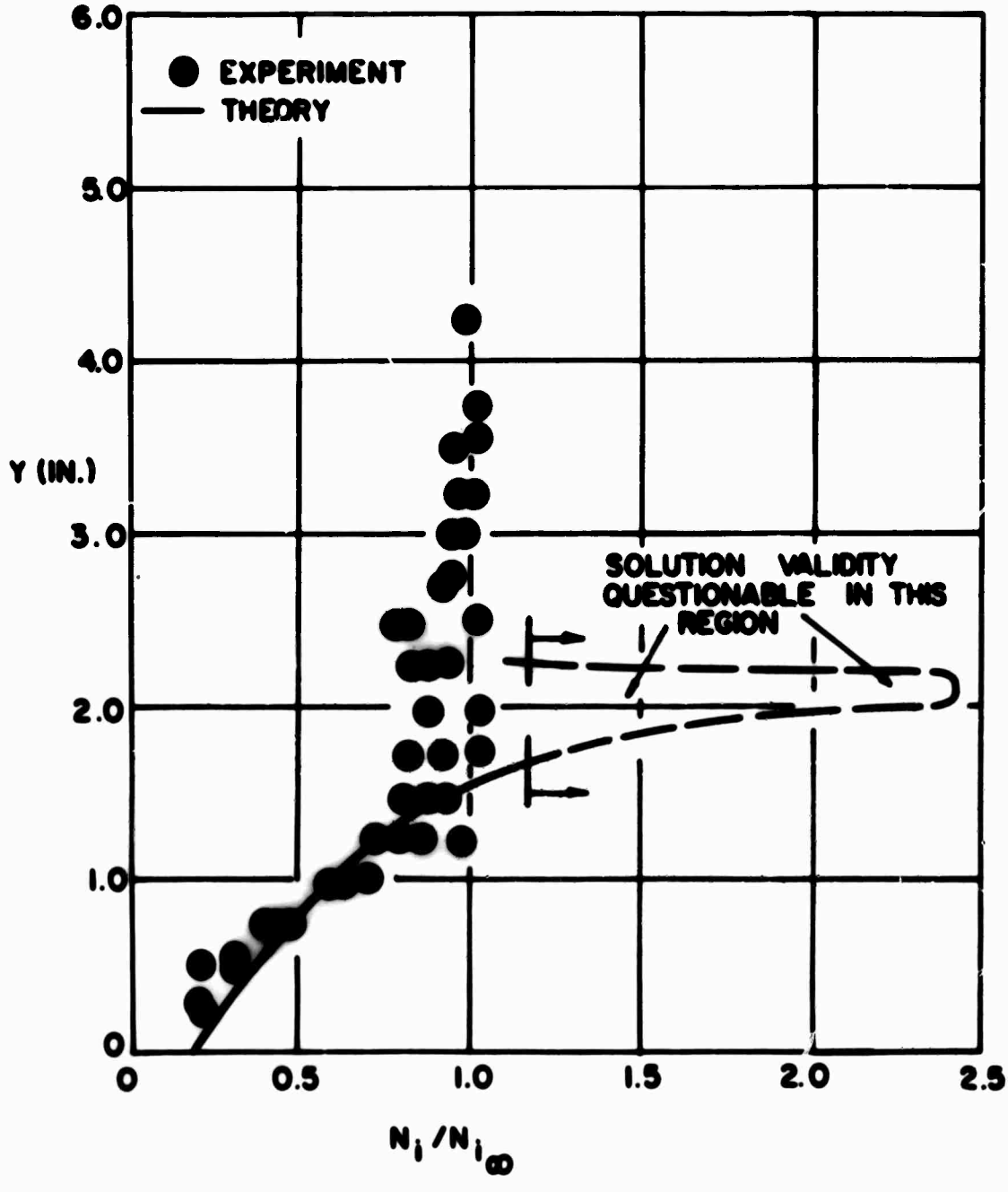

FIG. 28 NORMALIZED ION DENSITY PROFILE NORMAL TO THE PLATE AT X=9.0"

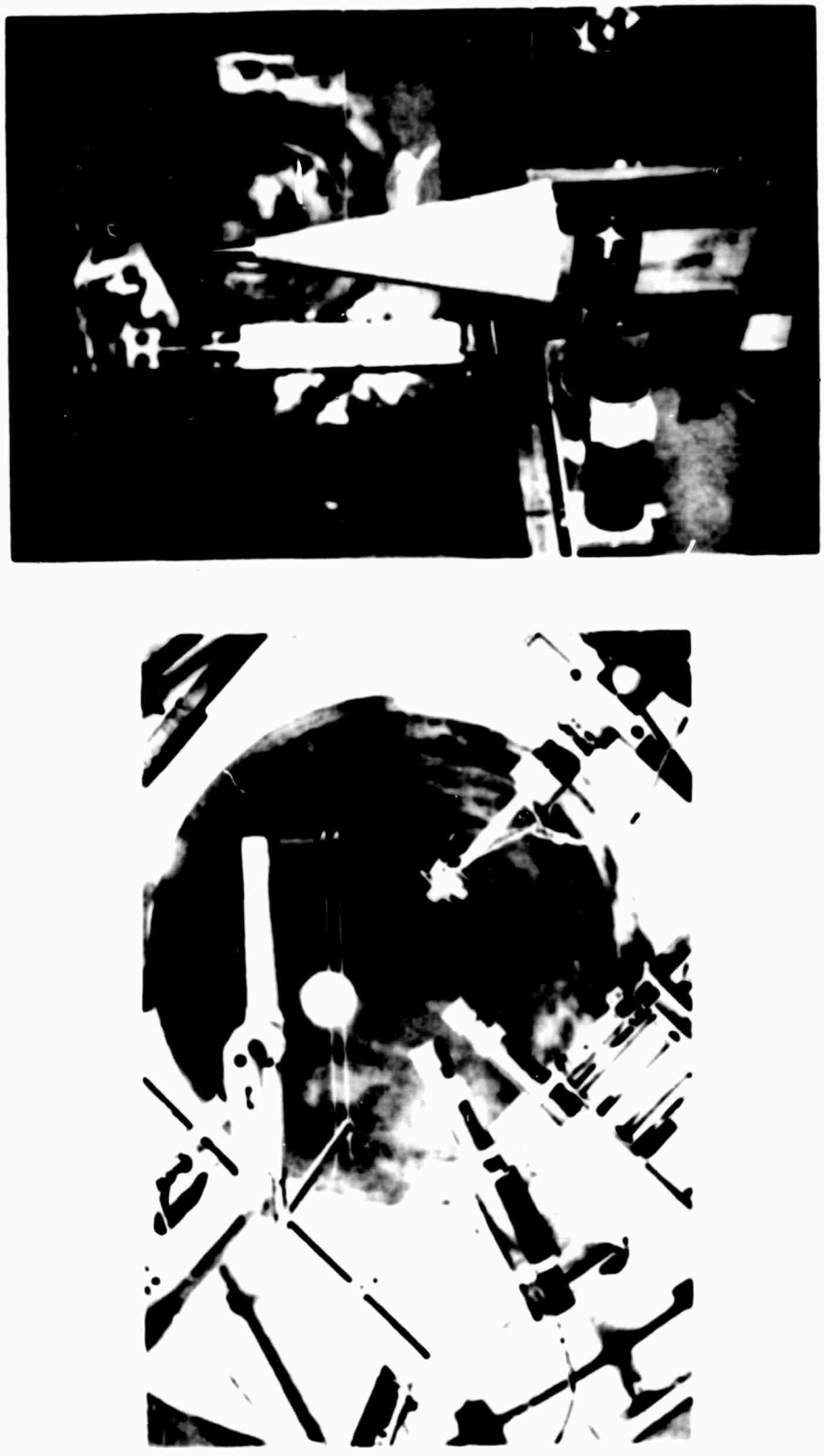

FIG. 20 PHOTOGRAPHIC VIEW OF THE CONE SUSPENDED IN THE TEST SECTION

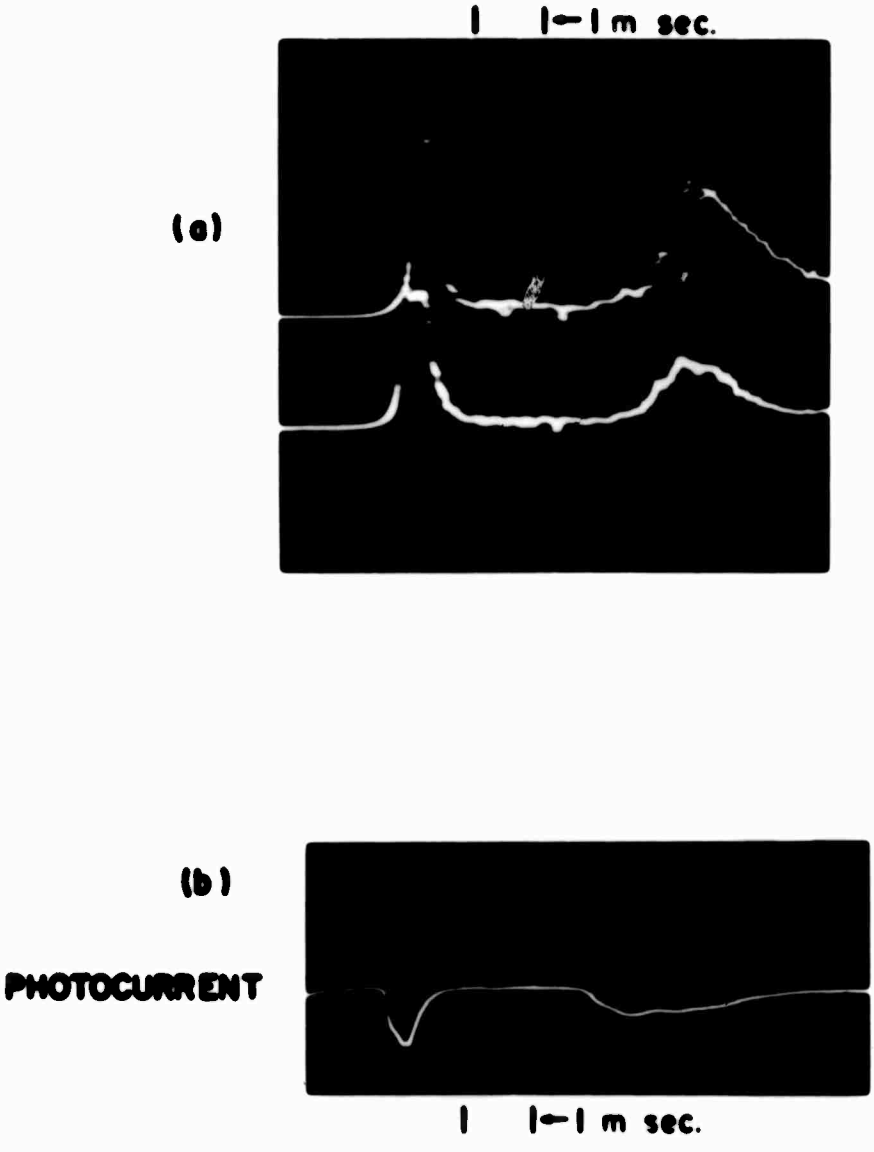

FIG. 21 (a) RESPONSE OF CYLINDRICAL ELECTROSTATIC PROBES
(b) FREE STREAM PHOTOCURRENT, NO ELECTRON BEAM

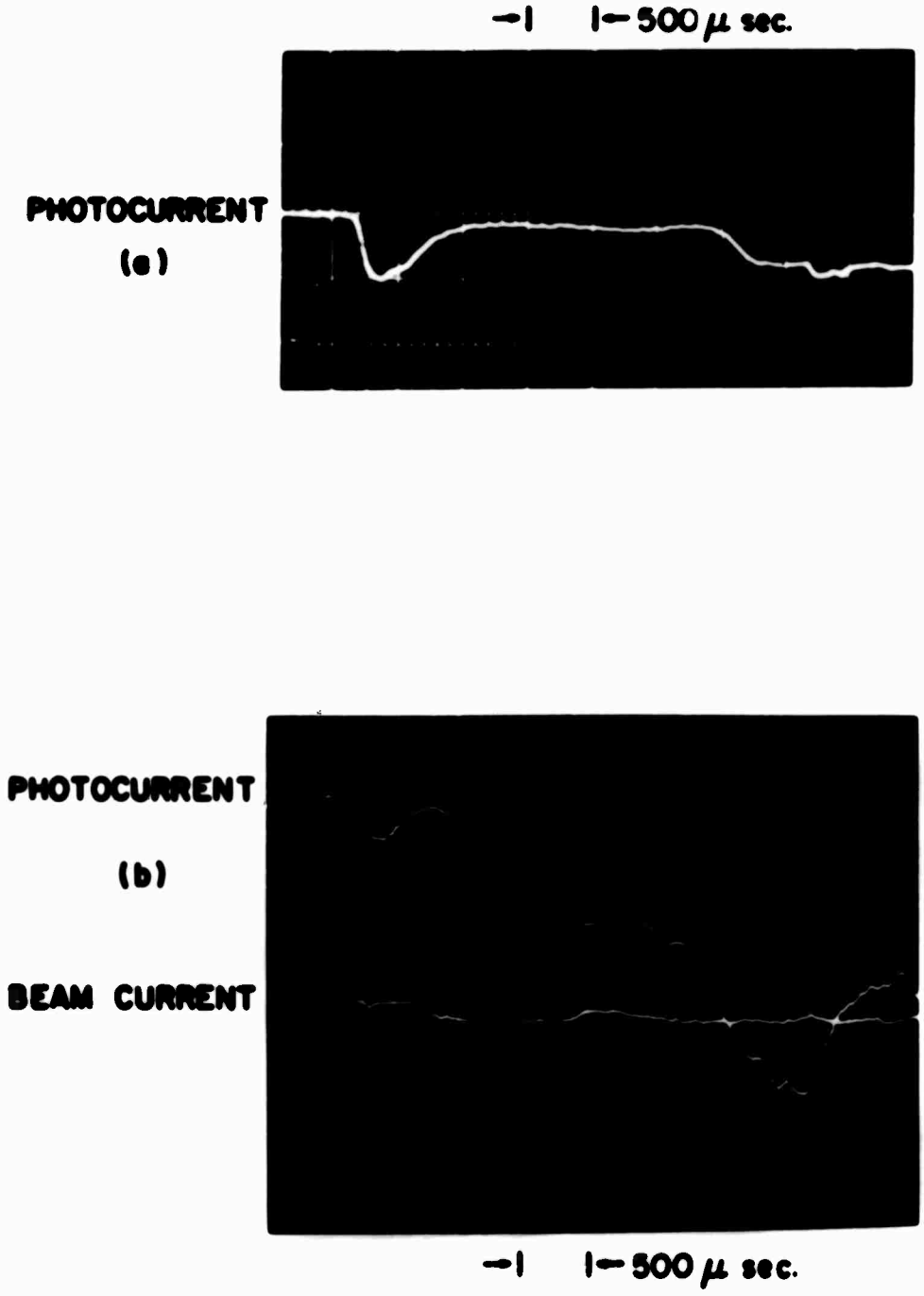

FIG. 22 (a) FREE STREAM PHOTOCURRENT, NO ELECTRON BEAM

(b) FREE STREAM PHOTOCURRENT, WITH ELECTRON BEAM

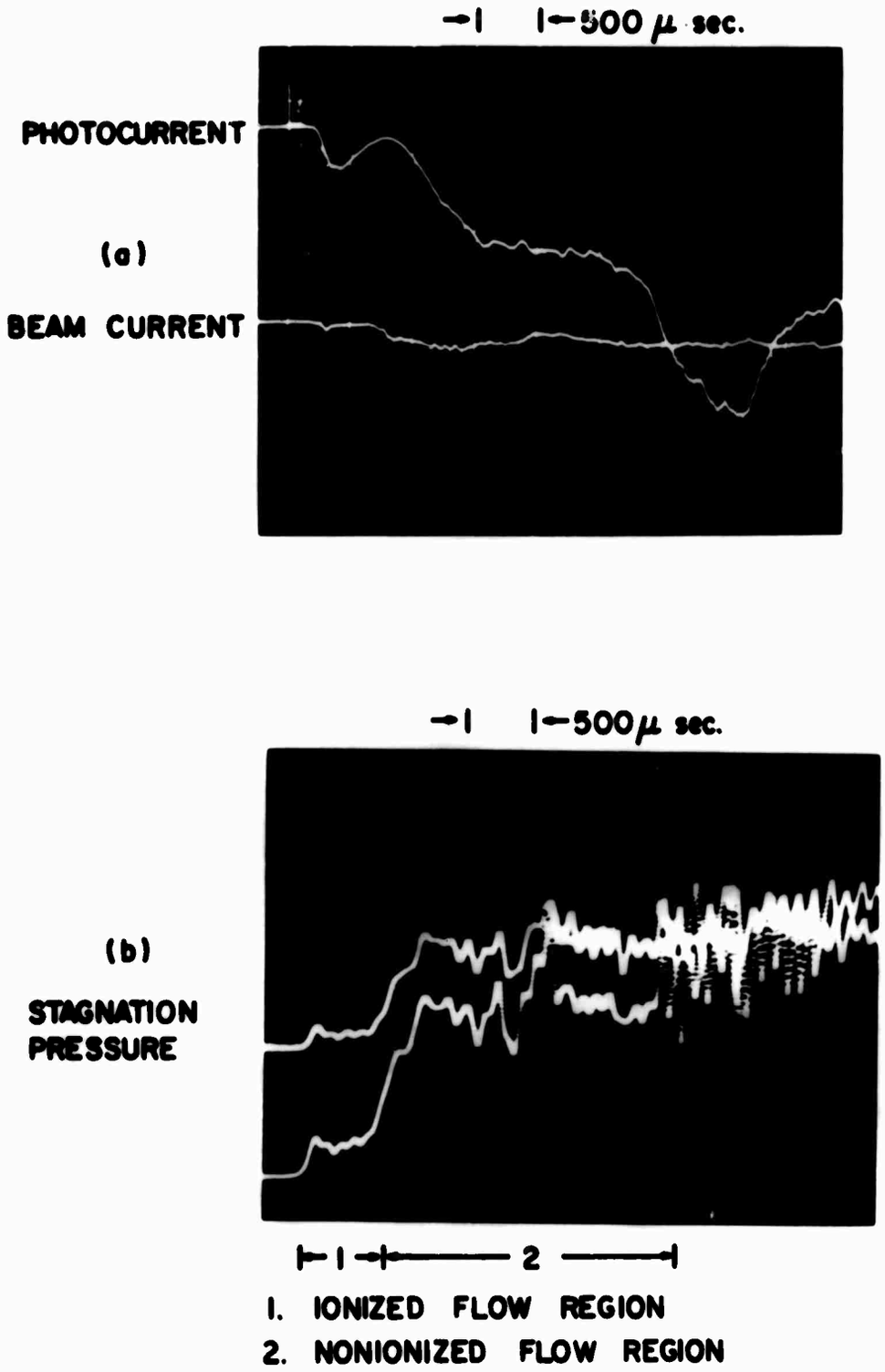

FIG. 23 (a) FREE STREAM PHOTOCURRENT, WITH BEAM
(b) FREE STREAM STAGNATION PRESSURE

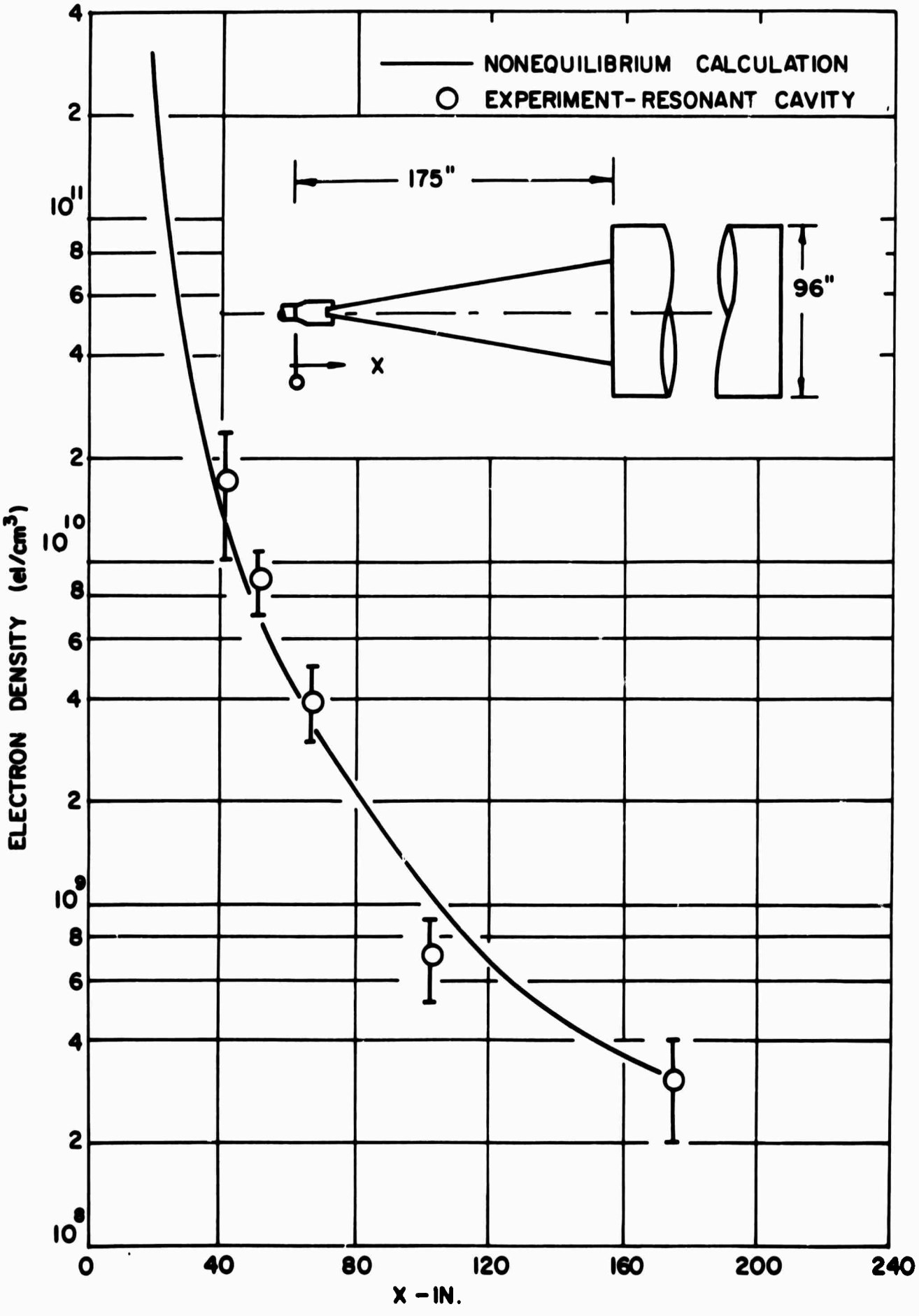

FIG.24 ELECTRON NUMBER DENSITY ALONG THE NOZZLE

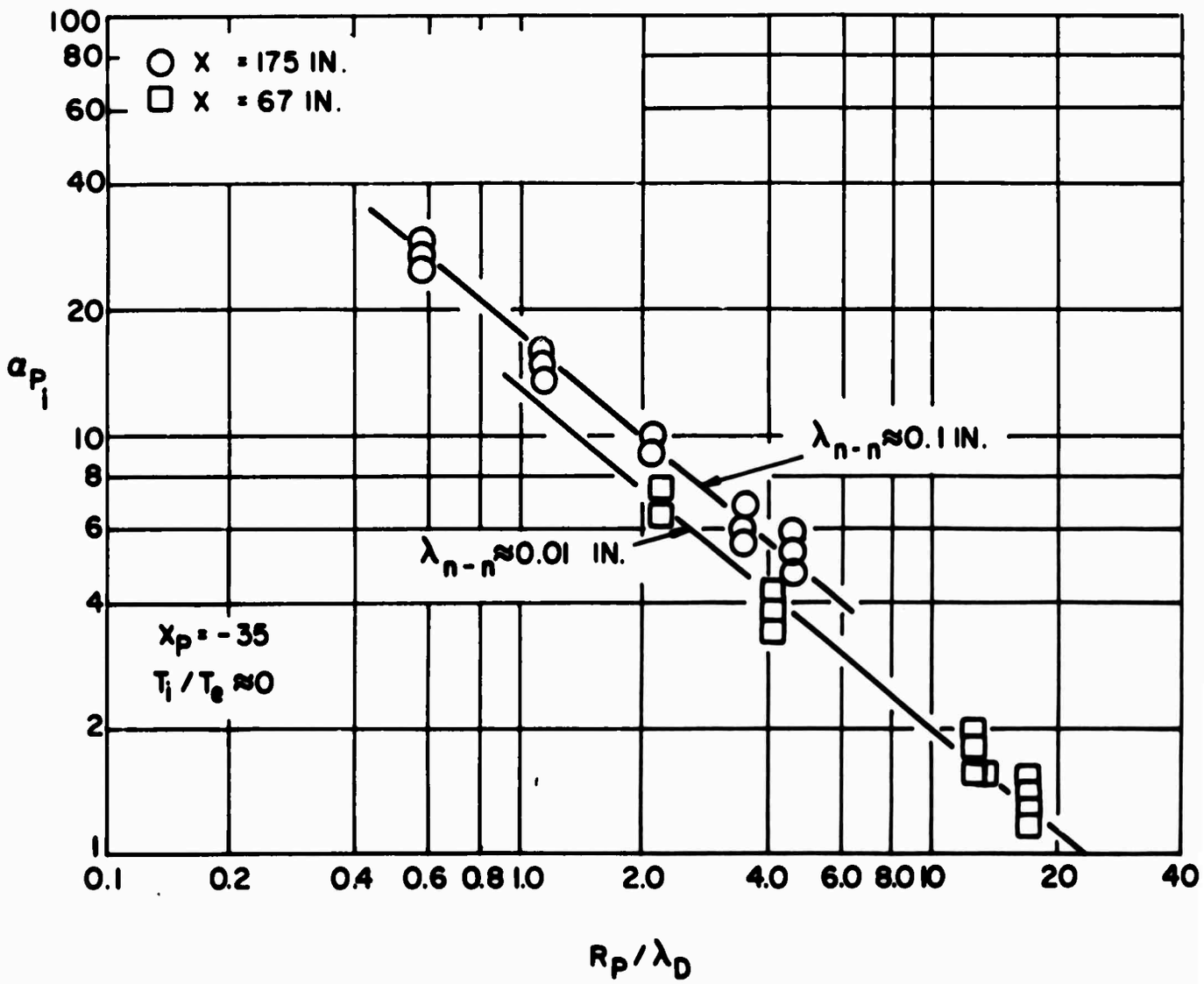

FIG. 25 DIMENSIONLESS ION CURRENT (α_{P_i}) DEPENDENC
ON NEUTRAL MEAN PATH λ_{n-n}

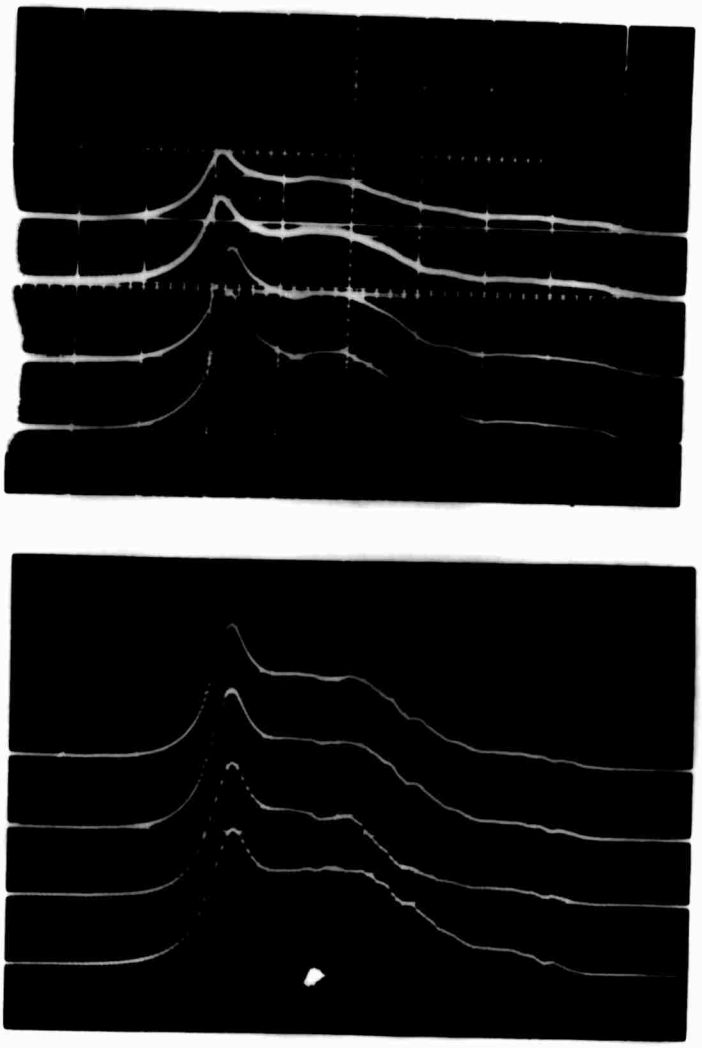

FIG. 26 RESPONSE OF ELECTROSTATIC PROBES IN THE FLOW ABOUT THE PLATE. TOP TO BOTTOM REPRESENT PLATE SURFACE TO FREE STREAM RESPONSE

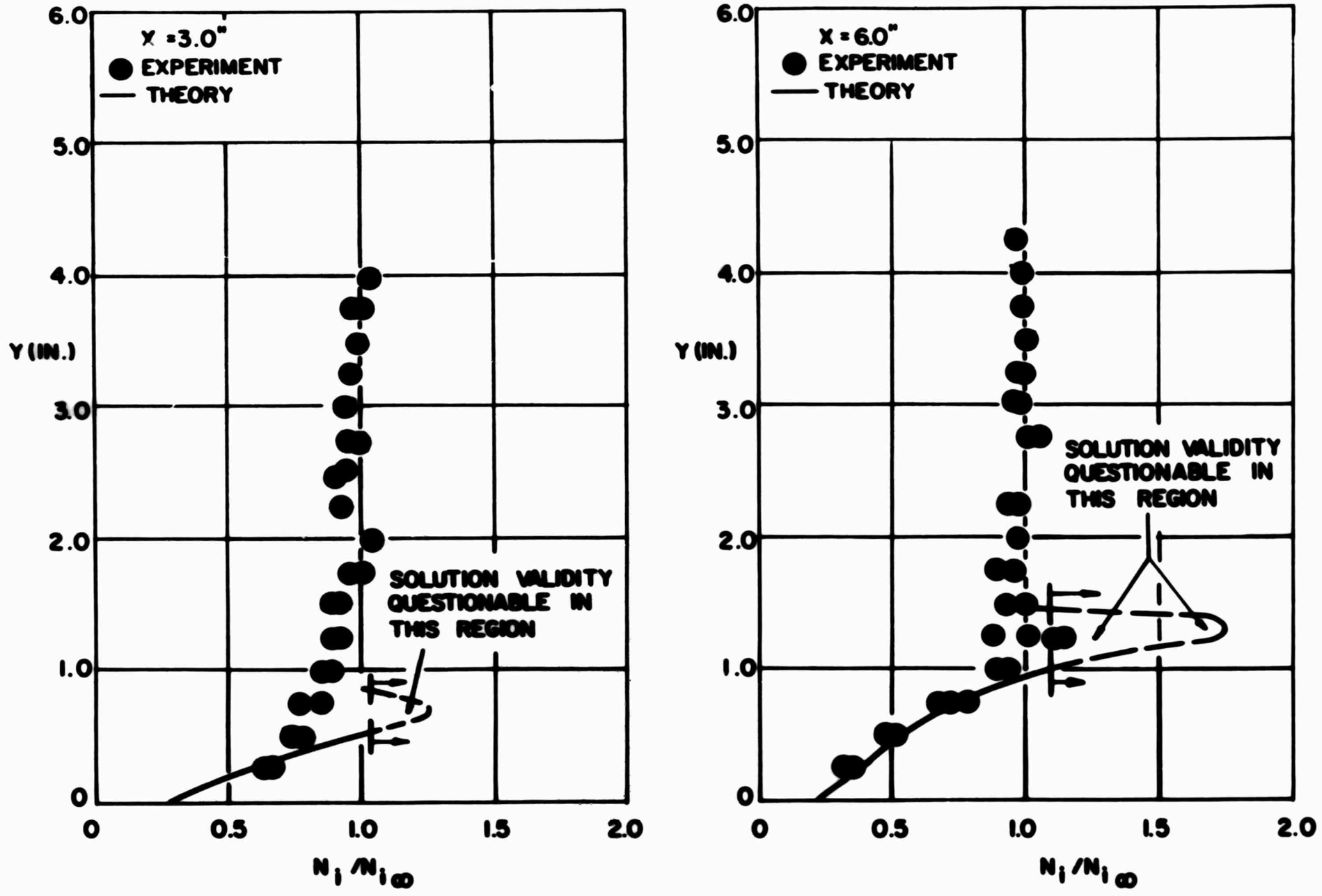

FIG. 27 NORMALIZED ION DENSITY PROFILE NORMAL TO THE PLATE

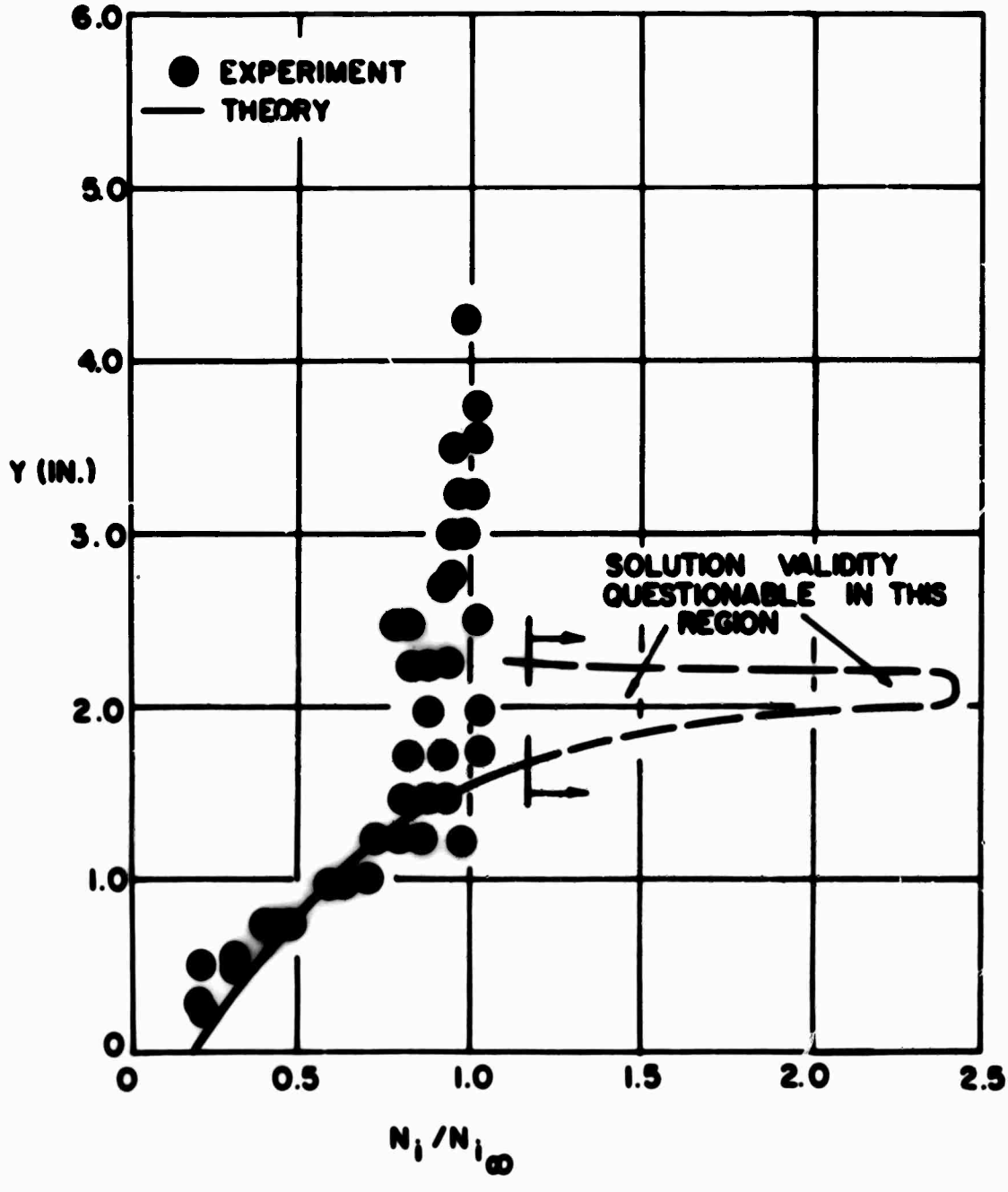

FIG. 28 NORMALIZED ION DENSITY PROFILE NORMAL TO THE PLATE AT X=9.0"

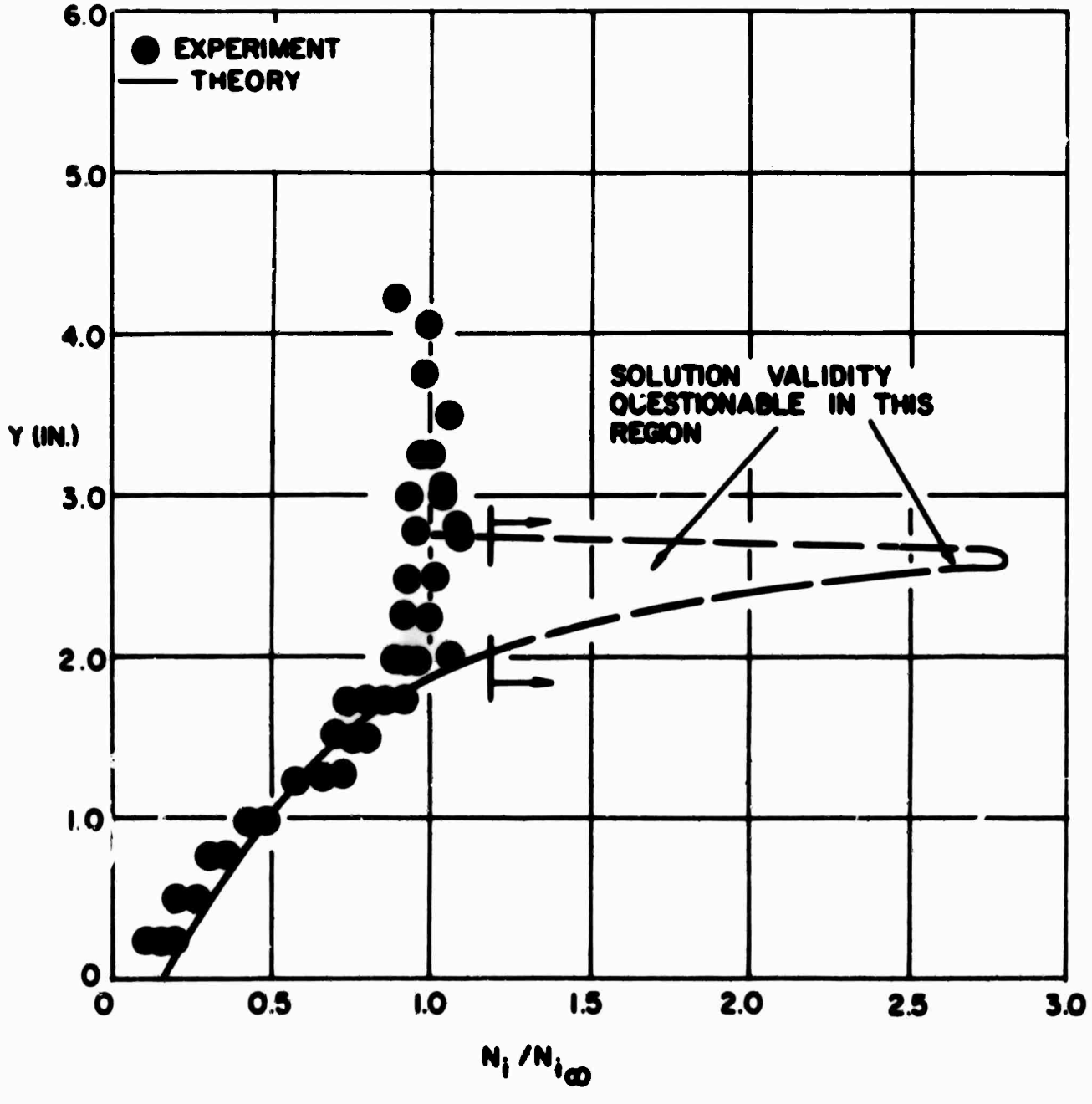

FIG. 29 NORMALIZED ION DENSITY PROFILE NORMAL TO THE PLATE AT X = 12.0"

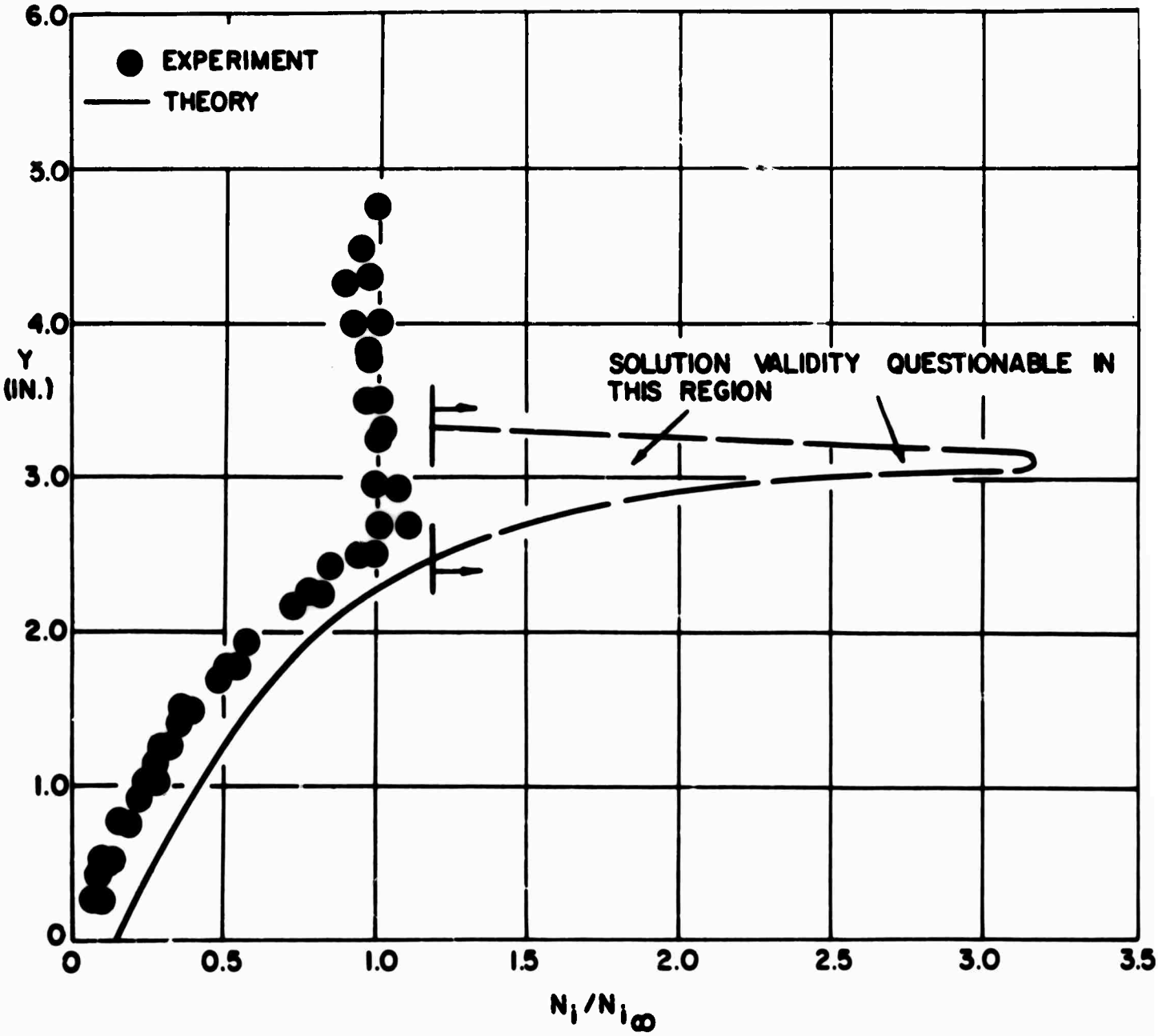

FIG. 30 NORMALIZED ION DENSITY PROFILE NORMAL TO THE PLATE AT X = 15.0"

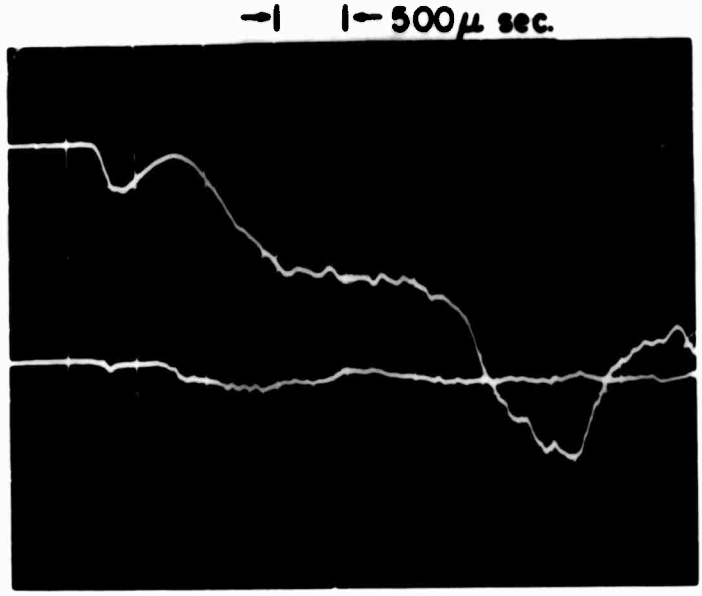

(a)

FREE STREAM

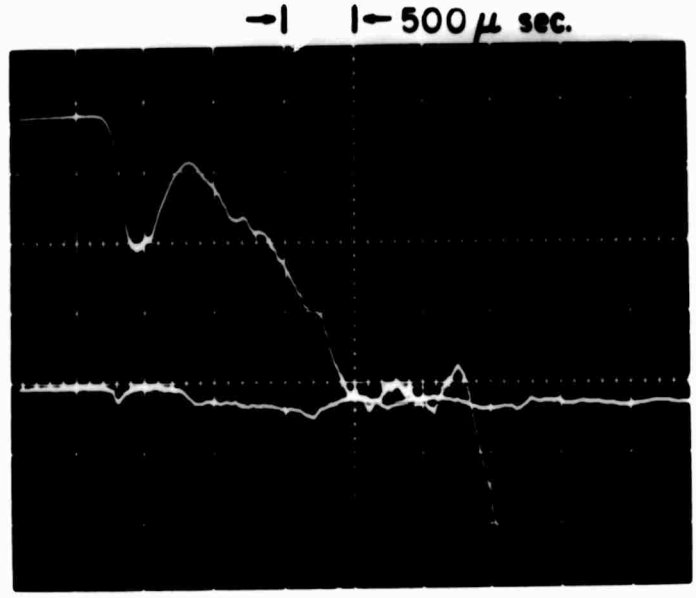

(b)

FLAT PLATE X = 9", Y = 1.8"

FIG. 31 PHOTOCURRENT DURING A TEST (BEAM ON)

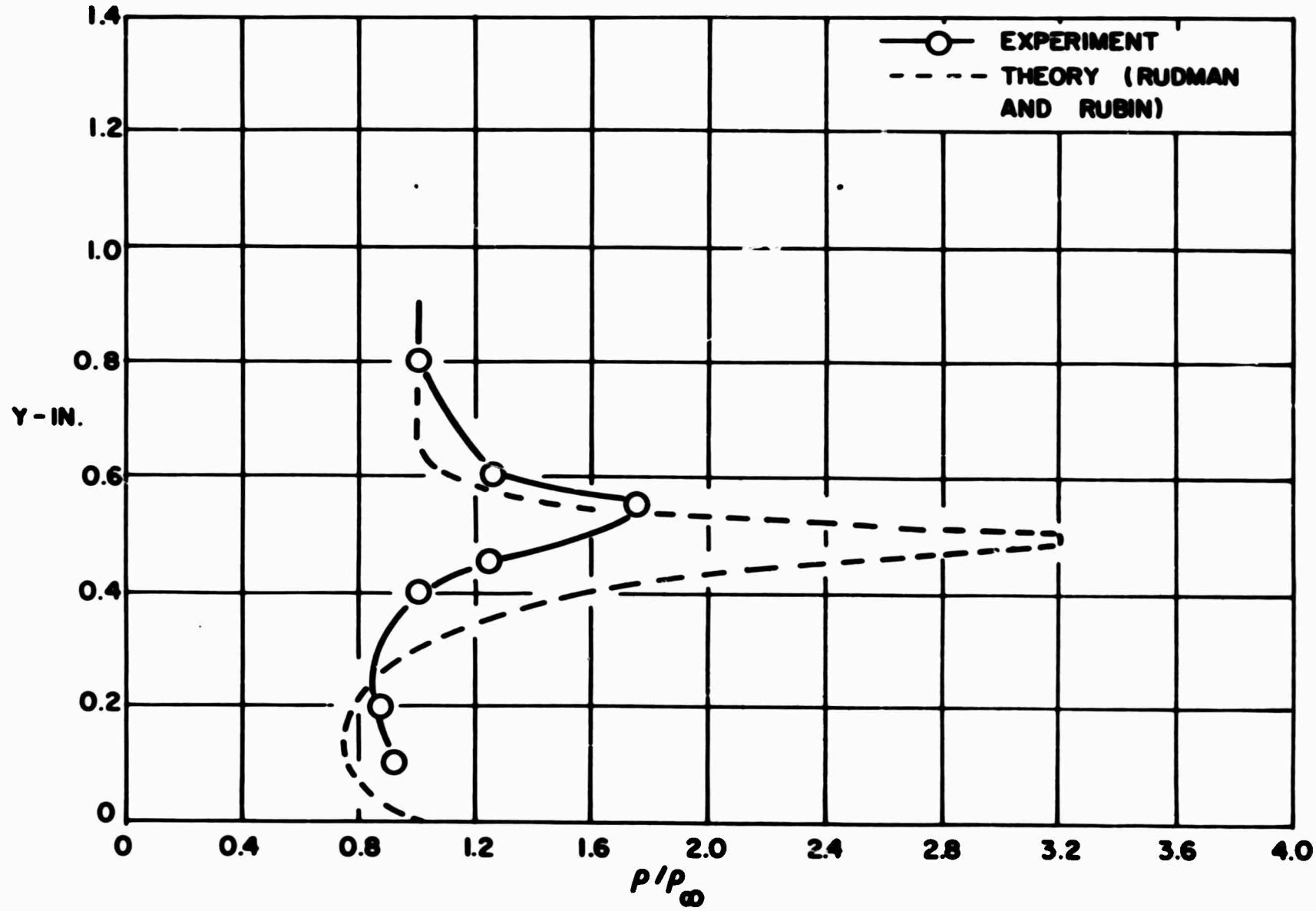

FIG. 32 NEUTRAL DENSITY NORMAL TO THE PLATE AT X = 2"

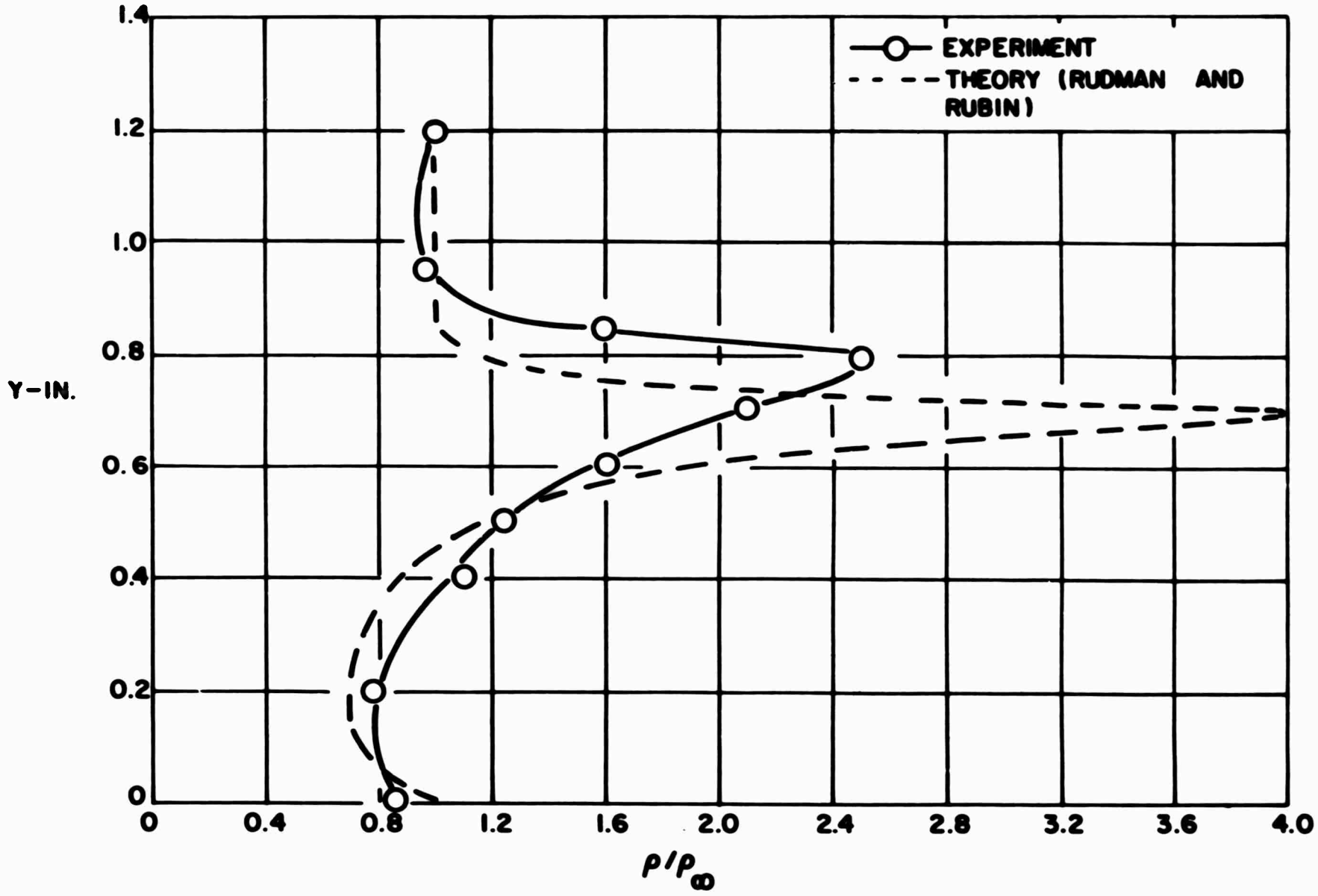

FIG. 33 NEUTRAL DENSITY NORMAL TO THE PLATE AT X=3"

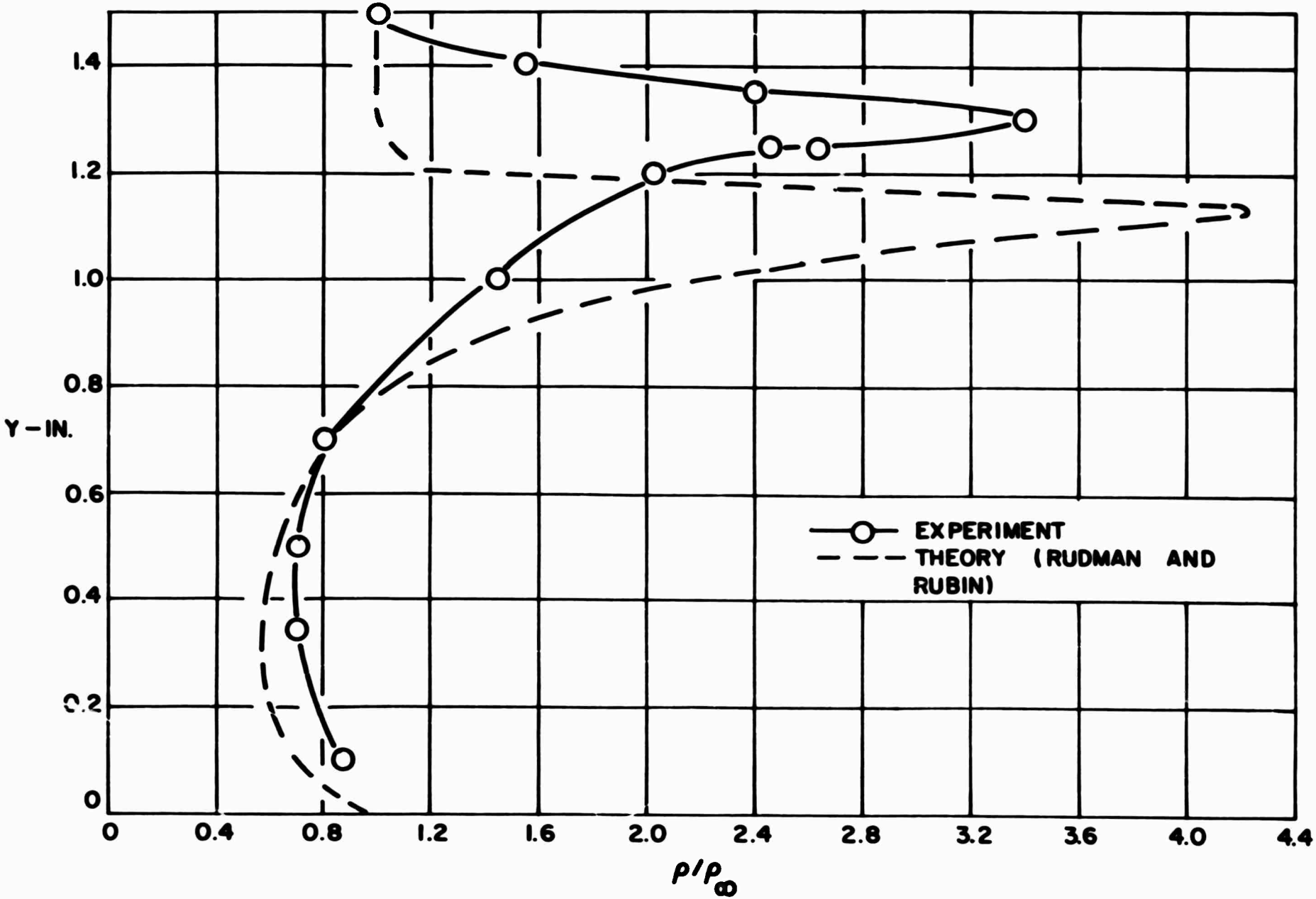

FIG. 34 NEUTRAL DENSITY NORMAL TO THE PLATE AT X=6"

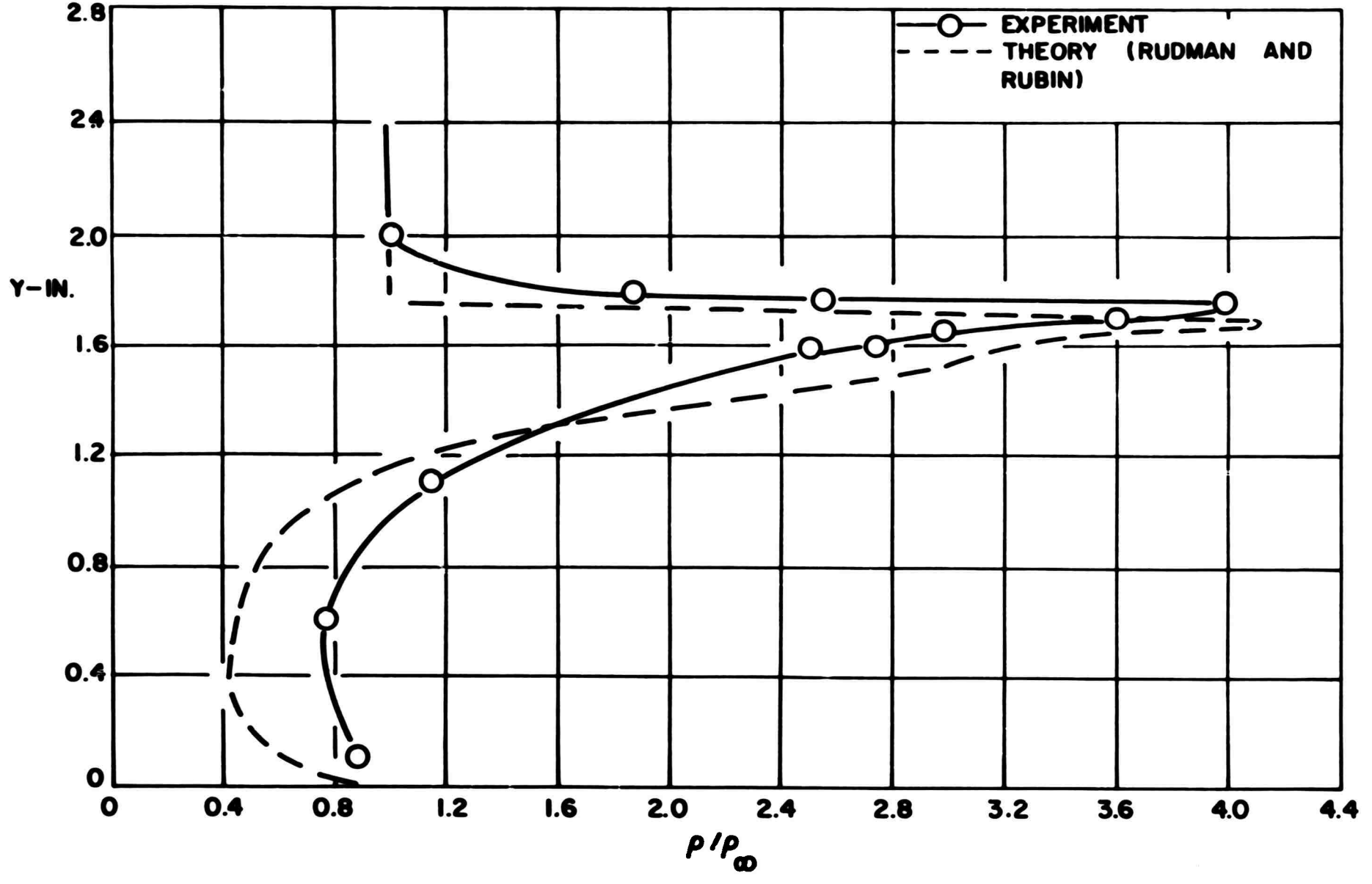

FIG. 35 NEUTRAL DENSITY NORMAL TO THE PLATE AT X = 9"

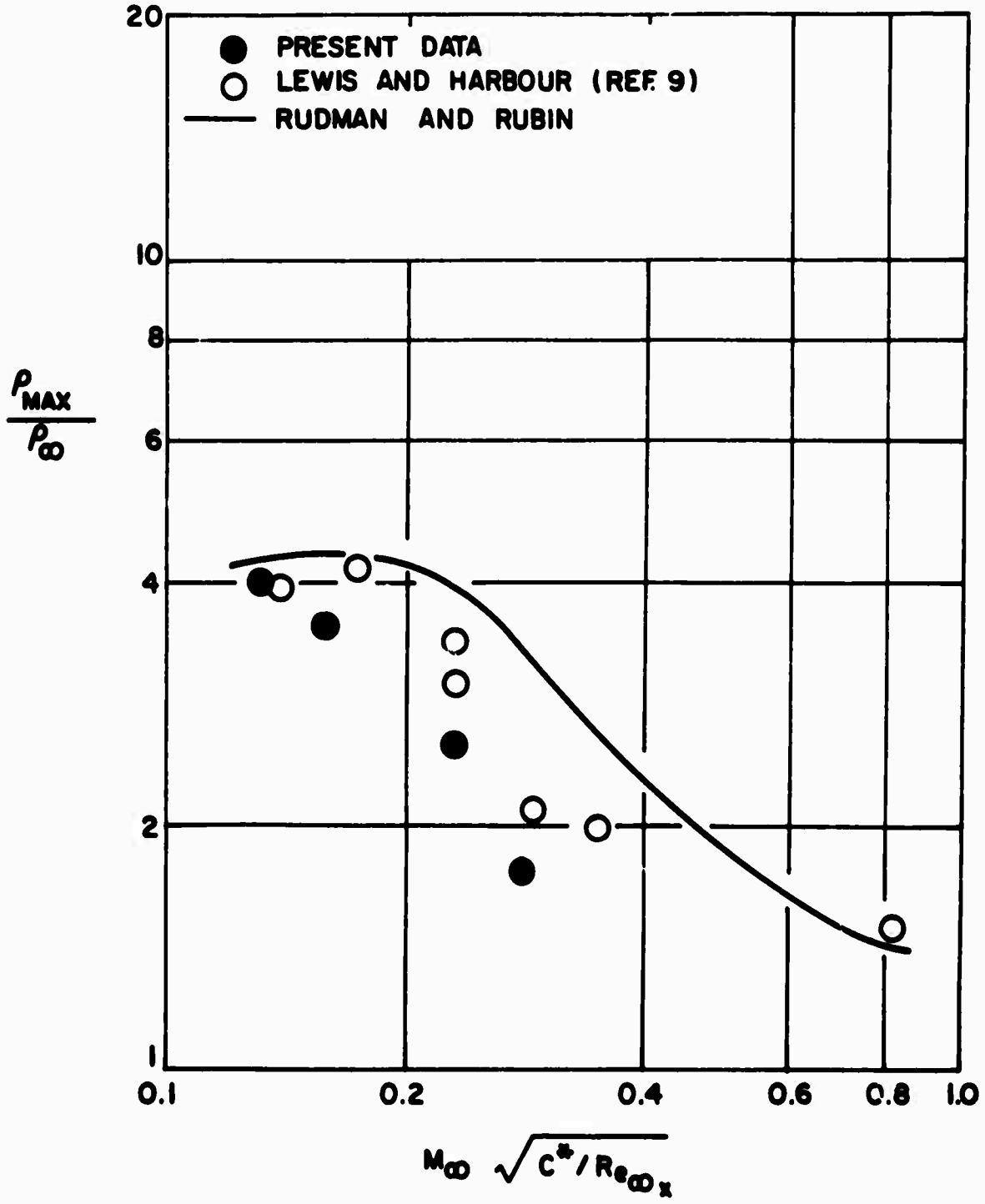

FIG. 36 DENSITY RATIO ACROSS THE SHOCK WAVE IN THE MERGED LAYER REGIME

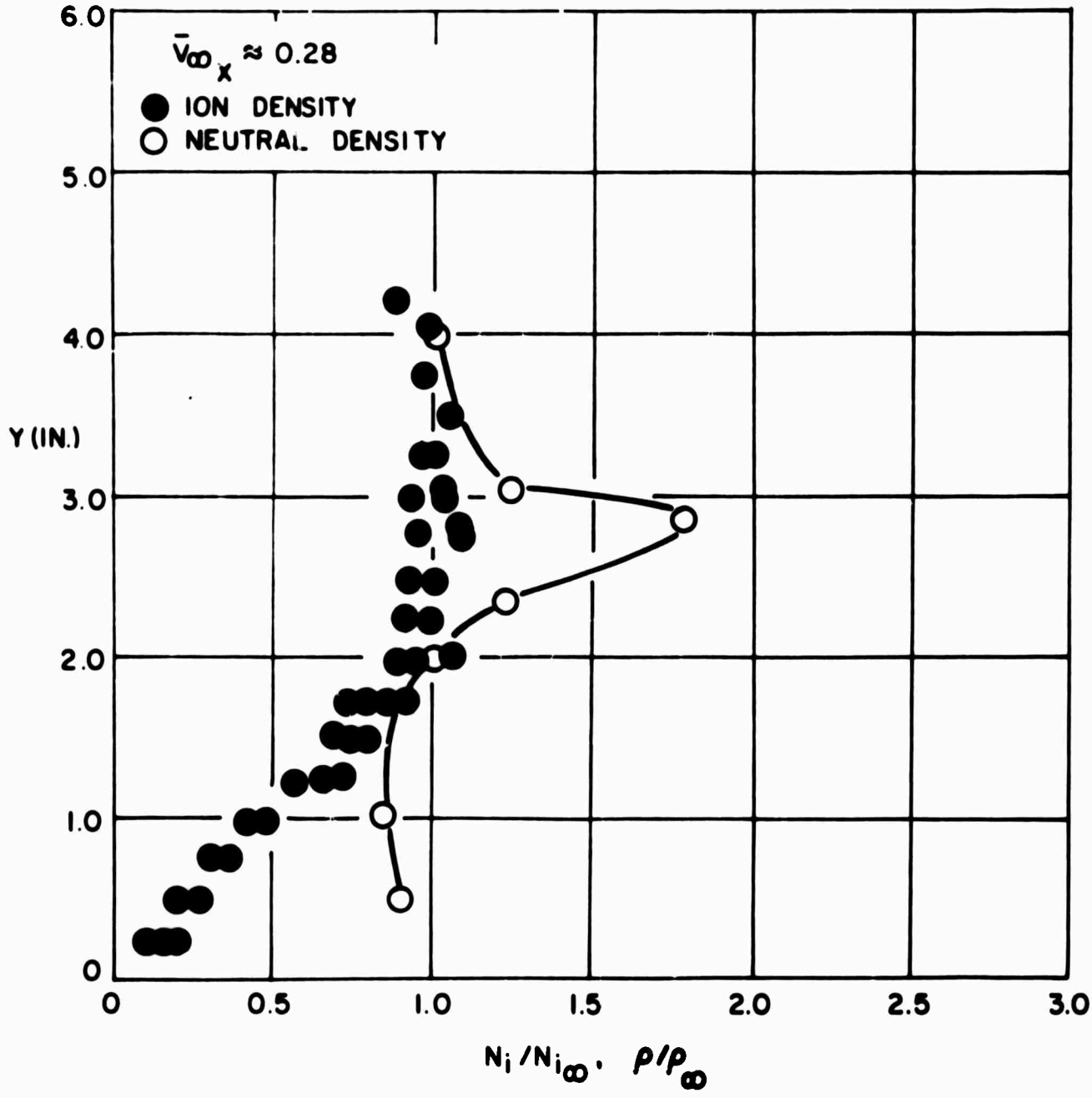

FIG. 37 NORMALIZED ION AND NEUTRAL DENSITY PROFILES NORMAL TO THE PLATE, $\bar{V}_{\infty_x} \approx 0.28$

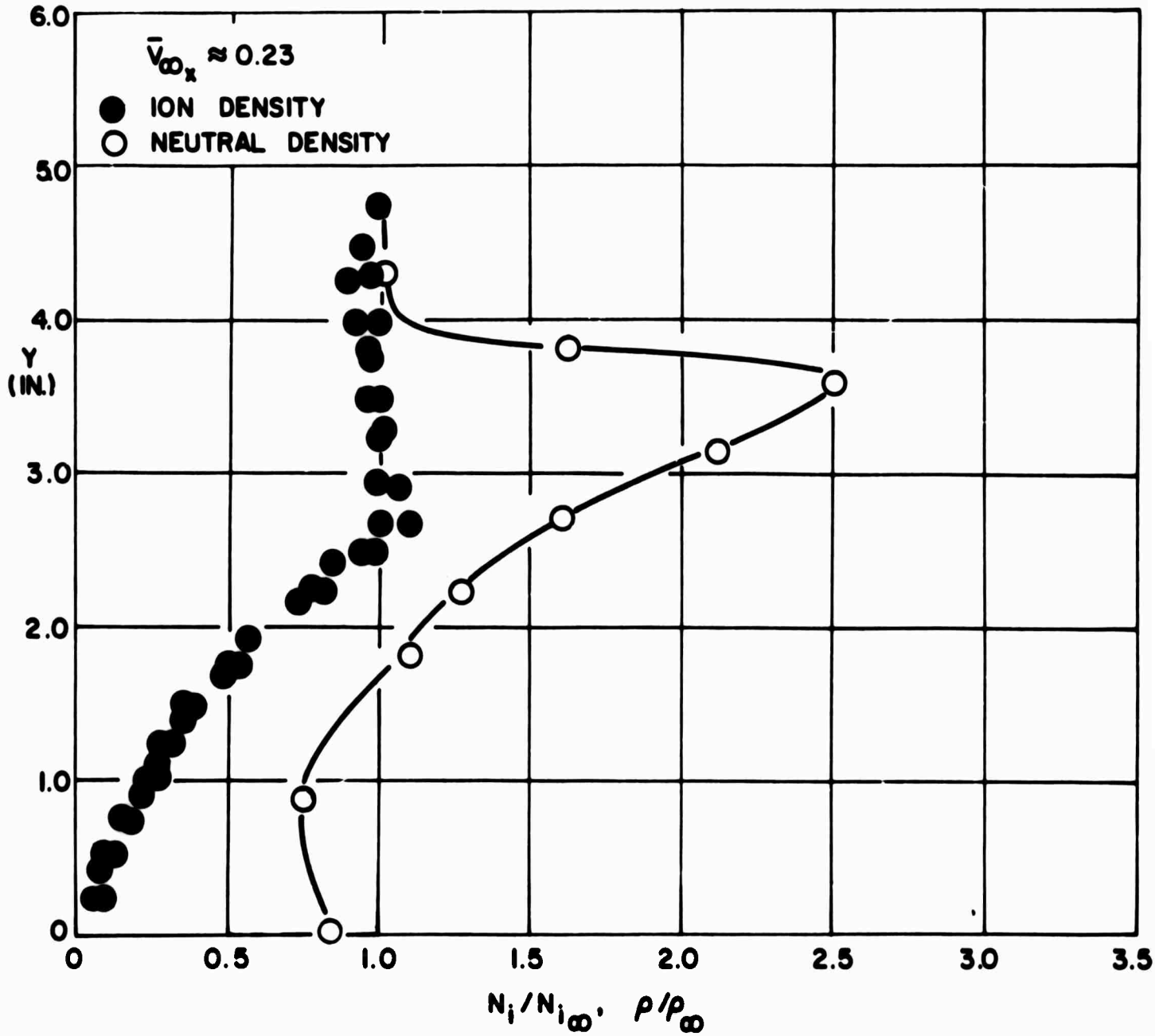

FIG. 38 NORMALIZED ION AND NEUTRAL DENSITY PROFILES NORMAL TO THE PLATE, $\bar{V}_{\infty_x} \approx 0.23$

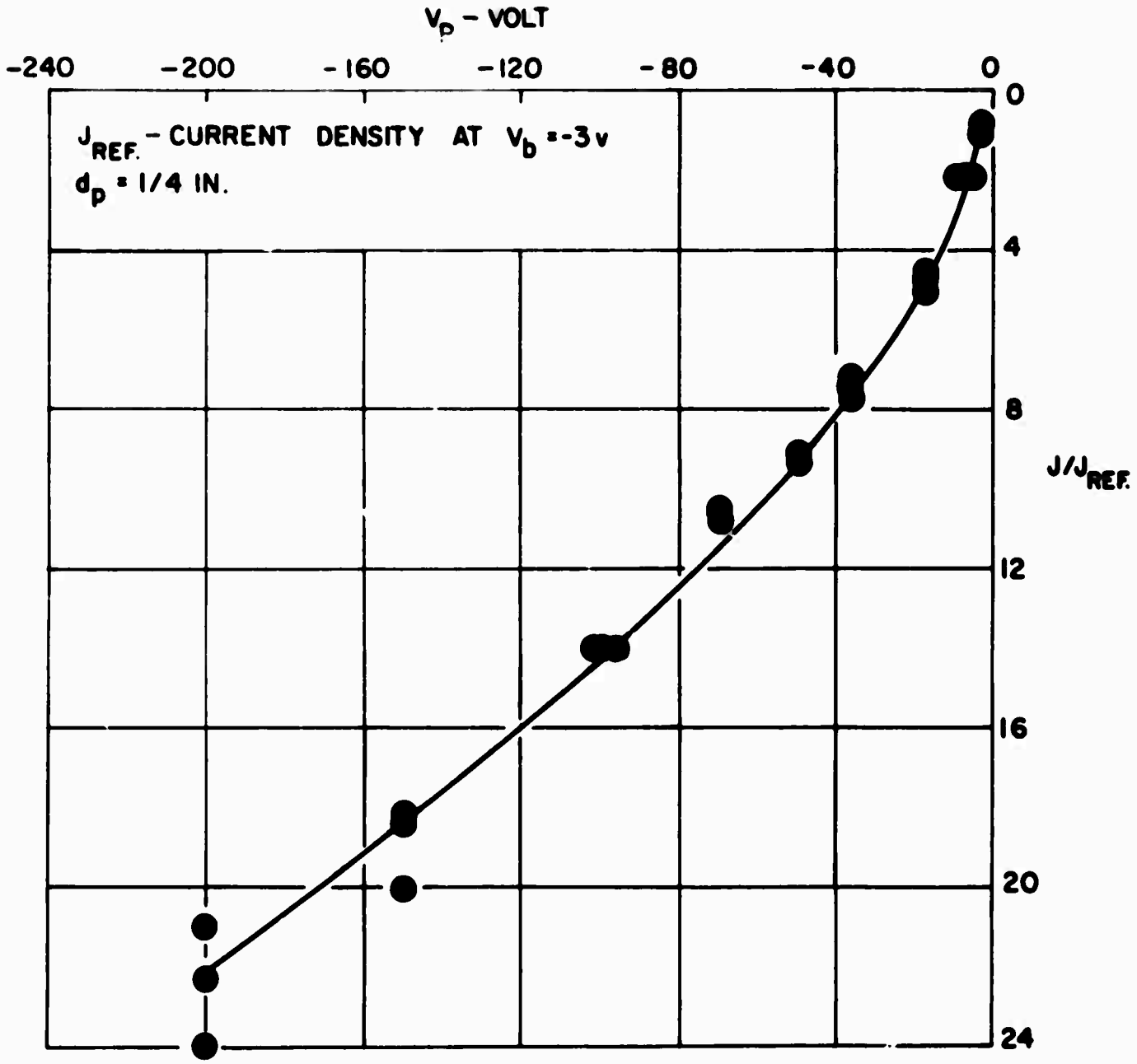

FIG. 39 VOLTAGE CURRENT CHARACTERISTIC FOR A FLUSH PROBE ($2R_p$ = 1/4")

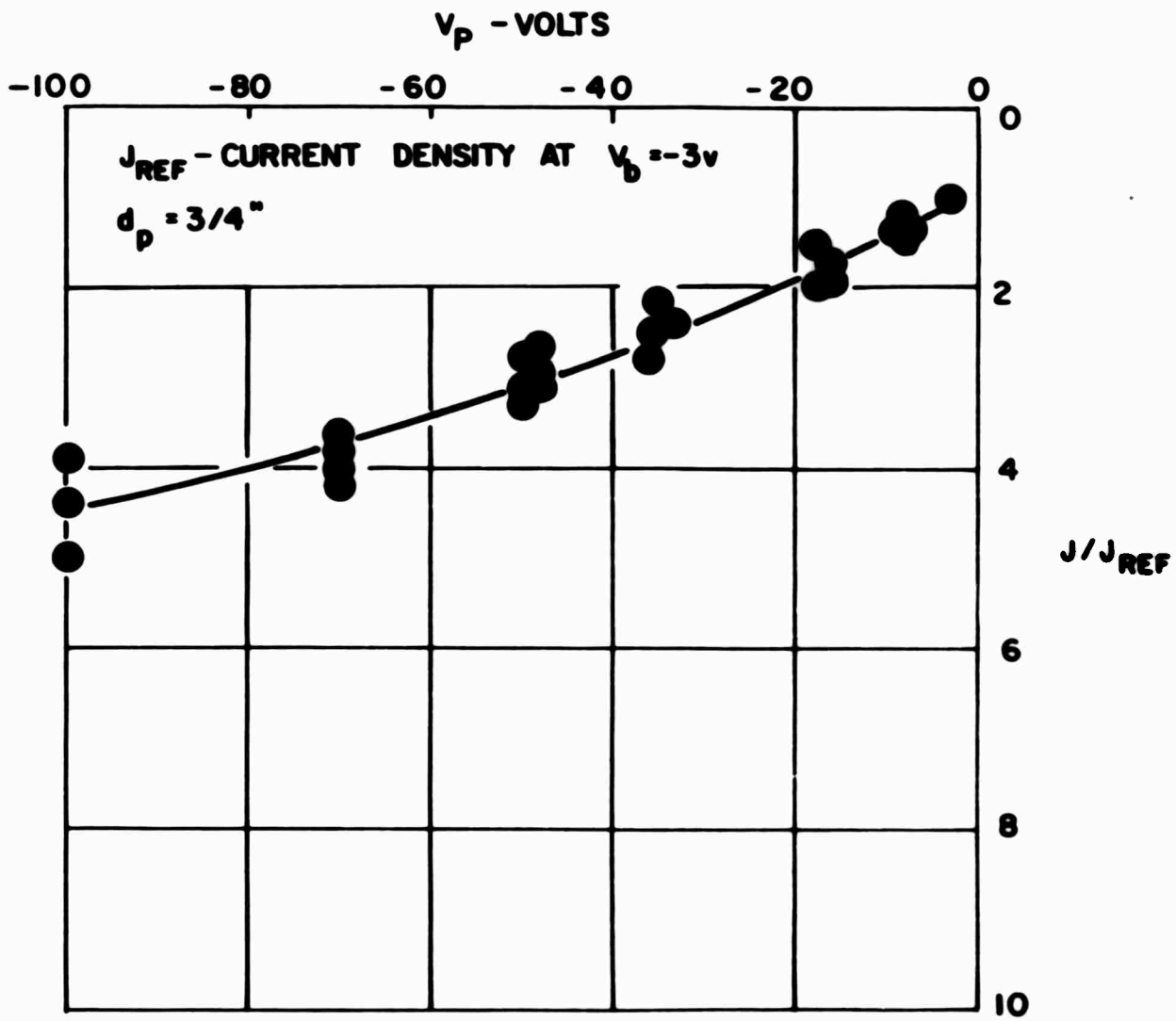

FIG. 40 VOLTAGE CURRENT CHARACTERISTIC FOR A FLUSH PROBE ($2R_p$ = 3/4")

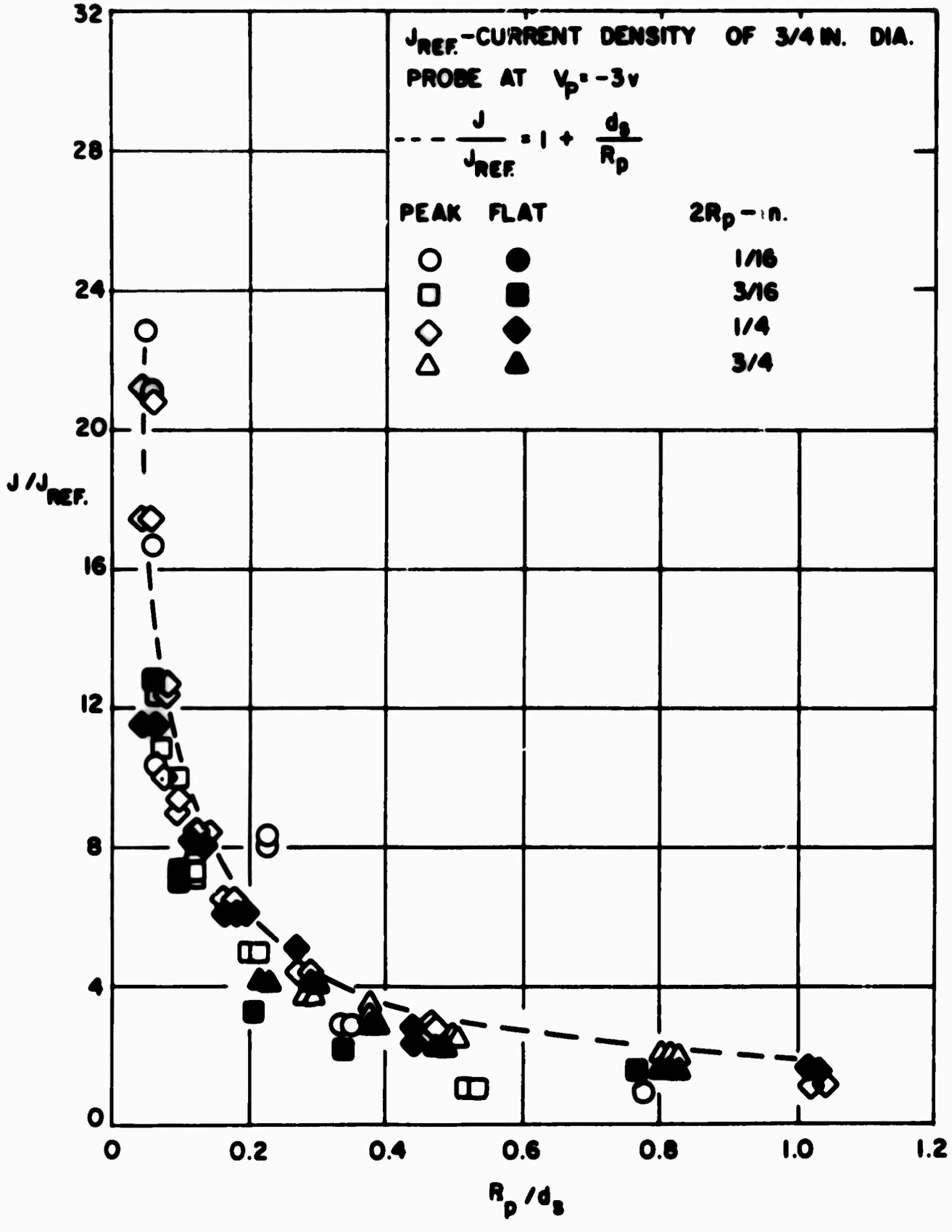

FIG. 41 NONDIMENSIONAL CURRENT DENSITY AS A FUNCTION OF THE RATIO OF R_p/d_s

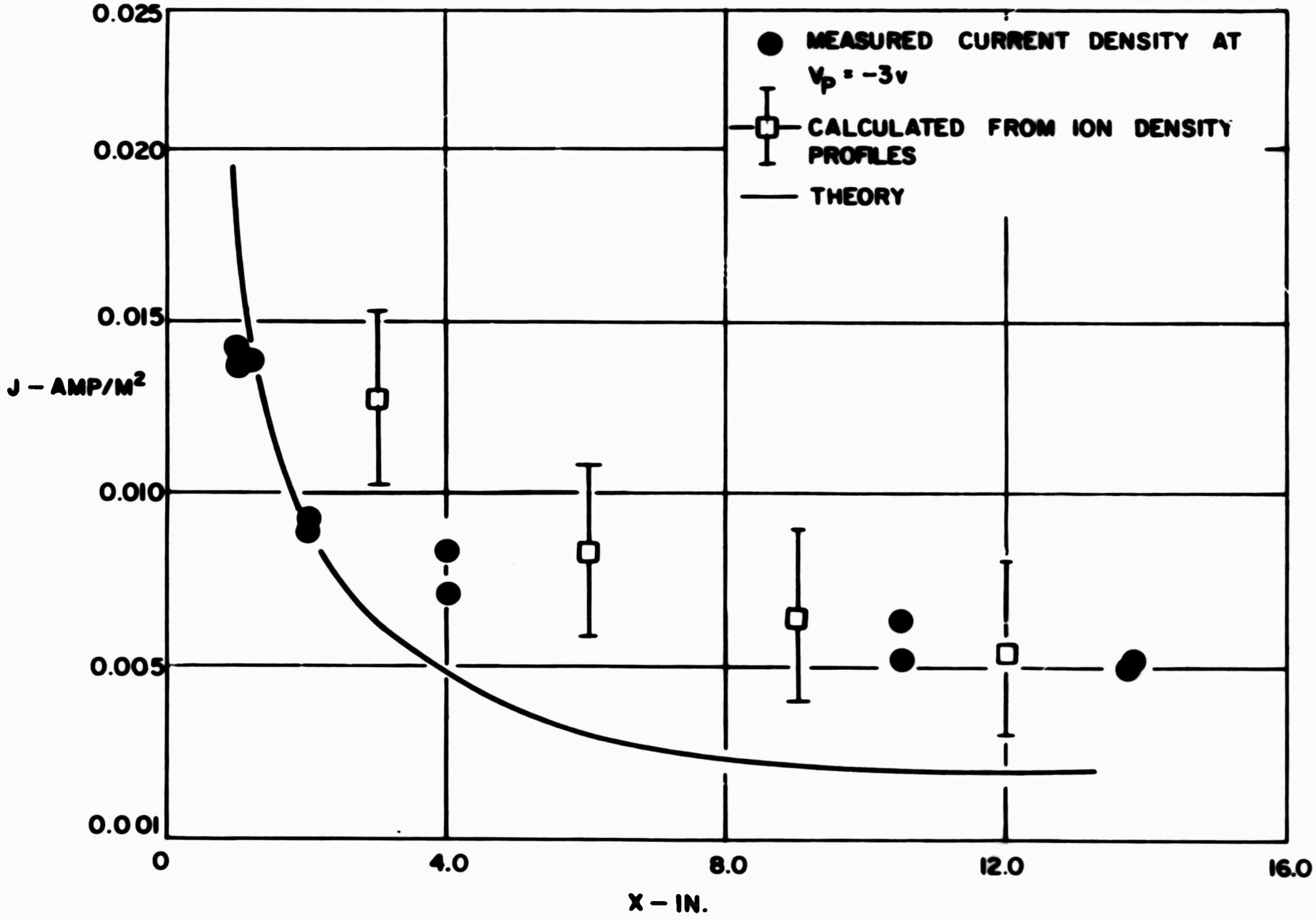

FIG. 42 AMBIPOLAR DIFFUSION FLUX TO THE PLATE

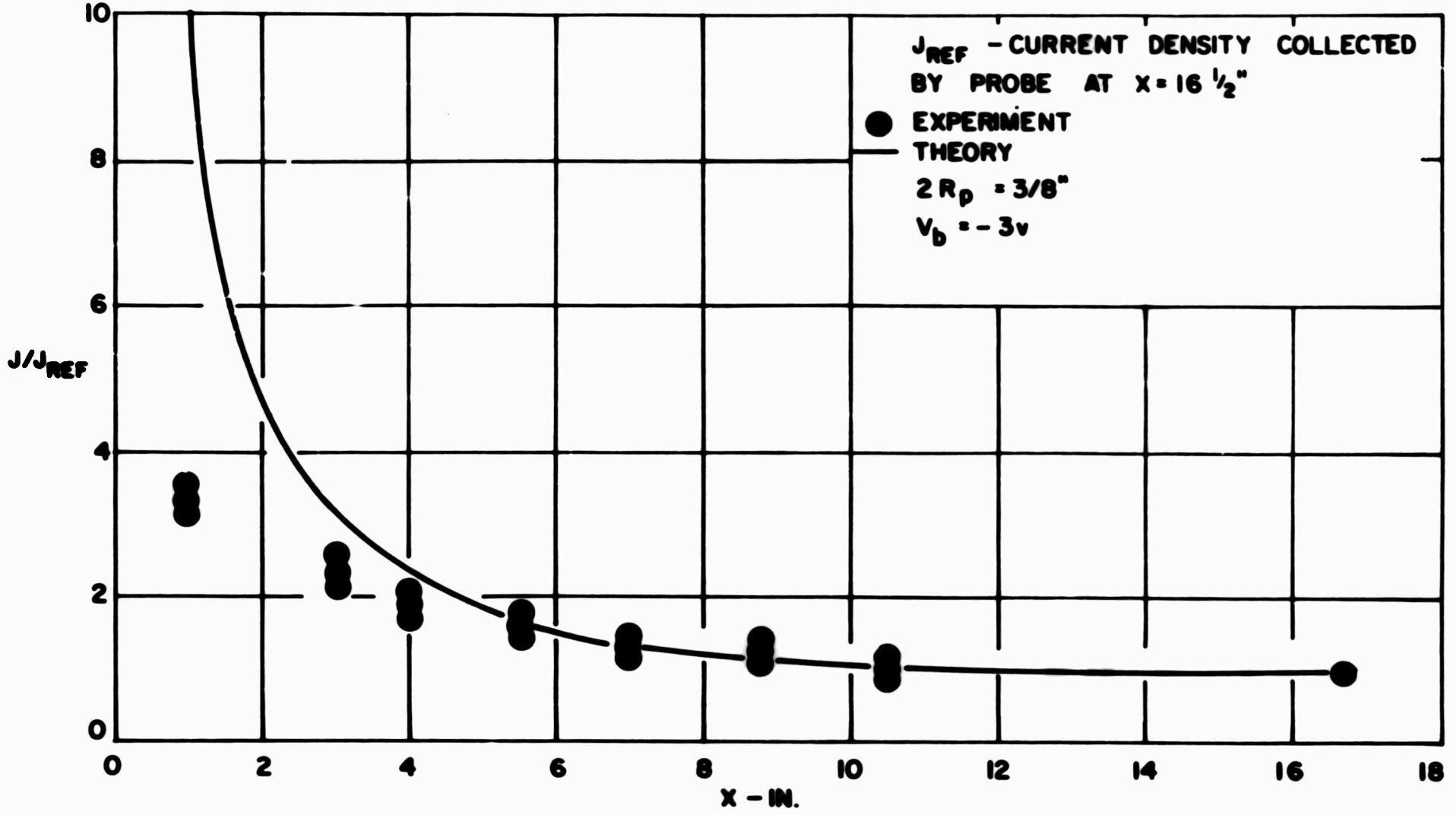

FIG. 43 NONDIMENSIONAL AMBIPOLAR FLUX TO THE PLATE

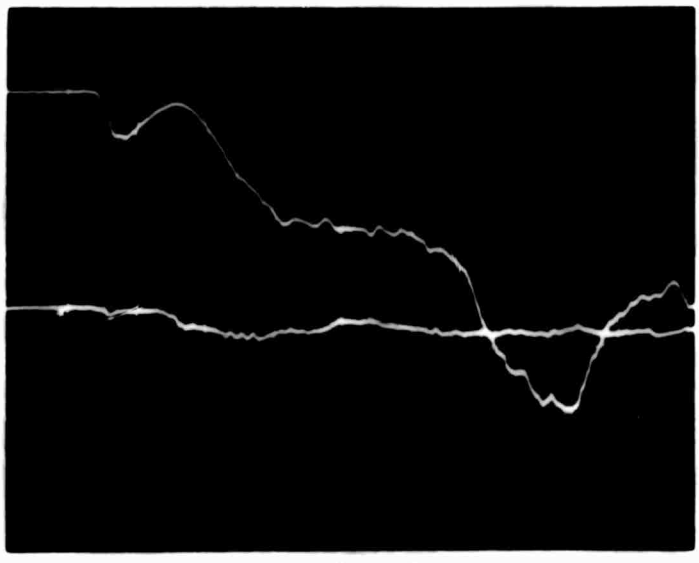

500 μ sec.

(a) FREE STREAM RUN

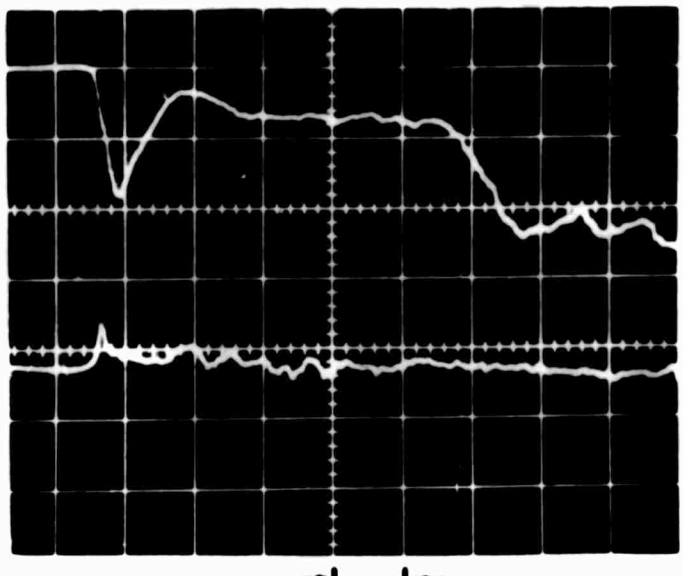

500 μ sec.

(b) WAKE RUN $X/D_B = 2.0$, $Y = 0$

FIG. 44 PHOTOCURRENT TRACES DURING A TEST (BEAM ON)

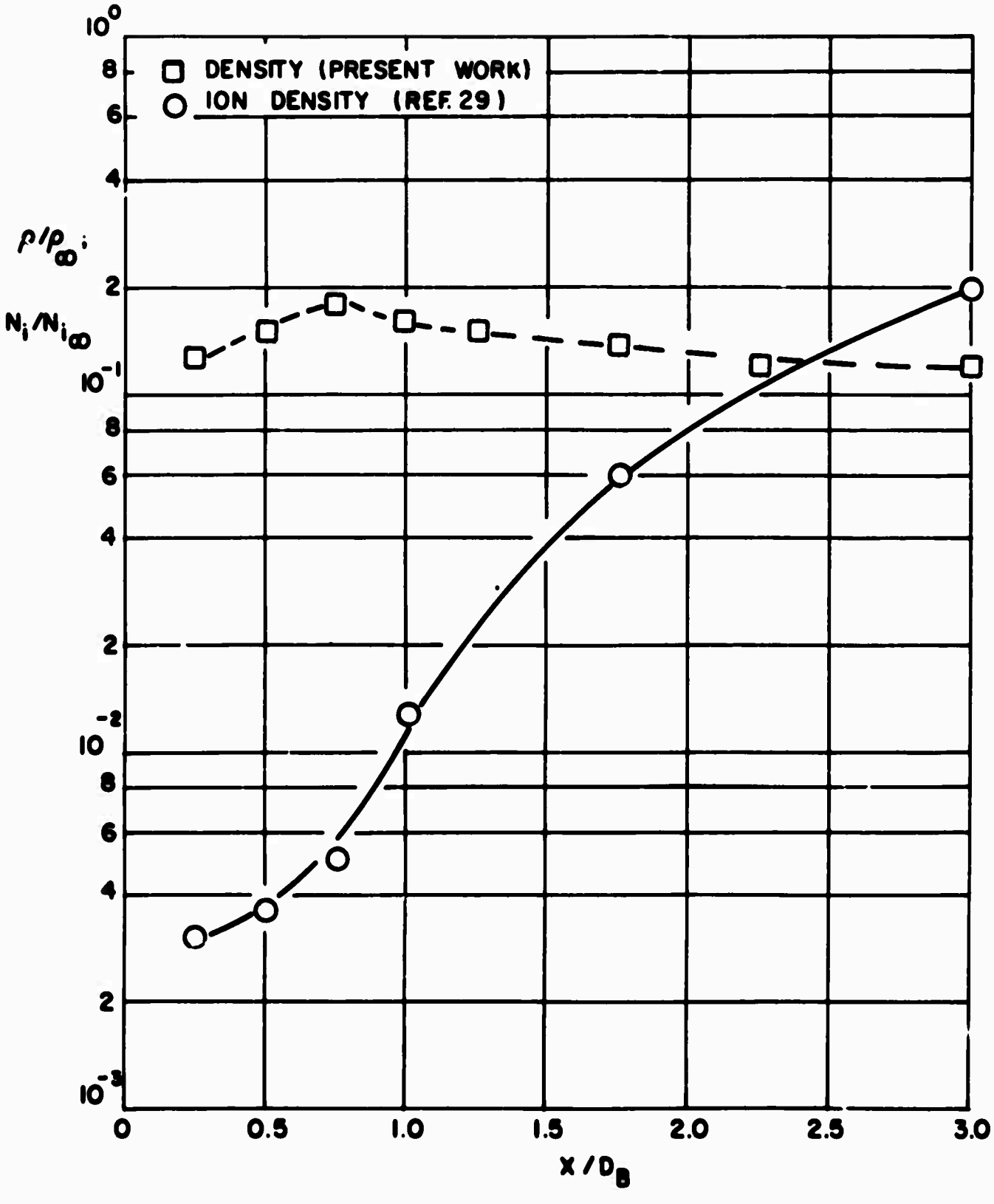

FIG. 45 NORMALIZED AXIAL NEUTRAL DENSITY AND ION DENSITY DISTRIBUTION IN THE NEAR WAKE OF THE CONE

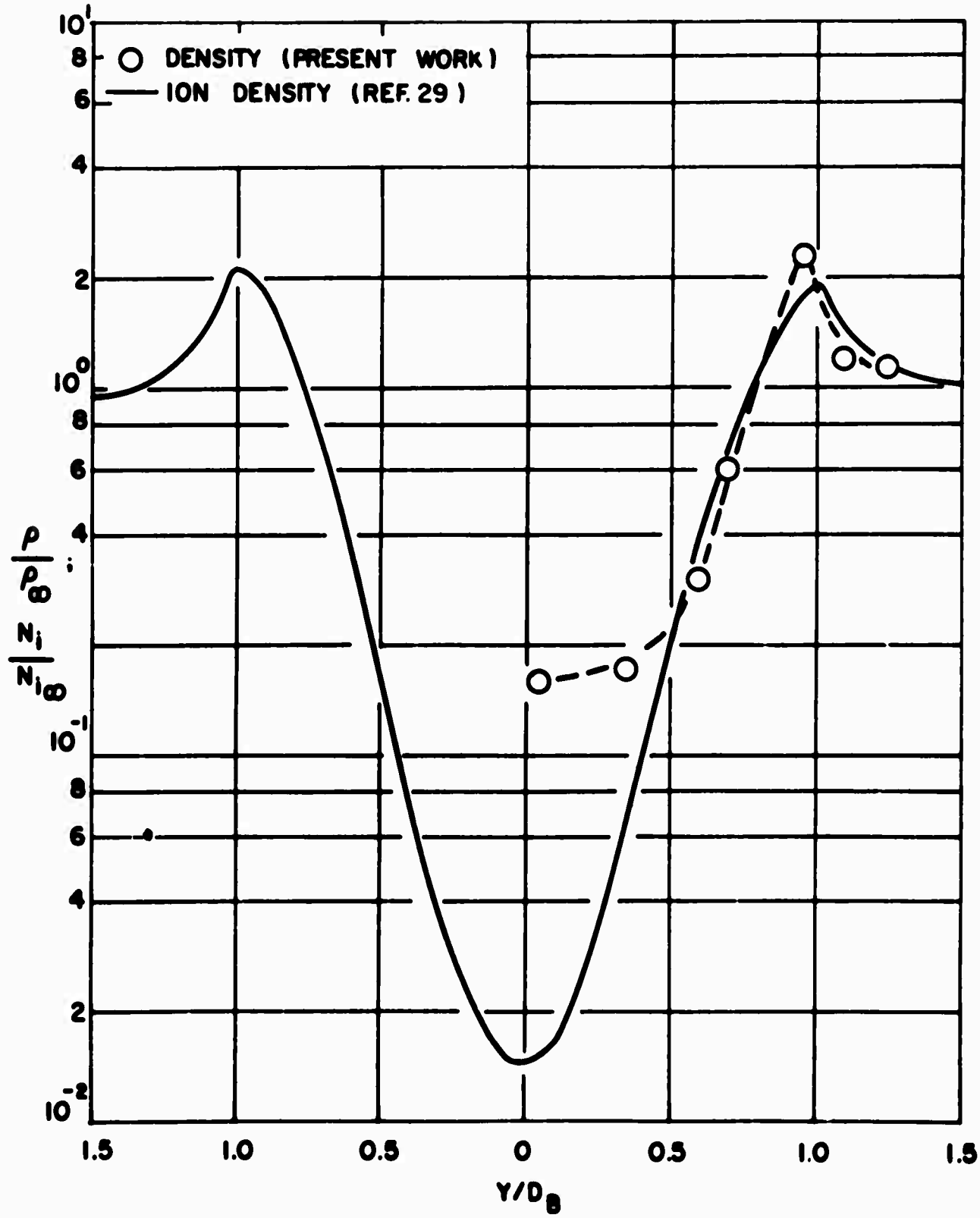

FIG. 46 NORMALIZED RADIAL NEUTRAL AND ION DENSITY PROFILE IN THE WAKE OF THE CONE AT $X/D_B = 1.0$

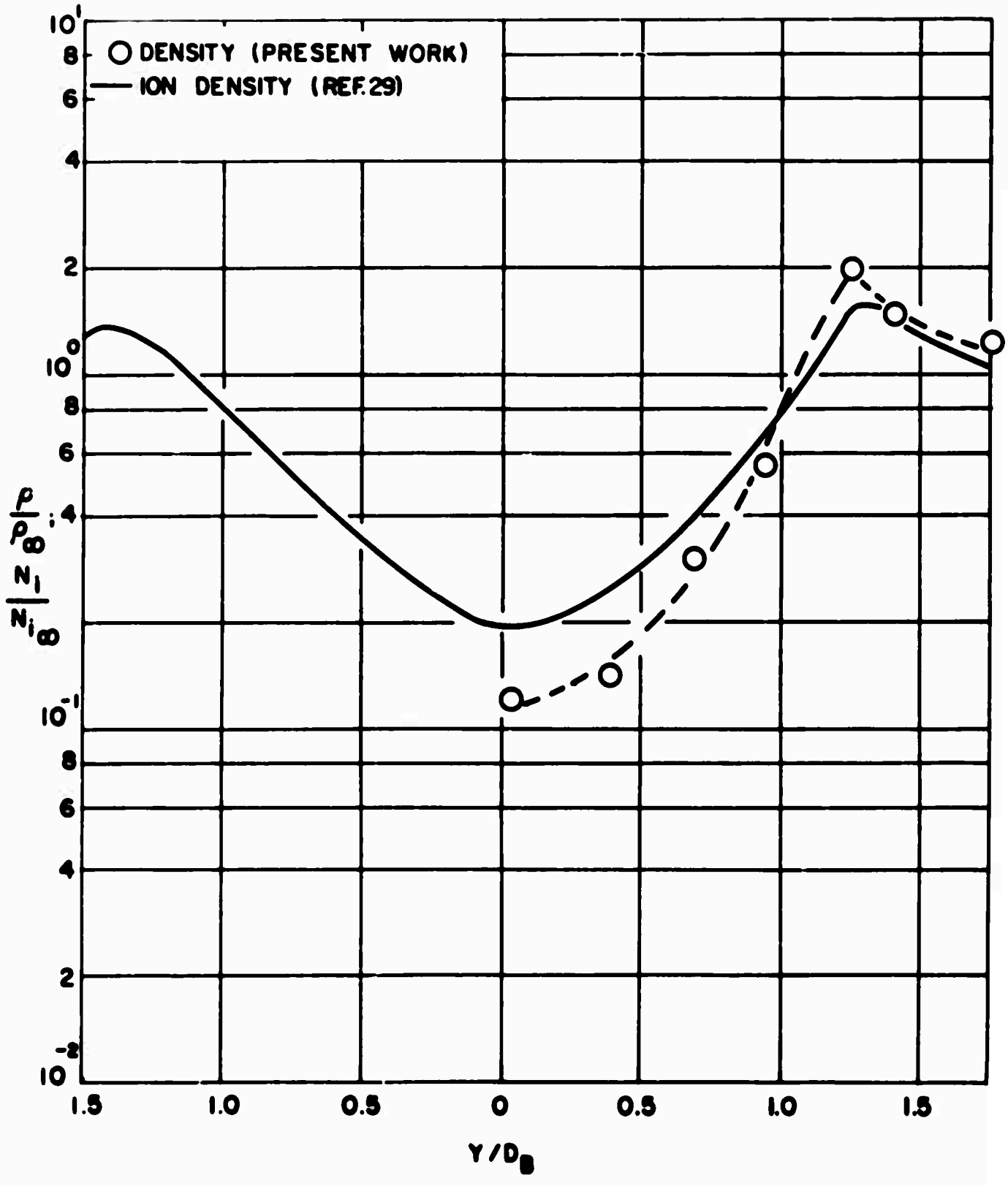

FIG. 47 NORMALIZED RADIAL NEUTRAL AND ION DENSITY PROFILE IN THE WAKE OF THE CONE AT $X/D_B = 3.0$